QATAR UNIVERSITY

COLLEGE OF ENGINEERING

DEVELOPMENT OF NOVEL MAGNETIC BENTONITE BASED ADSORBENTS COMBINED WITH DIFFERENT CARBON SOURCES FOR REMOVAL OF OIL CONTENT FROM PRODUCED WATER

BY

DINA MOHAMED AHMED MOHAMED AMR EWIS

A Thesis Submitted to

The College of Engineering

In Partial Fulfillment of the Requirements for the Degree of

Master of Science in Environmental Engineering

June 2021

COMMITTEE PAGE

The members of the Committee approve the Thesis of
Dina Mohamed Ahmed Mohamed Amr Ewis defended on 19/04/2021

Dr. Abdelbaki Benamor
Thesis/Dissertation Supervisor

Dr. Muneer M. Ba-Abbad
Thesis Associate Supervisor

Prof. Dominic C. Y. FOO
Committee Member

Dr.Anand Kumar
Committee Member

Dr. Galal Abdellah
Committee Member

Approved:

Khalid Kamal Naji, Dean, College of Engineering

ABSTRACT

EWIS, DINA, Mohamed,Masters:June:2021,

Masters of Science in Environmental Engineering

Title: Development of Novel Magnetic Bentonite Based Adsorbents Combined With Different Carbon Sources for Removal of Oil Content from Produced Water

Supervisor of Thesis: Dr. Abdelbaki Benamor .

Water scarcity is a challenge faced worldwide due to depleting sustainable good quality water resources. Produced water, associated with the production of gas and oil, usually comes as oil contaminated water, creating real problems in water resources' management. Therefore, removing oil content from produced water is crucial to meet the discharge limits set by governmental legislation. Compared to the current state of produced water treatment technologies, adsorption is envisaged as a promising technique due its simplicity, and ease of operation. For that, the development of adsorbents with high removal capability, good stability, high recoverability, inexpensive, and environmentally friendly nature is the most important step in adsorption process. Bentonite is a type of clay minerals that is inexpensive, non-toxic, and naturally occurring that have been utilized in water remediation applications. Thus, the aim of this work is to develop novel magnetic bentonite-based adsorbents combined with different carbon sources (reduced graphene oxide, and multiwall carbon nanotubes) for oil content removal. The developed adsorption composites were characterized using XRD, TGA, SEM, EDX, TEM, and BET analysis techniques. Furthermore, the adsorptive behavior of the developed composites was compared to magnetic bentonite under the same experimental conditions examining the effect of

various parameters on the adsorption capability. The experimental data were analyzed using three isotherm models including Langmuir, Freundlich and Sips models using non-linear regression fitting and were compared using Akaike Information Criterion statistical model. The results showed that developed composites attained enhanced adsorption capacity and had shorter equilibrium times compared to magnetic bentonite. Furthermore, the oil content removal performances of all synthesized composites reported in this study were investigated in a fluidized bed reactor and a possible adsorption mechanism was proposed. Overall, this work confirms the feasibility of the proposed adsorbents for oil removal in industrial adsorption process.

***Keywords*:** Magnetic bentonite, reduced graphene, Carbon nanotubes, Adsorption, Oil treatment.

DEDICATION

To my family, friends, and people who supported me during my downs.

ACKNOWLEDGMENTS

This publication was made possible by an Award [GSRA6-2-0516-19029] from Qatar National Research Fund (a member of Qatar Foundation). The contents herein are solely the responsibility of the author.

My deepest gratitude to Dr.Abdelbaki Benamor and Dr.Muneer Abaad for their continuous support and guidance to accomplish this study. I would like to extent my sincerest appreciation to Prof.Muftah El-Naas, Dr. Hazim Qiblawey, Prof.bassim hamid, and Dr.Mustafa Nasser for sharing their expertise and knowledge throughout my graduate study. Finally, I would like to acknowledge Mr.Dan cortes, and Dr.Ahmed Al Khattat for their valuable assistance in my experimental work.

TABLE OF CONTENTS

DEDICATION v

ACKNOWLEDGMENTS vi

LIST OF TABLES xi

LIST OF FIGURES xiii

NOMENCLATURE xvi

CHAPTER 1: INTRODUCTION 1

1.1 Research overview 1

1.2 Tangible objective 3

1.3 Research novelty 4

1.4 Thesis outline 5

1.5 Research outcome (publications) 5

CHAPTER 2: LITERATURE REVIEW 7

2.1 Produced water. 7

2.2 Environmental legislation 9

2.3 Treatment technologies 10

2.3.1 Chemical treatment technologies 10

2.3.2 Physical treatment technologies 12

2.4 Adsorption technology 14

2.5 Adsorbents 15

2.5.1 Clay minerals. 15
2.5.2 Carbon-based adsorbents. 19
2.5.3 Magnetic metals oxides 20
2.5.4 Modified adsorbents 21
2.5.5 Composites 21
2.6 Adsorbents synthesis methods 27
2.6.1 Co-precipitation 27
2.6.2 Hydrothermal 27
2.6.3 Solvothermal 28
2.6.4 Microwave-assisted 28
2.7 Adsorption isotherms 33
2.7.1 Langmuir model 33
2.7.2 Freundlich model 34
2.7.3 Sips model 34
2.8 Adsorption kinetics 34
2.8.1 Pseudo first order 35
2.8.2 Pseudo second order 35
2.8.3 Intraparticle diffusion model 35
2.9 Akaike Information Criterion 35
2.10 Performance in fluidized bed reactor 36

CHAPTER 3: MATERIALS AND METHODS 38
3.1 Materials and chemicals 38
3.2 Adsorbents preparation 38
3.2.1 Synthesis of iron oxide nanoparticles 38
3.2.2 Synthesis of graphene oxide 38
3.2.3 Synthesis of iron oxide/Bentonite composite 39
3.2.4 Synthesis iron oxide/bentonite/reduced graphene oxide 39
3.2.5 Synthesis of iron oxide/bentonite/multiwall carbon nanotubes 40
3.1 Adsorbents characterization 40
3.2 Synthesis of produced water 40
3.3 Adsorption experiments 41
3.4 Fluidized bed experiments 42
CHAPTER 4: RESULTS AND DISCUSSION 44
4.1 Characterization 44
4.1.1 X-ray diffraction 44
4.1.2 Thermogravimetric analysis 47
4.1.3 Scanning electron microscope/ Energy-dispersive X-ray spectroscopy 48
4.1.4 Transmission electron microscopy 52
4.1.5 Brunauer Emmett Teller 54
4.2 Adsorption results 55

4.2.1 Performance of iron oxide/Bentonite 55

4.2.2 Performance of Fe_3O_4/Bent/rGO and Fe_3O_4/Bent/MWCNTs 69

4.3 Performance in fluidized bed 79

4.4 Adsorption mechanism 81

4.5 Comparison of adsorbents 85

CHAPTER 5: CONCLUSION AND FUTURE PERSPECTIVE 88

APPENDIX 116

LIST OF TABLES

Table 1: The adsorption performance of various composites towards produced water organic constituents. 24

Table 2: The advantages and disadvantages of using microwave heating in absorbents preparation. 32

Table 3: Perfomance of fluidized bed reactor in organic polluants removal by adsorption.....37

Table 4: EDX analysis for Fe3O4/Bentonite/ Fe3O4/Bent/rGO and Fe3O4/Bent/MWCNTs. 50

Table 5: BET analysis of the synthized composites. 54

Table 6: Isotherm parameters for Langmuir, Freundlich and Sips models for oil adsorption onto Fe_3O_4/Bentonite. 61

Table 7: A comparison of the adsorption isotherm models for oil adsorption onto Fe_3O_4/bentonite. 62

Table 8: Kintic models parameters for oil adsorption onto Fe_3O_4/Bentonite. 65

Table 9: Isotherm parameters for Langmuir, Freundlich and Sips models for oil adsorption onto the novel composites. 74

Table 10: A comparison of the adsorption isotherm models for oil adsorption onto Fe_3O_4/Bent/rGO. 75

Table 11: A comparison of the adsorption isotherm models for oil adosrption onto Fe_3O_4/Bent/MWCNTs. 75

Table 12: The kinetics parameters for oil adsorption onto novel composites. 79

Table 13: Comparsion between the performance of different adsorbent twoards emlusifed oil.....87

Table 14: Raw data for the effect of varying Fe_3O_4/Bentonite dosage on its removal capability 116

Table 15: Raw data for the effect of varying solution pH on Fe_3O_4/Bentonite removal capability. 117

Table 16: Raw data for effect of initial oil concentration on Fe_3O_4/Bentonite removal capability. 118

Table 17: Raw data for effect of varying contact time on Fe_3O_4/Bentonite removal capability. 119

Table 18: Raw data for effect of varying initial oil concentration on Fe_3O_4/Bent/rGO removal capability. 120

Table 19: Raw data for the effect of varying contact time on Fe_3O_4/Bent/rGO removal capability. 121

Table 20: Raw data for the effect of varying initial oil concentration on Fe_3O_4/Bent/MWCNTs removal capability. 122

Table 21: Raw data for the effect of contact time on Fe_3O_4/Bent/MWCNTs removal capability. 123

Table 22: Raw data for performance of Fe_3O_4 NPs, Fe_3O_4/Bentonite, Fe_3O_4/Bent/rGO, and Fe_3O_4/Bent/MWCNTs in fluidzied bed reactor. 124

LIST OF FIGURES

Figure 1: Constituents of produced water. 7

Figure 2: A schematic diagram of Electrodialysis system. 13

Figure 3: Crystaline structure of Clay minerals (a) Octahedral (b) Tetrahedral 16

Figure 4: Bentonite structure 18

Figure 5: Schematic diagram of Microwave system. 29

Figure 6: Heat flow in direction in Microwave and conventional heating systems 30

Figure 7: Microwave heating system. 30

Figure 8: The adsorption experiment procedure. 41

Figure 9: Fluidized bed setup. 43

Figure 10: XRD pattern for Fe_3O_4, raw bentonite, Fe_3O_4/Bentonite, Fe_3O_4/Bent/rGO, and Fe_3O_4/Bent/MWCNTs. 46

Figure 11: TGA specturm for Fe_3O_4/Bentonite, Fe_3O_4/Bent/rGO and Fe_3O_4/Bent/MWCNTs. 48

Figure 12: SEM images (a) rGO at 50 μm (b) Bentonite at 50 μm (c) Fe_3O_4 NPs at 0.5 μm(d) Fe_3O_4/Bentonite at 3 μm (e) Fe_3O_4/Bent/rGO at 5μm (f) Fe_3O_4/Bent/rGO at 3μm (g) Fe_3O_4/Bent/MWCNTs at 5μm (h) Fe_3O_4/Bent/MWCNTs at 3μm 51

Figure 13: TEM image (a) Fe_3O_4 NPs at 100 nm (b) Fe_3O_4/Bentonite at 100 nm (c) Fe_3O_4/Bent/rGO at 50nm (d) Fe_3O_4/Bent/rGO at 100nm (e) Fe_3O_4/Bent/MWCNTs at 100 nm (f) Fe_3O_4/Bent/MWCNTs at 50 nm. 53

Figure 14: Effect of Fe_3O_4/Bentonite dosage on the removal of oil at 6.5 pH, 298K, oil concentration of 100 ppm, and contact time 90 min. 56

Figure 15: Effect of pH on oil removal by Fe_3O_4/Bentonite 298K ,dosage concentration of 0.1g, 90 min contact time and oil concentration 100 ppm. 57

Figure 16: Effect of contact time on oil removal by Fe_3O_4/Bentonite at 298 K, initial concentration 100 ppm, 0.1 g dosage concentration and 6.5 pH 58

Figure 17: Effect of initial oil concentration on Removal percent using Fe_3O_4/Bentonite after 180 minutes at 298 K, dosage concentration 0.1 g and 6.5 pH. 59

Figure 18: Non-linear isotherm model fitting for oil adsorption onto Fe_3O_4/Bentonite adsorbent. 60

Figure 19: Separation factor (R_L) of emulsified oil adsorption onto Fe_3O_4/Bentonite. 62

Figure 20: Kinetics models fitting for oil adsorption onto Fe_3O_4/Bentonite using (a) PFO (b) PSO (c) intraparticle diffusion model. 64

Figure 21: FTIR spectra of Fe_3O_4/Bentonite (a) before oil adsorption (b) after oil adsorption.....67

Figure 22: The possible adsorption mechanism of diesel oil by Fe_3O_4/bentonite. 68

Figure 23: Effect of time on the adsorption capacity (Dosage 0.1 g, Oil Concentration 120 ppm, 6.5 pH and Temperature 303 K. 70

Figure 24: Effect of initial concentration on the adsorption capacity (Dosage 0.1 g, Time 210 minutes, 6.5 pH and Temperature 303 K).....72

Figure 25: Non-linear isotherm model fitting for oil adsorption onto Fe_3O_4/Bent/rGO. 73

Figure 26: Non-linear isotherm model fitting for oil adsorption onto Fe_3O_4/Bent/MWCNTs. 73

Figure 27: Kinetics models fitting for oil adsorption onto Fe_3O_4/Bent/rGO using (a)

PFO (b) PSO (c) intraparticle diffusion model. 77

Figure 28: Kinetics models fitting for oil adsorption onto Fe_3O_4/Bent/MWCNTs using (a) PFO (b) PSO (c) intraparticle diffusion model. 78

Figure 29: performance of Fe_3O_4 NPs, Fe_3O_4/Bentonite, Fe_3O_4/Bent/rGO and Fe_3O_4/Bent/MWCNTs in fluidized bed reactor. 80

Figure 30: FTIR spectra of (a) Fe_3O_4/Bent/rGO before adsorption (b) Fe_3O_4/Bent/MWCNTs before adsorption (c) Fe_3O_4/Bent/rGO after adsorption (d) Fe_3O_4/Bent/MWCNTs after adsorption. 83

Figure 31: The possible adsorption mechanism of oil onto the novel composites. 84

NOMENCLATURE

PW	Produced water
DS	Dissolved solids
PAH	Polycyclic aromatic hydrocarbon
BTEX	Benzene, toluene, ethyl benzene, and xylene
COD	Chemical oxygen demand
BOD	Biological oxygen demand
EC	Electrocoagulation
ED	Electrodialysis
IEM	Ion-exchange membrane
CM	Clay minerals
AC	Activated carbon
ACF	Activated carbon fiber
MW	Microwave
TGA	Thermogravimetric analysis
FTIR	Transform Infrared Spectroscopy
SEM	Scanning Electron Microscopy
EDX	Energy-dispersive spectrometer
TEM	Transmission electron microscope
XRD	X-ray diffraction
BET	Brunauer-Emmett-Teller
PFO	Pseudo first order
PSO	Pseudo second order
AIC	Akaike Information Criterion

FBR	Fluidized bed reactor
Fe_3O_4 NPs	Iron oxide nanoparticles
Fe_3O_4/Bentonite	Iron oxide/Bentonite
Fe_3O_4/Bent/rGO	Iron oxide/Bentonite/reduced graphene oxide
Fe_3O_4/Bent/MWCNTs	Iron oxide/Bentonite/multiwall carbon nanotubes
MW	Microwave
CNTs	Carbon nanotubes

CHAPTER 1: INTRODUCTION

1.1 Research overview

Deterioration of water quality due to the continuous discharge of contaminated water induced by the world's population growth, modernization, and rapid industrialization has become a global issue of concern [1, 2]. This situation is getting worse in the Gulf cooperation council (GCC) countries, with less than 1% of the total available freshwater resources worldwide available for 6% of the world population [3]. The frequent and continuous discharge of produced water that results from oil and gas industry became one of the serious problems worldwide causing considerable impact on ecological equilibrium, environment, and economy [4, 5]. Produced water (PW) is wastewater that is produced during the exploration and production of gas and oil [6]. It represents around 80% of the residuals and wastes produced, and its quantity rises significantly to reach up to 98% in depleted fields [7]. The composition of produced water varies according to the location and the type of the oil and gas fields, but generally, it is characterized by high content of oil and dissolved organics [8].It primarily consists of dissolved oil, hydrocarbon gases, organic acids, phenols, metals, and various chemical additives. The dissolved oil contaminants contain recalcitrant organic compounds such as benzene, toluene, xylene, , waxes, and surfactants [9]. The disposal of PW without proper treatment can interfere with the environmental sustainability harming aquatic life, thus, produced water remediation is a crucial task [10]. Strict governmental legislation to limit the amount of oil and grease in discharged produced water was set. According to the U.S. Environmental protection Agency, the allowable produced water on monthly and daily average are 29 mg/L and 42 mg/L, respectively [11]. Therefore, it is crucial to treat produced water prior to discharge into reservoir.

Several treatment technologies have been used for oil contaminants removal. For

instance, membranes and advanced oxidation are used for oily water treatment; however, their use is limited due to high capital and maintenance cost. Chemical flocculation attains high removal efficiency and requires small floor space, but it consumes huge amounts of energy. Biological treatment is also used despite causing secondary pollution that requires further treatment and consumes time [12, 13]. Compared to the current state of produced water treatment technologies, adsorption is envisaged as a promising technique due its simplicity, ease of operation and high removal capability [14]. Nevertheless, the main drawback associated with adsorption technology is the adsorbents high cost, which in turn elevates the cost of the treatment process [15]. Therefore, it is important to develop adsorbents with high efficiency, low cost, great selectivity, and excellent recyclability.

The utilization of low-cost adsorbents can potentially reduce the cost of insulation and maintenance. Besides, it is important to consider the recyclability, porosity, and separation efficiency of the adsorbents for an effective adsorption process [16]. Chitosan is a type of adsorbent that is known for good adsorption capacity along with low cost and non-toxicity [17]. However, it has low mechanical strength, low solubility in acidic solutions and can be deformed after drying [18]. Zeolites and biomass have been suggested as adsorbents, but their applications are limited due to low adsorption rates [18]. Clay minerals (CMs) are known for their excellent adsorption capabilities, but their applications are limited because of their high dispersion of CMs in aqueous solutions, which makes them difficult to recycle and reuse [19]. Among CMs, Bentonite is available abundantly, inexpensive, contains wide interlayer spacing, attains ion exchange capacity and has high specific surface area [20, 21]. Even though bentonite has high dispersity in aqueous solution that renders its ability to be recovered and regenerated, it can be combined with other adsorbent, such as iron oxide nanoparticles

(Fe_3O_4 NPs) to facilitate its separation from aqueous solution. Fe_3O_4 NPs are known for their biological adaption, magnetic property, and large surface to volume ratio, environmentally friendly nature, and their high ability to remove organic contaminates from wastewater [22, 23]. Encapsulating Fe_3O_4 NPs into inorganic matrix (e.g bentonite) facilitate the magnetic composite separation from aqueous solution in the presence of external magnetic field due to Fe_3O_4 NPs magnetic property. Besides, the fabricated magnetic composite could have exceptional physicochemical properties including large specific surface area , enhanced Fe_3O_4 NPs chemical stability, and availability of a wider range of active sites [24]. Furthermore, carbonaceous adsorbents including activated carbon (AC), activated carbon fiber (ACF), and carbon nanotubes (CNTs) are known for high adsorption capacity, surface reactivity, and high surface area [25, 26]. More recently, the development of clay/carbon composites have received attention due to their enhanced properties including high recyclability, adsorption capacity, surface area, and porosity compared to the composite's individual components. Liang et al.[27], fabricated carbon/bentonite composite for alkaline industrial wastewater treatment. The composite attained around 91% removal for initial COD value of 79,834 mg/L. In addition, the composite showed a high removal efficiency for nine regeneration cycles. Yet, there is a growing focus on the development of low cost, and sustainable adsorbents that possess high adsorption ability for wide range of organic and inorganic contaminants.

1.2 Tangible objective

Considering the above-mentioned characteristics of a desired adsorbent for organic contaminants removal, the objectives of this study are:

I. To investigate the adsorptive capability of Fe_3O_4/Bentonite composite towards emulsified oil by examining the effect of adsorbent dosage, initial oil

concentration, solution pH, and contact time in a batch mode experiment.

II. Evaluate the adsorption capacity of Fe_3O_4/Bentonite for emulsified oil removal by conducting isotherm and kinetics study as well as assessing the adsorption mechanism.

III. To develop novel magnetic bentonite-based composites combined with reduced graphene oxide and multiwall carbon nanotubes (Fe_3O_4/Bent/rGO and Fe_3O_4/Bent/MWCNTs) for emulsified oil removal.

IV. To investigate the adsorptive capability of Fe_3O_4/Bent/rGO and Fe_3O_4/Bent/MWCNTs composite by examining the effect of initial oil concentration and contact time in a batch mode experiment.

V. Evaluate the adsorption capacity of Fe_3O_4/Bent/rGO and Fe_3O_4/Bent/MWCNTs composites towards emulsified oil by conducting isotherm and kinetics study as well as assessing the adsorption mechanism.

VI. To investigate the performance of Fe_3O_4 NPs, Fe_3O_4/Bentonite Fe_3O_4/Bent/rGO and Fe_3O_4/Bent/MWCNTs towards emulsified oil removal in a fluidized bed reactor.

VII. Conduct a comparison between Fe_3O_4/Bentonite and the developed composites in term of morphology, physiochemical properties, adsorptive capability and uptake mechanism.

1.3 Research novelty

Even though the synthesis of Fe_3O_4/Bentonite composite and its utilization for organic and inorganic water contaminants removal was reported in the literature, this work includes the composite synthesis and reports its adsorptive behavior towards emulsified oil under various parameters for the first time. In addition, in this work, novel Fe_3O_4/Bent/rGO and Fe_3O_4/Bent/MWCNTs composites were synthesized through co-

precipitation method for emulsified oil removal. The composites morphology, surface characteristics and physiochemical properties were investigated. Finally, the adsorptive behavior of Fe_3O_4 NPs, Fe_3O_4/Bentonite, Fe_3O_4/Bent/rGO and Fe_3O_4/Bent/MWCNTs towards emulsified oil in fluidized bed reactor was investigated.

1.4 Thesis outline

This research comprises five chapters. The first chapter introduces the research work, emphasizes the research novelty, and highlights the publications generated from this work. Chapter 2 offers an overview on PW sources, constituents, and management, legislation, and treatment technologies. The chapter also includes an overview on adsorption technology and the performance of various adsorbents in oil removal reported in the last decade. The chapter explains the theory of various types isotherm and kinetic models used in this work as well as Akaike Information Criterion (AIC), which was used to compare between the models. Chapter 3 includes the materials and chemicals used in this study, the synthesis procedures for all adsorbents as well as the synthetic produced water preparation. Chapter 4 represents the adsorbents characterization analysis and the adsorption results of Fe_3O_4/Bentonite, Fe_3O_4/Bent/rGO and Fe_3O_4/Bent/MWCNTs. In addition, the chapter emphasizes on the adsorption mechanism of emulsified oil onto the above-mentioned adsorbents and their performance in a fluidized bed reactor. Chapter 5 includes the main outcomes of the research work highlighting the future work.

1.5 Research outcome (publications)

I. **Ewis, D.**, Benamor, A., Ba-Abbad, M. M., Nasser, M., El-Naas, M., & Qiblawey, H. (2020). Removal of oil content from oil-water emulsions using iron oxide/bentonite nano adsorbents. *Journal of Water Process Engineering, 38,* 101583. doi:10.1016/j.jwpe.2020.101583

II. **Ewis, D.**, Ismail, N. A., Hafiz, M., Benamor, A., & Hawari, A. H. (2021). Nanoparticles functionalized ceramic membranes: Fabrication, surface modification, and performance. *Environmental Science and Pollution Research*. doi:10.1007/s11356-020-11847-0

III. **Ewis, D.,** Hameed, BH. (2021). article A review on microwave-assisted preparation of adsorbents and its application in the removal of water pollutants. Journal of Water Process Engineering, 41, 102006. doi.org/10.1016/j.jwpe.2021.102006

IV. **Ewis, D.**, Mahmud, N., Benamor, A., Ba-Abbad, M. M., Nasser, M., & El-Naas, M. (2021). Development of Novel Magnetic Bentonite Based Adsorbents combined with different Carbon Sources for Removal of Oil Content from Produced Water. *Colloids and Surfaces A: Physicochemical and Engineering Aspects. submitted.*

V. **Ewis, D.**, El-Naas, M., Ba-Abbad, M., Benamor, A. (2021). Adsorption of Organic Water Pollutants by Clay Minerals composites: A Review. *Applied Clay Science. Under preparation.*

CHAPTER 2: LITERATURE REVIEW

2.1 Produced water.

Produced Water (PW) associated with oil and gas exploration and production is one of the largest wastewater streams generated. PW consist of mainly dissolved oil and grease, polycyclic aromatic hydrocarbon (PAH), chemical additives, BTEX, organic acids, inorganic compounds, and dissolved solids (DS) [9]. Figure 1 shows the composition of PW.

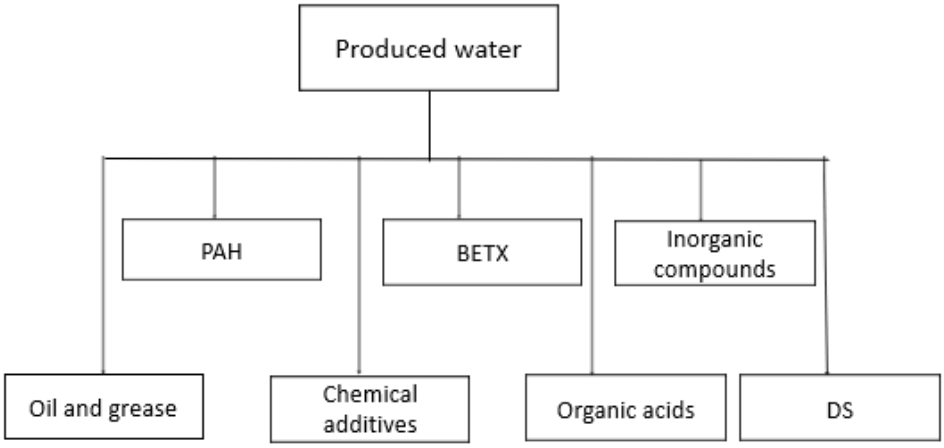

Figure 1: Constituents of produced water.

The composition of PW varies according to various factors including age and depth of geological formation, the field geographic location, type of produced hydrocarbon and the chemical composition in the oil and/or gas reservoir. Generally, the amount of DS ranges between 100 and 300,000 mg/L. The major contributor to the value of DS are mainly chloride and sodium ions, which are originally from water salinity. Inorganic compounds such as sodium, chloride, calcium, cobalt, mercury, magnesium, sulfate, carbonate, and lead are also present in PW [28, 29]. The concentration of sodium and chloride can vary from 0-150,000 mg/l and 0-270,000 mg/l, respectively. While other metals can vary from 0 to few thousands in ppm concentration [30]. The concentration of oil in PW associated with natural gas ranges between 6-60 mg/l [31].

Another study indicated that the concentration of oil in produced water ranges between 40 and 2000 mg/l [32]. Organic acids present in PW are mainly formic acid and acetic acid. The concentration of formic acid ranges from 0 up to 68 mg/l, whereas acetic acid ranges from 8 up to 5735 mg/l [33]. Moreover, BTEX are aromatic compounds that are present in oil and gas products, which can easily escape to the atmosphere due to their low boiling point. Dorea et al.[34] reported that benzene represents the highest concentration among BTEX solution with a concentration that ranges between 0.44-2.80 mg/l. Furthermore, phenols in gas-field PW presents in greater amounts compared to oil-field PW. The concentration of phenols ranges between 0.36 up to 16.8 mg/l [35, 36].Table 1 shows a typical concentration and characteistics of PW.

Table 1: Typical concentration and characteistics of PW.

Parameter	**Unit**	**Concentration**
TOC	mg/l	0-1500
COD	mg/l	0-1220
pH	-	4.3-10
TSS	mg/l	1.2-1000
Total Oil	mg/l	2-565
BTEX	mg/l	0.39-35
Sulfate	mg/l	2-1650
Ammonium	mg/l	30-300
Phenols	mg/l	9.7-600

The environmental effect of PW is catastrophic. For instance, phenols, and BTEX can

harm human causing poisoning, skin and eye irritation, cancer, inhalation injuries, kidney damage, leukemia etc., which, on a long-term exposure can lead to death [37, 38]. Furthermore, PAHs have carcinogenic properties, and cause DNA damage. Marine environments are also affected by PAHs as heavy PAHs can cause carcinogenicity and problems to fish's reproductive system [39]. Moreover, heavy metals have constituted a great concern due to their toxic effect on aquatic organisms and birds if accumulated in high concentrations [40].

During oil and gas production, PW represents around 80% of the residuals and its amount can reach up to 98% in depleted fields [41]. Moreover, the ratio of water to oil is 3:1 and this ratio may increases to reach 12:1 in some cases [42-44]. In 2009, the amount of PW generated worldwide was estimated to be more than 70 billion barrels per annum [45]. In Qatar, the amount of PW associated with gas production is estimated to be 50,508,816.54 barrels per annum [46]. The expansion of oil and gas industry and their end products wide applications are responsible for the increase in PW volume on a yearly basis and consequently increase the amount of contaminants released into waterbodies [47]. However, some studies have indicated that the main risk is the concentration of PW constituents rather than the volume of PW discharged. Therefore, it is important to manage the amount of PW released to the environment as well as ensuring that its constituents are kept within the allowable discharge limits.

PW water management could be through either minimizing its production through PW reinjection into the well or release it to the environment to be used for irrigation. However, treatment of PW prior to discharge is required.

2.2 Environmental legislation

Strict legislations have been set by the authorities for PW discharge. United States Environmental Protection Agency (USEPA) set a daily allowable discharge of oil and

grease 42 ppm. China set a monthly average limit of oil and grease discharge as well as COD of 10 ppm and 100 ppm, respectively [28, 48]. In 2000, the EU water Framework Directive (WFD) has adopted zero discharge in order to protect the marine environment. Since then, countries around the world started to adopt the zero discharge of contaminants in PW. Recently, countries started to adopt new technologies that are economically visible to reuse PW in industry or for agriculture after proper treatment [48].

2.3 Treatment technologies

PW treatment requires series of individual units due to its complex constituents that could not be eliminated in a single process. The treatment of PW includes the removal of oil, suspended solids, soluble organics, inorganic compounds, bacteria, and chemicals. For that, the treatment usually involves a combination of physical, biological, and chemical processes. PW treatment process involves three stages: pre-treatment, main treatment, and final polishing. The pre-treatment stage concerned with the removal of large oil droplets and coarse particles. The main treatment stage consists of primary and secondary steps in which small oil droplets and particles are removed. The primary step is employed through different techniques such as API separators. In the secondary step, smaller oil droplets and particles are removed using techniques such as biological treatment, membrane, and gas floatation. The polishing step is implemented to remove ultra-small particles and droplets using technologies, such as reverse osmosis, adsorption, advanced chemical oxidation, and photochemical [7, 9, 49]. In this section, insights into the polishing step technologies are discussed, highlighting the advantages and disadvantages of each one.

2.3.1 Chemical treatment technologies

2.3.1.1 Chemical advanced oxidation

Chemical Oxidation working mechanism is based on oxidizing the contaminant in wastewater stream to carbon dioxide or transfer the nature of the contaminant into other metabolite product. This process is achieved through using strong oxidizers such as Ozone (O_3), hydrogen peroxide (H_2O_2), and chloride (Cl_2) that interact with the contaminant through oxidation-reduction reactions. In addition, other techniques are used to increase the removal effect through using ultraviolet (UV) light along with a strong oxidizer [50]. Chemical oxidation is able to remove the COD, BOD, organic materials, some types of inorganic materials, color and odor from PW. The removal is achieved through the release of OH· that is able to oxidize the contaminant existing in PW. This process does not include wastes' production, can achieve high water recovery rate (~100%), has small footprint, and does not need pre-treatment process. However, it is associated with high chemical cost, regular maintenance, and production of byproducts that need to be removed [7]. Furthermore, the process is associated with high energy consumption if ozone is used as an oxidant [51].

2.3.1.2 Electrocoagulation

Electrocoagulation (EC) is a process that combines coagulation, flotation and electrochemistry. EC is comprised of an electrolytic cell with anode and cathode electrodes immersed in the wastewater. The electrodes are connected to external DC power source that apply electrical field. In the EC cell, the anode dissociates to produce metal cations when DC passes and serve as a coagulant. Whereas, on the cathodic electrode, hydrogen bubbles are evolved and OH- ions are released into the solution. Meanwhile, electrons flow freely to destabilize surface charges of the containments, which leads to the formation of large flogs that eventually precipitate [52]. Esmaeilirad et al.[53], reported that EC system was able to reduce the concentration of Calcium, Magnesium, Strontium, Barium, Boron, and TOC in produced water in a batch mode

experiment by 90%, 70%, 61.1%, 74.2%, 74%, and 64% respectively. Another study indicated that hardness and COD in PW in a pilot scale were reduced by 85.81% and 66.64%, respectively [54].

EC technology offers several advantages including elimination the production of secondary pollution and the need for chemical addition. Furthermore, the technology is simple and able to produce odorless, colorless and clear effluent [55-57]. On the other hand, this technology is limited by high operating cost, regular replacement of anode, and fluctuation of EC efficiency due to cathode passivation (precipitation of ion on the cathode surface) [55, 56].

2.3.2 Physical treatment technologies

2.3.2.1 Electrodialysis

Electrodialysis (ED) is an electromechanical separation technique that is based on using ion-exchange membranes (IEM) within an electrical filed for ion separation. This technology is able to treat sea water and wastewater including PW [58]. It has been implemented on an industrial scale 50 years ago[59]. ED system consist of IEM, power supply, ED stack and auxiliary materials, (electrodes, spacers, Gasket seal).

The ED system consists of two plates. Inside the ED system, anodic and cathodic exchange membrane exist for the separation of charged particles. In addition, series of electrodes, spacer and gasket seal. The spacer gasket is used to separate IEM and create concentrate and dilute compartments. The membranes act as a barrier to nutrient migration in which it allows the ion passage according to its electric charge. Furthermore, ED system includes two electronic devices that are responsible on converting ions current into an electrons current [58]. Figure 2 shows a schematic diagram of ED system.

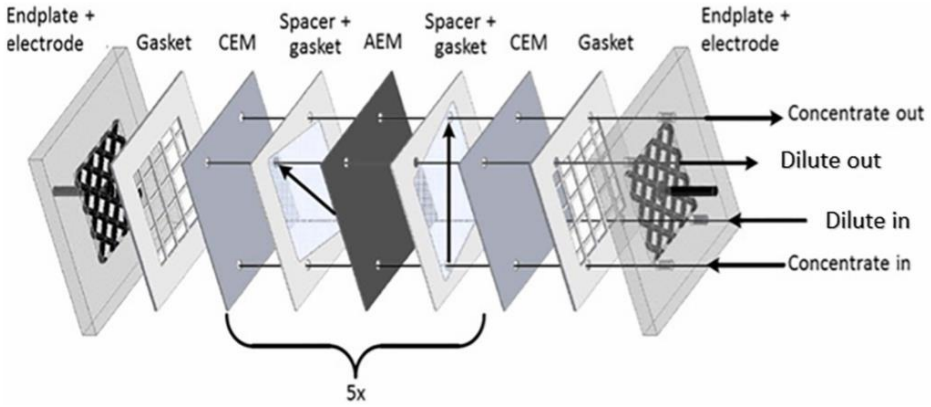

Figure 2: A schematic diagram of Electrodialysis system[60].

The concept of ED is based on applying a voltage between cathodic and anodic electrodes that is pass through IEM inside the ED cell, which causes the charged species to separate from uncharged matter [58].

ED technology is a promising for wastewater treatment including PW as it offers higher water recovery rate compared to RO, ease of operation, long membrane lifetime, flexible operating conditions, and eliminates the need for pre-treatment or post-treatment [58]. However, the high capital and operating cost that mainly from the high cost of the IEM limit their application in wastewater treatment. Furthermore, other concerns associated with ED are rapid fouling especially with saline streams, non-ionic contaminants cannot be removed, and the need for highly skilled and trained labor for maintenance and operation [61].

2.3.2.2 Membrane technology

Membrane technology is one of the most effective technologies available for desalination and wastewater treatment. Water filtration using membrane technology is characterized by several features, such as small footprint, ease of operation, low operating temperature, and high removal efficiency [13]. Membranes are classified according to their pore size into microfiltration (MF), ultrafiltration (UF), nanofilteration (NF), and reverse osmosis (RO). MF membranes attain pore size

ranging from 0.1-10 μm, which is suitable for most types of bacteria and suspended solids removal [62]. This type of membrane is used in pre-treatment stage of PW [63, 64]. UF membranes have pore size ranging between 0.01 and 0.1 μm in which it is able to remove bacteria, proteins, plastics and PW dissolved constituents [65]. NF membranes pore size ranging between 0.001 and 0.01 μm. NF membranes can provide rejection of divalent ions > 99%. Moreover, NF membranes can reject COD contaminants, oil particles, nitrate, and sulfate. However, NF membrane are not able to reject sodium and chloride ions [66]. The pore size of RO is <0.001 μm. This technology has been proved to be efficient in PW treatment as it is able to reject solutes > 99% [67]. More recently, a combination of two membrane systems has been implement by several researchers. For instance, Maltos et al.[68], reported the performance of Forward osmosis/reverse osmosis (FO/RO) for PW treatment on a pilot plant scale. The results indicated that the system reached >99% and >95% rejection of all ions and hydrocarbon, respectively.

Membrane technology is able to produce effluent with excellent quality, occupy small footprint, and does not produced secondary products (e.g. sludge). However, membrane fouling (accumulation of the particles on membrane surface), and the high capital and operating cost are a major concern [69].

2.4 Adsorption technology

Adsorption is the adhesion of a substrate in a gas or a liquid phase to the adsorbent surface's functional groups [70]. In wastewater treatment, adsorption technology is used extensively, mostly as a polishing step rather than standalone technology. The technology is based on using an adsorbent that interacts chemically or physically with the water contaminant. The adsorbent can be re-generated and utilized in the adsorption process. Compared to the above-mentioned technologies, adsorption is one of the most

economically feasible and efficient process that is widely used for wastewater treatment applications. The major advantages of adsorption technology are low capital and operating cost, high treatment efficiency, ease of operation, and low energy requirement compared to other technologies. However, the major drawback is the high cost of adsorbents, which can be eliminated by using economical, and highly efficient adsorbents [3]. For these reasons adsorption process is widely used in several wastewater treatment technologies such as, Total Oil Remediation and Recovery (TORR) [71].

2.5 Adsorbents

The selection of the suitable adsorbent is a crucial matter as it contributes to the adsorption process cost. A suitable adsorbent should have the following characteristics [72]:

(1) High removal capability for wide range of contaminants.

(2) Environmentally friendly nature.

(3) Inexpensive.

(4) Can be regenerated and used for several cycles.

(5) High stability.

In this section, the most commonly used adsorbents for PW treatment are discussed, highlighting their performance, and physiochemical properties.

2.5.1 Clay minerals.

CMs fall under Phyllosilicates family in which their structure consists of one or two silica tetrahedral sheets with alumina based octahedral sheets (plate-like structure) [73]. The tetrahedral sheets are composed of $Si_2O_6(OH)_4$ in which each unit consists of a silicon atom surrounded by four hydroxyl atoms. Whereas octahedral unit consist of Aluminum (Al), magnesium (Mg) or iron (Fe) surrounded by six oxygen or hydroxyl

atoms in an octahedral as shown in Figure 3.

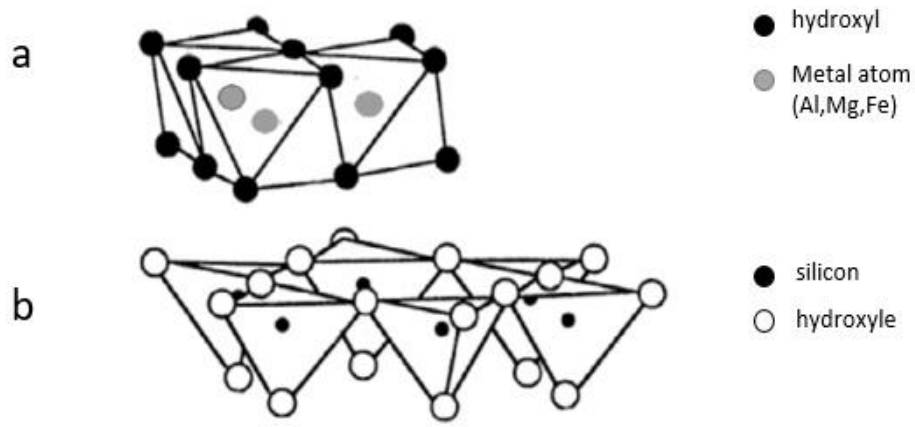

Figure 3: Crystaline structure of Clay minerals (a) Octahedral (b) Tetrahedral (re-drawn from [74]).

CMs have three surfaces: outer surface, edges and interlayer space between the layers. The outer surface and interlayer space are susceptible to alteration through two distinct processes: adsorption and ion exchange. Furthermore, CM edges may develop charge depending on the environment's pH that affects the bond of Al-O and Si-O [73].

CMs including kaolinite (1:1), montmorillonite (2:1), bentonite (2:1) as well as illite (2:1) are utilized as adsorbents [75]. They have received considerable attention due their high adsorption capability and unique physiochemical characteristics. Among clay minerals, bentonite has been reported in previous studies as an adsorbent for various types of water contaminants. Bentonite is composed of smectite clay minerals such as montmorillonite, and hectorite. The chemical composition of bentonite is $(Na)_{0.7}(Al_{3.3}Mg_{0.7})Si_8O_{20}(OH)_4.nH_2O$. Its structure consists of three layers, an aluminum based octahedral sheet that is surrounded by two tetrahedral silica sheets (Figure 4). Bentonite possess a net negative charge due to the isomorphic substitution of Al atoms by lower valence elements (Fe and Mg). Furthermore, silica atoms are prone to substitution by Al atoms, which contributes to the negative surface charge [73].

Bentonite results from the volcanic ash alteration. It attains a distinct 2D layer structure and excellent properties including ion exchange capacity, high surface area ,and charged surface and edges [76]. The interlayer space enable to trap the water contaminants within its structure, which is known as swelling capacity [77]. The charged edges, large surface area, interlayer spacing, and existence of exchangeable ions such as H+, Na^+ and Mg^+ empower bentonite with good adsorption capability. These unique characteristics increase bentonite affinity towards cationic and anionic water contaminants removal from aqueous solutions.

The main drawback of using bentonite, or clay minerals in general, in adsorption process is that they have high dispersity in aqueous solutions, which limits their ability to be separated and re-generated [19].

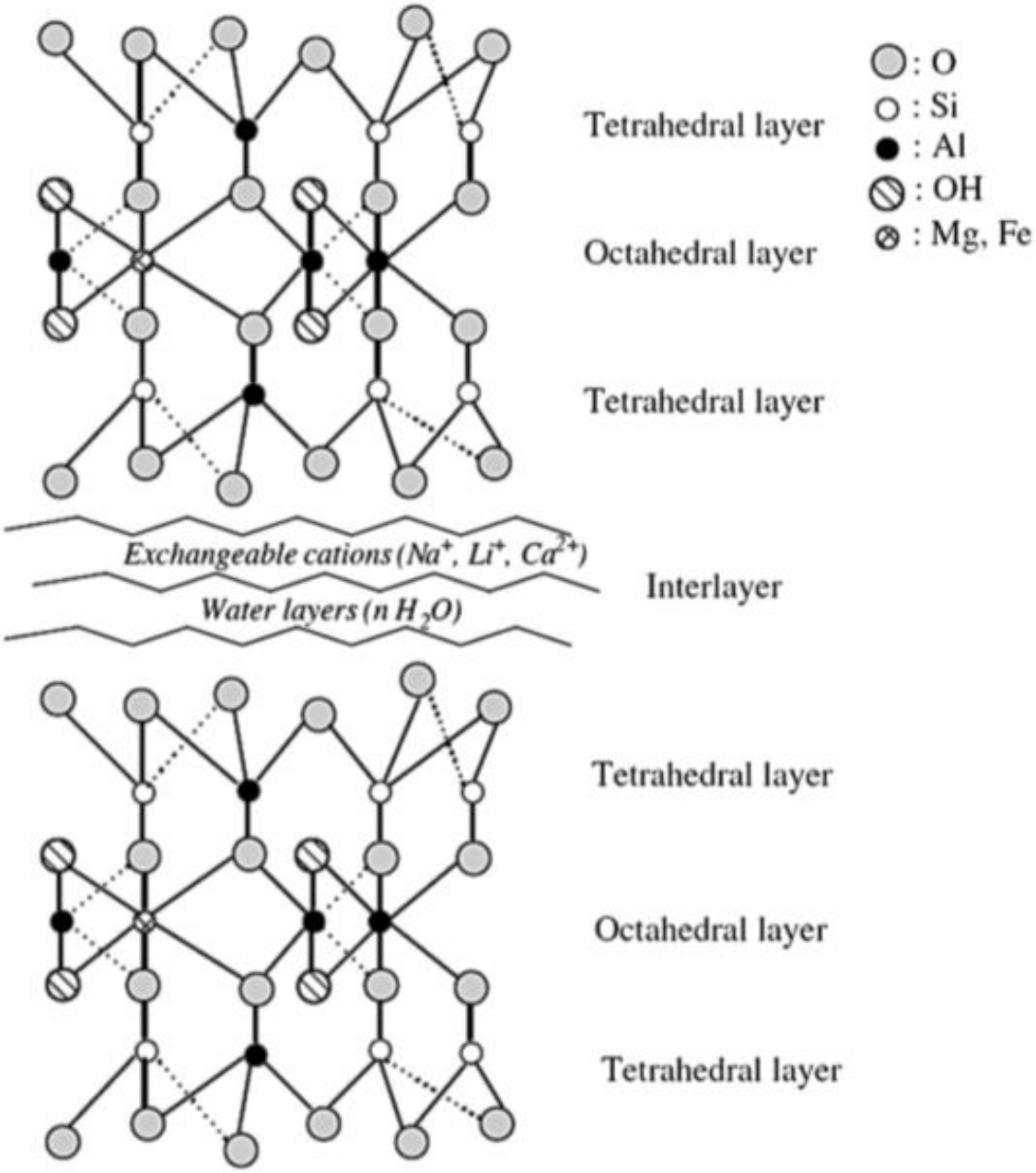

Figure 4: Bentonite structure [78].

2.5.2 Carbon-based adsorbents.

Carbon-based adsorbents including AC, ACF and other carbonaceous adsorbents, such as graphene, are widely used for water remediation applications. Carbon-based adsorbents vary in their adsorption performance due to their variation in surface area, porosity, and surface functional groups. AC is widely used as an adsorbent in water treatment applications due to its high surface area, good mechanical strength, reactive surface, and high stability [79-81]. It is produced from several precursors that results in adsorbents with different properties and adsorption efficiency depending on the nature of the precursors [82]. AC can be produced via carbonization and activation techniques [83, 84]. Carbonization involves exposing the carbonaceous substrate to high temperature in the presence of nitrogen gas. Whereby, the activation of AC is achieved by two approaches, which are physical activation using oxidative gases such as steam or carbon dioxide, or by chemical activation using chemical reagents such as potassium hydroxide, potassium carbonate, sodium hydroxide, zinc chloride, phosphoric acid etc. AC prepared via physical activation is still a challenge due to its inferior textural properties compared to AC prepared by chemical activation method, which possesses high specific surface area and pore volume [85]. In addition, applying surface modification to AC can potentially enhance its adsorptive performance towards water pollutants [86]. The main problem associated with AC is the high cost of production and regeneration [87].

ACFs are microporous materials with negligible mesoporosity, which exhibit a well-defined porous structure in fibrous form. Despite the fact that ACFs show similar properties to AC such as porosity, they exhibit several advantages over AC owing to their structure [88]. Similar to AC, ACFs are produced from different precursors such as polyacrylonitrile (PAN) [89], coal tar pitch [90], petroleum pitch [91] etc.

AC, ACF can be produced via carbonization and activation techniques. However, prior to carbonization, a pretreatment is required to improve the yield and the strength of the final product [92]. In addition, physical and chemical activation are applied to ACF. The main advantage in activation processes is the removal of disorganized carbon, which consequently is reflected on the pore distribution. Other carbonaceous adsorbents such as graphene and CNTs are widely used for wastewater treatment, especially towards organic pollutants owing to their unique structure and physiochemical properties such as high pore volume, large specific surface area, and surface hydrophobic, and π-π interaction. In addition, they contain a large number of oxygen-containing functional groups, which are mainly responsible for their high adsorption performance [93]. The main concern associated with carbon-based adsorbents is that they are not easy to be separated from aqueous solutions for re-generation. The separation process is usually implemented through sedimentation process or by filter beds [94].

2.5.3 Magnetic metals oxides

Magnetic metals oxides such as MnO_3, Co_3O_4, Fe_3O_4 and NiO_2 have been used in adsorption processes extensively. They exhibit remarkable properties including, high specific surface area, good mechanical and chemical stability, tolerated size, biocompatibility, and low toxicity. Moreover, their magnetic properties enable their separation from aqueous solution by an external magnet [95]. Magnetic metals oxides exhibit good adsorption capability towards various water contaminants. However, their performance is poor compared to other adsorbents such as AC, and CMs towards organic water contaminants [95]. Therefore, most of the adsorption studies incorporate metals oxides to other adsorbents. The main reason is to facilitate the adsorbent separation from aqueous solution by an external magnet, and enhance the adsorbent

removal capability.

2.5.4 Modified adsorbents

Adsorbent modification includes physical and chemical treatment processes are applied to enhance the adsorbent structure, functional groups, stability, and morphology [96]. Physical modification process involves the application of high temperature that ranges between 120 ℃ and 700 ℃. Whereas, chemical modification involves the use of strong chemicals, such as acids. These processes contribute to the increase in the adsorbent cost and energy requirements, which elevates the overall adsorption process cost. In addition, even after the modification process, some adsorbents such as CMs still suffer from relatively poor-medium adsorption capacity towards organic water contaminants, especially in multipollutant system [97].

2.5.5 Composites

In the last decade, the literature witnessed an increasing number of research articles related to developing composites for wastewater treatment that exhibit enhanced adsorption capacity and physiochemical properties compared to the composites' individual components. For instance, the adsorption capacity of malachite green using graphene oxide/sodium montmorillonite composite was triple the adsorption capacity of raw montmorillonite and reduced graphene oxide towards the same water containments [98-100]. Ahmed et al.[101], reported that incorporation of adsorbents results in more stable structure, high removal capability and enhanced pore properties. The performance of various types of composites in real PW treatment or oily wastewater as representative of PW concentration was reported in a limited number of studies. Fe_3O_4/Bentonite composite was studied for BOD and COD removal with initial concentration of 394 mg/L and 1875 mg/L, respectively, which are a good representative of BOD and COD content in PW [102]. The study showed that the

composite attained a removal percentage of 84.88% and 88.8% for BOD and COD respectively. In another study, El-Dib et al. [103], studied the ability of Chitosan immobilized Bentonite composite for the treatment of industrial wastewater with initial COD of 10,1791 mg/L. The study indicated that the composite was able to reduce the COD concentration by 83% and the effluent color by 78% in 3 hours. The performance of bentonite with carbonaceous adsorbent for industrial wastewater treatment was better. Liang et al. [27], used bentonite/carbon composite for the treatment of alkaline wastewater with COD value of 79,834 mg/L. The results showed that the indicated composite was able to reduce the COD concentration by maximum 91% in 2 hours. Moreover, the composite was regenerated and used for 9 cycles and showed a removal percentage > 60% in all cycles.

The physiochemical characteristics of composites might be enhanced compared to the composites' individual components. For instance Dotto et al.[104], reported that chitosan/bentonite composite attained higher mechanical strength compared to raw chitosan. In another study, cross-linked chitosan coated bentonite (CCB) attained higher thermal stability compared to raw bentonite and chitosan. In addition, CCB exhibited porous and irregular surface, whereas, chitosan seemed fibrous, regular and loose [105]. The porosity and surface area might also increase after incorporation of two adsorbents together. A study confirmed that the porous structure of cellulose-derived carbon/montmorillonite (CMt) was responsible for rapid and high adsorption capability. The composite attained specific surface area of 41.8 m^2/g, meanwhile, acid activated montmorillonite attained 39.5 m^2/g [106]. The pore size of the composite was also higher than acid activated montmorillonite. The increase in pore size could be attributed to the introduction of carbonaceous materials into the interlayer region, destroying some main basal spacing of montmorillonite and caused the formation of

new mesopores on the composite. These factors resulted in an increase in the adsorption capacity of CMt composite. Xu et al.[107], confirmed that the increase in specific surface area enhances the adsorption capacity. The study involved the fabrication of graphene oxide/bentonite (BG) composite for toluidine blue removal. The results demonstrated that increasing graphene oxide content in the composite from 1wt% to 2wt%, has increased the specific surface area from 56.8 m^2/g to 63.4 m^2/g. Consequently, the adsorption capacity of the composite was increased from 458.7 mg/g to 471.7 mg/g. Table 2 summarizes the adsorption performance of various composites towards PW organic constituents.

Table 2: The adsorption performance of various composites towards produced water organic constituents.

Adsorbent	**Pollutant**	**Experimental conditions**	**Adsorption performance**		**Ref.**
			Adsorption capacity q_m (mg/g)	**Adsorption %**	
Fe_3O_4/Bentonite	BOD (394 mg/L)	pH (7.5-8.5), Room temperature	-	84.88	[102]
	COD (1875 mg/L)	pH (5.5-6.5), Room temperature	-	88.8	
Chitosan immobilized Bentonite	Industrial wastewater (COD=10,1791 mg/L)	298 K, pH=4.76	-	83	[103]
Lignin xanthateresin–bentonite	Doxycycline hydrochloride	298 K, initial concentration (0-600 mg/L),	438.75	-	[108]
montmorilonite/ poly (vinyl alcohol)/sodium dodecyl sulfate aerogel	Dodecane oil	-	23.6 (g/g)	-	[109]
	Motor oil		25.84 (g/g)	-	
Bentonite/carbon	alkaline water (COD=79,834 mg/L)	pH= 13.4, temperature 298 K	-	91	[27]

Adsorbent	Pollutant	Experimental conditions	Adsorption performance		Ref.
			Adsorption capacity q_m (mg/g)	Adsorption %	
Octadecyl trimethyl ammonium-Bentonite/Alginate beads	2,4-dichlorophenol	Temperature 297 K, pH= 6.4	392	-	[110]
Hexadecyl trimethyl ammonium-Bentonite/Alginate beads			185		
sulfur-doped titanium dioxide hollow spheres loaded on magnetic bentonite	bisphenol A	Room temperature	77.36	-	[111]
Magnetic molecularly polymers (MMIPs) based on kaolinite/Fe_3O_4	bisphenol A	Temperature 318 K	113.6	-	[112]
magnetic non-imprinted polymers based on kaolinite/Fe_3O_4		Temperature 298 K	112.4		

Adsorbent	Pollutant	Experimental conditions	Adsorption performance		Ref.
			Adsorption capacity q_m (mg/g)	Adsorption %	
Montmorillonite/alginate gel	polychlorinated biphenyl	Temperature 298 K	-	93	[113]

2.6 Adsorbents synthesis methods

The extensive use of adsorption technology in wastewater treatment and the essential need for low cost, effective, and non-toxic adsorbents with specific physiochemical characteristics caused rapid development of several synthesis techniques including co-precipitation, hydrothermal, solvothermal, ultrasound, and microwave-assisted (MW) method. These methods result in adsorbents with different morphology, surface characteristics, physiochemical properties as well as different adsorption behavior. This section highlights the most commonly used adsorbents synthesis techniques.

2.6.1 Co-precipitation

Chemical co-precipitation is the most common used method for adsorbents' synthesis. In this method, the precursors are reduced using reducing agents such as ammonia, and sodium hydroxide. The reducing agent's pH has a strong influence on the final adsorbent properties, structure, and adsorbent size. In addition, the adsorbent size can be controlled by temperature and ionic strength [114]. During adsorbent synthesis using co-precipitation method, the adsorbent particles might be agglomerated, especially for magnetic metal oxides nanoparticles. The agglomeration of nanoparticles reduces the uptake capability of the adsorbent and thus limits their utilization in the adsorption process. Therefore, co-precipitation is recently combined with ultrasound synthesis method to reduce the agglomeration of the nanoparticles over a support layer [102].

2.6.2 Hydrothermal

Hydrothermal fabrication technique was developed in the 19^{th} century. In this method, the precursors are placed inside a rector under high temperature and pressure for several hours. This

method is based on the reaction of the precursor mixture in the vapor phase with a solid material, which eventually leads to the deposition of small particles. The adsorbents fabricated through this method are smaller than those produced by co-precipitation method [114]. Furthermore, nanocrystals with high crystallinity are produced through this method with the desired size and shape [115]. However, the major disadvantages of this method is that the synthesis process is difficult to control and the limitation of reliability and reproducibility [116].

2.6.3 Solvothermal

The method is based on the preparation of nanomaterials in presence of water or other organic solvent. The reaction occurs in a pressure vessel in which the solvent is heated above its boiling point. The major advantage of this method is the preparation of high quality crystallized nanocrystals with high degree of crystallization [117].

2.6.4 Microwave-assisted

MWs are an electromagnetic radiation that have a wavelength ranging between 1 mm and 1 m and frequency between 300 MHz to 300 GHz. In industrial applications, the most common used frequencies for heating purposes are 915 MHz ,2.45 GHz, 5.8 GHz, and 22.125 GHz [118]. MW technology has been used in material science and processing including powder synthesis and polymers synthesis [119-121]. In particular, MW technology as a heating source has been used in adsorbents synthesis instead of conventional heating due to: (i) low energy consumption and processing time (ii) rapid and simple irradiation process (iii) uniform temperature throughout the material (iv) enhanced diffusion process [122]. In addition, MW energy reduces the risk of overheating that subsequently leads to the material combustion (e.g. AC) [123]. A schematic diagram of microwave heating system is shown in Figure 5.

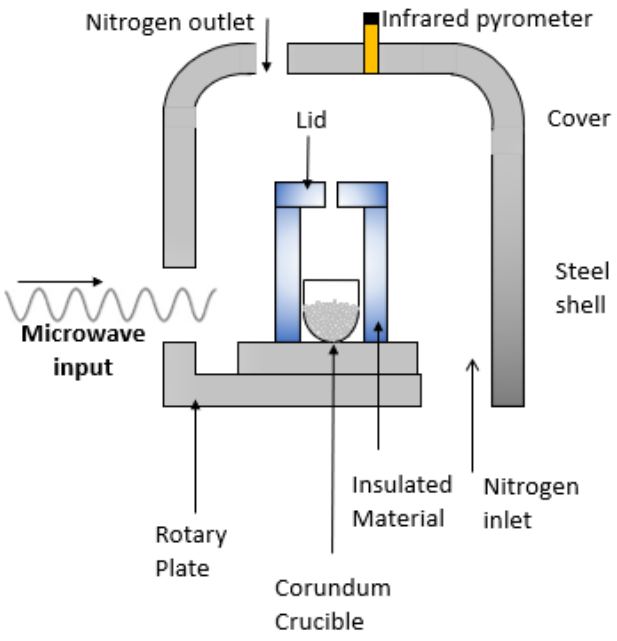

Figure 5: Schematic diagram of Microwave system(re-drawn from [124]).

In conventional heating technique, the material surface is heated first followed by the transfer of heat inwards. This occurs by heat transfer between objects by conduction, convection, and radiation. Whereas, in MW heating, the material couples with MW and absorbs the electromagnetic energy volumetrically. Then, energy is transformed into heat within the material and then transfers outwards as shown in Figure 6. As a result, the morphology and the physicochemical properties of the adsorbent are enhanced significantly compared to adsorbents prepared by conventional heating techniques [125-127].

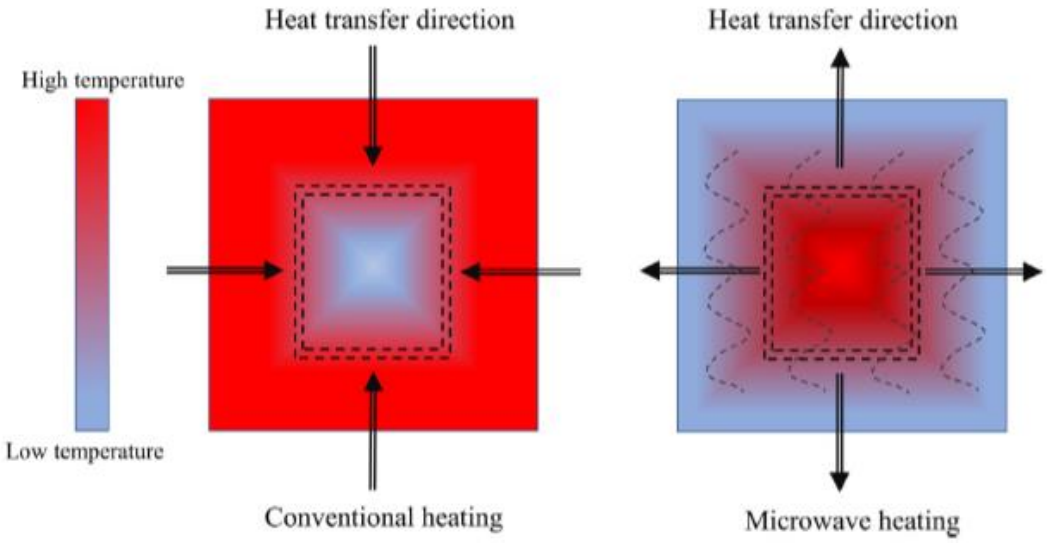

Figure 6: Heat flow in direction in Microwave and conventional heating systems [128].

The MW heating system consists of four basic components as shown in Figure 7, which are: power supply, magnetron, applicator and waveguide [118]. In this system, the material is placed in a metal applicator that varies according to the process specification and heated by MW energy that is directed by the waveguide. During the heating process, the material is moved through the oven by an insulated conveyor belt for better energy distribution [128].

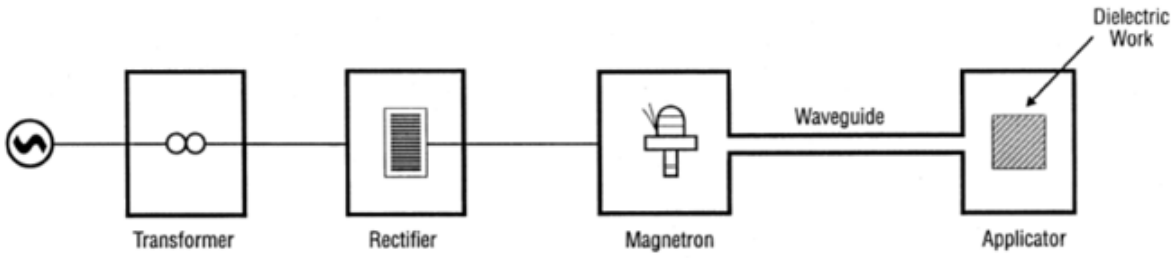

Figure 7: Microwave heating system [118].

The literature shows a lack of studies related to PW treatment using microwave-synthesized adsorbents. Nevertheless, extensive number of studies utilized microwave synthesized adsorbents for organic pollutants removal. Several authors studied the use of MW irradiation as an alternative

energy source for polymer-based adsorbents synthesis. Masinga et al. [129], compared the morphology and the adsorptive behavior of B-cyclodextrin/N-doped carbon nanotube polyurethane nanocomposite(N-CNTs/b-CD) synthesized by conventional and microwave heating techniques. It was found that the MW preparation of N-CNTs/b-CD reduced the synthesis time compared to conventional method from 24 hr to 10 minutes. A visual observation reveals that N-CNTs/b-CD synthesized using MW was soft and powdery. Whereas N-CNTs/b-CD composite prepared using conventional heating technique was in granular form and attained a coarse-like structure. In addition, the MW synthesized composite was less densely packed and had high surface area compared to conventionally prepared composites, which allowed more pollutant to be trapped. The adsorption experiment using both composites showed that MW synthesized composite had higher removal capability of nitrophenol even at ng/L pollutant concentration. Thermogravimetric analysis (TGA) revealed that MW synthesized N-CNTs/b-CD composite attained a slight shift in the decomposition. However, due to the use of low temperature in water purification, it is not expected to be an issue. Furthermore, the FTIR analysis showed that both composites showed identical surface functional group. These results indicate that MW irradiation does not affect the polymer's surface functional group, but it did affect the surface morphology and the adsorbent adsorptive capability. MW provides uniform heat distribution that might cause an enhancement in pore structure, surface properties and adsorbent stability. However, the microwave irritation time and power should be optimized to avoid collapse in the adsorbent morphology. In addition, the setup area should be secured, and proper safety measurements should be considered to avoid human body exposure to microwaves as they can damage the body tissues. Consequently, these drawbacks limit the application of MW technology in adsorbents synthesis. Table 3 summarizes the advantages and disadvantages of using MW in adsorbents preparation.

Table 3: The advantages and disadvantages of using microwave heating in absorbents preparation.

Advantages	Disadvantages	Ref.
• Results in more homogeneous, even, and highly porous structure.	• Might cause the absence of some functional groups.	[130-132]
• Homogenous distribution of nanoparticles over a support surface. • Decrees in thermal energy required for adsorbent synthesis	• Might cause a collapse in the carbonaceous material pore structure at high microwave power due to carbon calcination, which decreases the adsorbent pore volume.	[133-135]
• Prevent the aggregation of reduced graphene oxide sheets. • Results in polymeric adsorbents with less densely packed structure. • Might Increase the material purity. • Minimize the synthesis time to few minutes. • Minimize defects in polymeric adsorbents integrity.	• Microwave heating power and irritation time should be optimized to avoid a collapse in the adsorbent morphology and structure. • The setup area should be secured, and proper safety measurements should be considered to avoid human body exposure to microwaves as it can damage the body tissues.	[136, 137]
• No major changes in the adsorbent morphology after several regeneration cycles. • Might increase the adsorbent specific surface area. • Increase the adsorbent removal capability. • Enhances the reaction rate and the degree of functionalization.	-	[129, 138-141]

2.7 Adsorption isotherms

The relation between the equilibrium contaminant concentration in aqueous media and the equilibrium adsorption amount on the solid phase at constant temperature and pH is referred as isotherm. Generally, adsorption isotherm models, which are mathematical models that are based on certain assumptions, provide insights into the process of a substance release from aqueous media to a solid phase. From these models, adsorption information including the adsorption mechanism, adsorption capacity, degree of affinity of the adsorbents, and the adsorbent surface properties can be obtained [142, 143].

Several adsorption isotherm models were proposed over the years using three fundamental approaches: kinetics in which the rate of adsorption and desorption are equal, thermodynamics, and potential theory. The main difference between the isotherm models is the derivation in more than one approach, which leads to difference physical interpretation of isotherm model parameters [143]. The most commonly used adsorption models for the removal of PW organic constituents are described below.

2.7.1 Langmuir model

Langmuir model was initially developed to describe the adsorption of gaseous components onto activated carbon (solid phase). Later, it was extended to describe the relation between liquid phase and solid phase at equilibrium. The model assumes a monolayer adsorption in which the adsorption can only occur on a fixed number of sites that are identical and equivalent. In addition, the model assumes that each molecule of adsorbate possess constant enthalpy and adsorption activation energy [144]. Langmuir mathematical model is described by Equation 1.

$$Q_e = \frac{q_m K_L C_e}{(1+K_L C_e)} \quad 1$$

Where, K_L (L/mg) and q_m (mg/g) represent the Langmuir constant, and the maximum

adsorption capacity, respectively.

One of the most important features of Langmuir isotherm is a constant called separation factor, which is expressed as follows [145]:

$$R_L = \frac{1}{1+K_L C_0} \quad (2)$$

The separation factor (R_L) indicates the type of the adsorption according to the RL value compared to 1 in which: (1) Unfavorable when $R_L>1$, (2) Linear when $R_L=1$, (3) favorable when $0 < R_L <1$, (3) Irreversible when $R_L=0$.

2.7.2 Freundlich model

Freundlich isotherm model assumes the adsorbent surface is heterogeneous. The major problem associated with this model is the lack of thermodynamic fundamentals as it does not reduce to Henry's law at low concentration. The model can be represented by Equation 3:

$$Q_e = K_f . C_e^{1/n} \quad (3)$$

Where, n is the Freundlich empirical constant and it indicates the adsorption efficiency. K_f $(mg.g^{-1})(L.mg^{-1})^{1/n}$ is associated with the adsorption capacity.

2.7.3 Sips model

Sips isotherm model is a combination of Langmuir and Freundlich model that is applied for describing the adsorption on a heterogeneous adsorbent surface and eliminate the restriction of limited adsorbate concentration range implied by Freundlich mode. At low concentration range, the model reduces to Freundlich model; while at higher concentrations, sips model predicts Langmuir monolayer adsorption. The model is described by Equation 4.

$$Q_e = \frac{q_m b C_e^{1/n}}{1+b{C_e}^{1/n}} \quad (4)$$

Where b (L/mg) is related to energy of adsorption and n is sips isotherm constants.

2.8 Adsorption kinetics

Adsorption kinetics are vital in determining the rate at which the contaminant is removed from a solution by the adsorbent at constant temperature. In addition, adsorption kinetic models (e.g. intra-particle diffusion model) can identify the adsorption-controlling step. The most commonly used kinetics models are pseudo-first-order (PFO), pseudo-second-order (PSO) and intra-particle diffusion model.

2.8.1 Pseudo first order

PFO model assumes that the adsorption rate is proportional to the number of available sites. This model is described by Equation 5 in linear form,

$$Ln(q_e - q_t) = \ln(q_e) - k_1 t \quad (5)$$

Where qt (mg/g) corresponds to the adsorption capacity at time t and k_1 (min^{-1}) is the first order rate constant.

2.8.2 Pseudo second order

PSO model is based on the adsorption equilibrium capacity and it is described by Equation 6.

$$\frac{t}{q_t} = \frac{1}{{k_2}^2 q_e} + \frac{t}{q_e} \quad (6)$$

Where, k_2 (g/mg.min) is the second-order rate constant.

2.8.3 Intraparticle diffusion model

Intraparticle diffusion model is an important model as it indicates the rate controlling step during the adsorption process. The model can be expressed using the following equation:

$$q_t = k_i\sqrt{t} + C \quad (7)$$

Where, ki (mg/g $min^{0.5}$) is the rate constant and C (mg/g) is the intercept.

2.9 Akaike Information Criterion

AIC method compares between different models and identify the best model that fits

the experimental data. The best model attains the lowest AIC value and it is expressed as [146, 147]:

$$AIC = 2p + N \ln\left(\frac{SSE}{N}\right) \quad 8$$

Where p and N are the degree of freedom and sample size, respectively. Small sample size (N/P<40) implies the use of second-order AIC (AIC_c), which is defined as [147]:

$$AIC_c = AIC + \left[\frac{2p(p+1)}{N-p-1}\right] \quad 9$$

The model that attains the most statistical confidence is the one that has the highest value of information criterion weight (w_i) and it is defined as [147]:

$$w_i = \frac{\exp\left(-\frac{1}{2}\Delta AIC_{c(i)}\right)}{\sum_{i=r}^{R} \exp\left(-\frac{1}{2}\Delta AIC_{c(i)}\right)} \quad 10$$

Where ΔAIC_c is the difference between the information criterion value of i model relative to the best candidate model and it is expressed as:

$$\Delta AIC_c = \Delta AIC_{c(i)} - \Delta AIC_{c(\min)} \quad 11$$

2.10 Performance in fluidized bed reactor

Fluidized bed reactor (FBR) is used extensively in wastewater treatment, especially in advanced oxidation and biological processes. The working mechanism of FBR involves the suspension of particles in a fluid (liquid phase medium). This is achieved by passing the fluid with a superficial velocity that is enough to suspend the particles. This process facilitates uniform temperature distribution, good mixing, and high mass transfer rate. Besides, FBR operating cost is relatively low, which caused FBR to become one of the most important reactor systems in chemical and biological applications [148, 149].

Adsorption is conducted in a batch, and/or fixed bed column [150, 151]. However, problems such as non-uniform temperature distribution, dead zones in which the contact between adsorbent and the adsorbate is eliminated, clogging are encountered. These drawbacks are eliminated in FBR, which caused growing interest on the

application of FBR in adsorption. Zhou et al.[152], studied the removal of phenol using SiO_2/AC composite in a fluidized bed integrated with flocculation system. The results showed the adsorption in fluidization regime was higher than fixed bed regime at low hydraulic retention time (HRT) (below 50 minutes). In addition to HRT, the adsorption depends on initial solution concentration, gas and liquid velocity, fluidized bed particle size, as well as the column specification, such as internal diameter [152-154]. The performance of adsorbents in PW consistent removal is presented in Table 4.

Table 4: Perfomance of fluidized bed reactor in organic polluants removal by adsorption.

Adsorbent	**Pollutant**	**Operational condition**	**Removal %**	**Ref.**
SiO_2/AC	Phenol	U_L= 4-8 mm/s *HRT*= 7 s	80%	[152]
AC	Phenol	U_g=0.0219 m/s	95 %	[155]
AC	Phenol	Q= 0.15-0.35 dm^3/min U_{mf} = 0.0085 m/s	62 %	[156]
Formulated clay-lime	Congo red	Q_a= 1 L/min	99%	[157]

Q: liquid flow rate, U_L: liquid superficial velocity. *HRT* hydraulic retention time, U_g: gas superficial velocity, U_{mf}: minimum fluidization velocity, Q_a: air flow rate

CHAPTER 3: MATERIALS AND METHODS

3.1 Materials and chemicals

Ferric chloride ($FeCl_3.6H_2O$) (99%, purity), graphite powder (C) (99%, purity), sodium nitrate ($NaNO_3$) (99.5%, purity), potassium permanganate ($KMnO_4$) (99%, purity), hydrogen peroxide (H_2O_2) (30%, purity), hydrochloric acid (HCl) (35-38%, purity), sulfuric acid (H_2SO_4) (98%, purity), ferrous chloride ($FeCl_2.4H_2O$) (99%, purity), and ammonia 25% (NH_4OH) were supported from Research-Lab, India. Diesel oil was purchased from Local petrol station in Doha, Qatar. MWCNTs were obtained from NanoKarbon Co., Ltd,Korea. ethyle-enediamine-tetrakis-tetrol (≈100%, purity) (non-ionic surfactant) and raw-Bentonite were purchased from Sigma-Aldrich.

3.2 Adsorbents preparation

3.2.1 Synthesis of iron oxide nanoparticles

Fe_3O_4 NPs were synthesized using the conventional Co-precipitation method as described by N.Balaji et al. [158]. Briefly, 1.72 g of ferric chloride ($FeCl_2.4H_2O$) and 4.72 g of ferrous chloride ($FeCl_3.6H_2O$) was dissolved in 80 ml of distilled water under nitrogen environment. After that, 10 ml of ammonia (25%) were added to the final solution and stirred for 1 hr under nitrogen environment at 80 ℃. Finally, the magnetic nanoparticles were dried in a Vacuum oven.

3.2.2 Synthesis of graphene oxide

Graphene oxide was prepared using modified Hammers method [159, 160]. In brief, 5 grams of graphite and 2.5 grams of $NaNO_3$ was dissolved in 115 mL H_2SO_4 and the mixture was stirred for two hours at room temperature. After that, 20 g of $KMnO_4$ was added to the solution in an ice bath to maintain the overall temperature at 15 ℃. The mixture was left under stirring for 2 more hours during which the color of the solution gradually turned from black to greenish black. Then, the temperature of mixture was

raised to 35 ℃ and stirred for an additional hour. Afterwards, 230 mL of distilled water was slowly added to the solution under continuous mixing while maintaining the temperature was maintained at 90 ℃. Finally, the solution was diluted with 250 mL, followed by the addition of 10 mL of 30% H_2O_2 that caused the solution color to turn into yellow. The product was then washed with 5% HCl to removed imputers, and left overnight to settle down. Finally, the product was washed several times till the pH reaches near neutral, centrifuged and freeze-dried to obtain graphene oxide powder.

3.2.3 Synthesis of iron oxide/Bentonite composite

Fe_3O_4/Bentonite was prepared using ultrasound assisted co-precipitation method, following the procedures with adjustments reported by Khatamian et al. [161]. Briefly, solution A was prepared by dissolving 2.5 grams of ferrous chloride ($FeCl_2.4H_2O$) and 1.5 grams of ferrous chloride ($FeCl_3.6H_2O$) in 100 ml of distilled water under continuous stirring in a Nitrogen environment. Solution B was prepared by dispersing 2 g of raw bentonite in 15 ml of ammonia (25%) at a temperature of 50 ℃. Generally, Ammonia and sodium hydroxide (NaOH) are used as reducing agents in co-precipitation. However, Ammonia is preferred as it is a better stabilizer than sodium hydroxide (NaOH) and help in the growth of nanoparticle unlike NaOH [162].Then solution A was added gradually to solution B and left under continuous stirring for 1 hr. The obtained mixture was moved to an ultrasonic bath for 3h. The synthesized composite material was separated using a magnet and washed with distilled water and ethanol. This process was repeated 3-5 times. Finally, the magnetic nanocomposite placed in a vacuum oven to dry.

3.2.4 Synthesis iron oxide/bentonite/reduced graphene oxide

Fe_3O_4/Bent/rGO was fabricated using co-precipitation method. Solution I was prepared by dissolving 2.5 g of ($FeCl_2.4H_2O$), and 1.5 g of ($FeCl_3.6H_2O$) in 100 ml of distilled

water, under stirring at 60 ℃. Solution II was prepared by dispersing 0.2 grams and 0.1 grams of GO and bentonite, respectively, in 100 ml distilled water for 30 minutes at 50 ℃ by the application of ultrasound. Then, solution II was added to solution I under stirring. The temperature of the solution was raised up to 80 ℃. Then, 20 ml of ammonia (25%) was added to the mixture. The mixture was left for 3 hours for the reaction to occur and the final product was separated by a magnet and washed several times with distilled water and ethanol. Finally, the obtained nanocomposite was dried in a under vacuum at 70 ℃.

3.2.5 Synthesis of iron oxide/bentonite/multiwall carbon nanotubes

Similar to Fe_3O_4/Bent/RG, Fe_3O_4/Bent/MWCNTs was fabricated using the same procedure expect dispersing commercial MWCNTs instead of GO in solution II.

3.1 Adsorbents characterization

The surface morphology was visualized via Scanning Electron Microscopy (SEM) (Nova Nano SEM 450, USA) coupled with an energy-dispersive spectrometer (EDS) to reveal the surface elemental composition. The morphology within the composite was observed using transmission electron microscope (TEM) (TECNAI G2 TEM, TF20). The surface functional group before and after oil adsorption was detected by Fourier Transform Infrared Spectroscopy (FTIR) using Perkin Elmer spectrum one analyzer. The structure of the crystalline material was detected by X-ray diffraction (XRD) patterns using Rigaku MiniFlex-600 ° instrument. The composites thermal stability was tested using Thermogravimetric analysis TGA Q500 TA instrument (USA). The samples were heated from 30℃ to 850℃ at a heating rate of 10 ℃/min. The BET surface area and pore volume were conducted using Brunauer Emmett Teller (BET, Micromeritics, Tristar II series).

3.2 Synthesis of produced water

Water-in-oil emulsion solution was prepared by mixing deionized water with a surfactant followed by adding diesel oil droplets. The solution was homogenized for 20 minutes at temperature of 296 K. The concentration of oil was varied from 20 to 160 mg/L [163]. The ratio of oil droplets and surfactant were adjusted to obtain the intended concentration.

3.3 Adsorption experiments

The adsorption experiments were conducted by varying adsorbent dosage, solution pH, oil initial concertation and contact time at 200 rpm rotational speed, temperature of 303 K. After experiment completion, the adsorbents were separated by external magnet and samples were analyzed using *Shimadzu TOC* 5000 *analyzer*. All experiments were conducted in triplicate form for data accuracy. Figure 8 shows the experimental procedure.

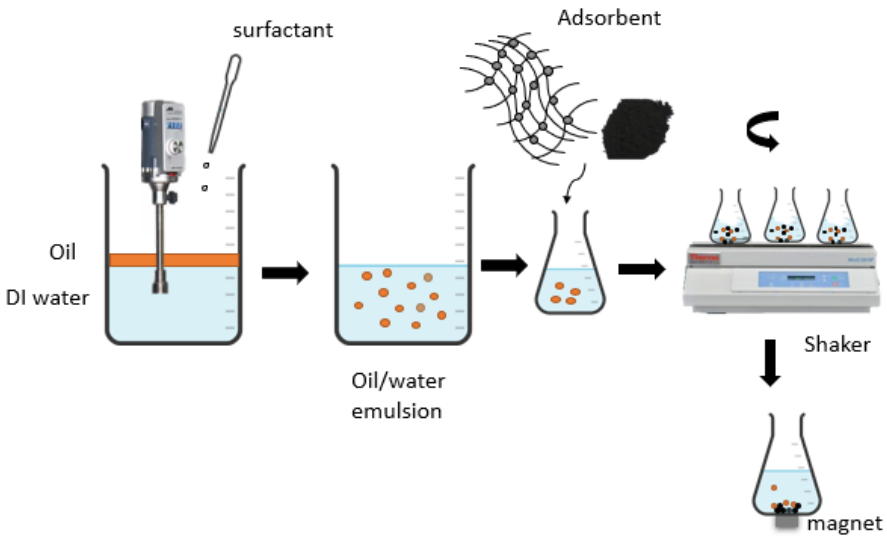

Figure 8: The adsorption experiment procedure.

The adsorbent adsorption capacity in mg oil/g composite was calculated using Equation 12:

$$Q_e = \frac{C_o - C_e}{m} V \quad (12)$$

Where, C_0 is the initial concentration (mg/L) and C_e is the equilibrium concentration (mg/L). m is the mass of the nanocomposite (grams), and V is the water-in-oil solution volume (L).

The removal efficiency was evaluated using Equation 13.

$$Removal\ efficiency\ \% = \frac{C_o - C_e}{C_o} x100 \quad (13)$$

3.4 Fluidized bed experiments

A laboratory scale fluidized bed made of Pyrex column with internal diameter of 25 mm and height of 202 mm was used. The fluidized bed was equipped with porous gas distributor plate that is connected to an air pump from the bottom of the column. The column was operating at atmospheric pressure and room temperature (297 K) in a batch mode experiment (without regeneration column). The experimental was conducted under pH 6.5, air flow 24 L/min for 180 minutes. Figure 9 shows the fluidized bed structure used.

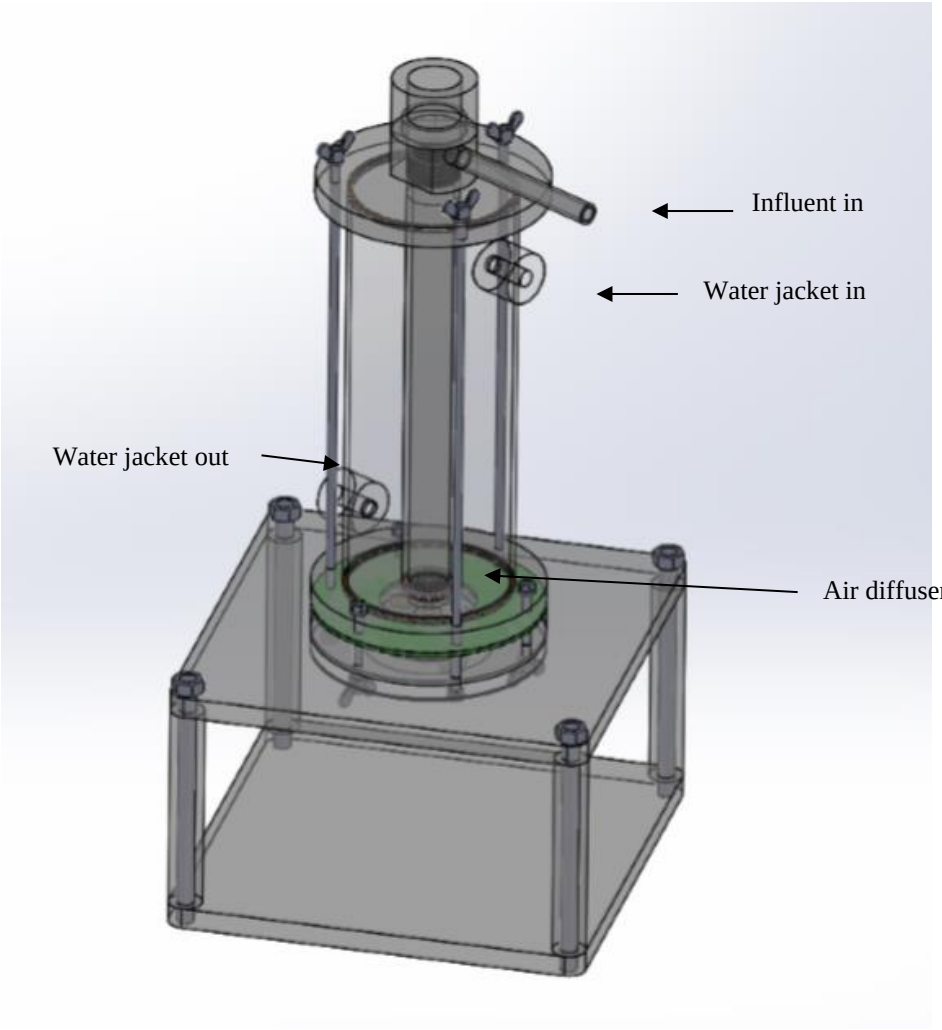

Figure 9: Fluidized bed setup.

CHAPTER 4: RESULTS AND DISCUSSION

4.1 Characterization

4.1.1 X-ray diffraction

The XRD pattern for Fe_3O_4 NPs, raw bentonite, Fe_3O_4/Bentonite, Fe_3O_4/Bent/rGO and Fe_3O_4/Bent/MWCNTs are presented in Figure 10. For raw bentonite, montmorillonite is the main phase exist with characteristic peaks 2θ = 7.26°, 19.75° ,21.87°, 29°, 35°,55°, and 62.9°. In addition, other phases including Plagioclase, Quartz, Gypsum, Kaolinite and Illite present as impurities [102, 164]. The absorption peaks of Fe_3O_4 NPs are in 2θ = 30.24°, 35.62° ,43.26°, 53.56°, 57.12°, and 62.78°. These values correspond to (220), (311), (311), (400), (422), (511) and (440) planes. The observed XRD pattern indicate that Fe_3O_4 NPs possess face-centered cubic lattice (fcc) crystal structure [165]. After loading Fe_3O_4 NPs onto the surface Bentonite, XRD patterns show only peaks of Fe_3O_4 nanoparticles (30.24°, 35.62°, 43.26°, 53.56°, 57.12°and 62.78°) with no other peaks which confirms that Fe_3O_4 NPs cover the entire Bentonite surface. For Fe_3O_4/Bent/rGO, the XRD pattern shows obvious peaks at 2θ= 7.26°, 19.75°, and 21.87°, which are for bentonite; while, the absorption peaks at 2θ= 30.24°, 35.62°, 43.3°, 53.56°, 57.5° and 62.9° are for Fe_3O_4 NPs. The absorption peak at 2θ= 26.25° corresponds to the presence of reduced graphene oxide [166]. These results affirm the successful synthesis of Fe_3O_4/Bent/rGO composite. For Fe_3O_4/Bent/MWCNTs, the XRD pattern shows peaks similar to Fe_3O_4/Bent/rGO that correspond to the existence of Fe_3O_4 NPs and bentonite, but with less intensities. The peaks observed at 2θ= 28.8° indicate the presence of MWCNTS [167]. The slight spikes of Fe_3O_4/Bent/rGO sample are observed due to the agglomeration of many Fe_3O_4 particles on the surface of rGO, which caused a growth on these particles. However, few smaller particles of Fe_3O_4 with less agglomeration attached on MWCNTs surface, which had no effect on their overall

size observed in TEM and EDX analysis. Overall, the lattice strain was one of the major factor affecting nanoparticle synthesis and crystal growth [168].

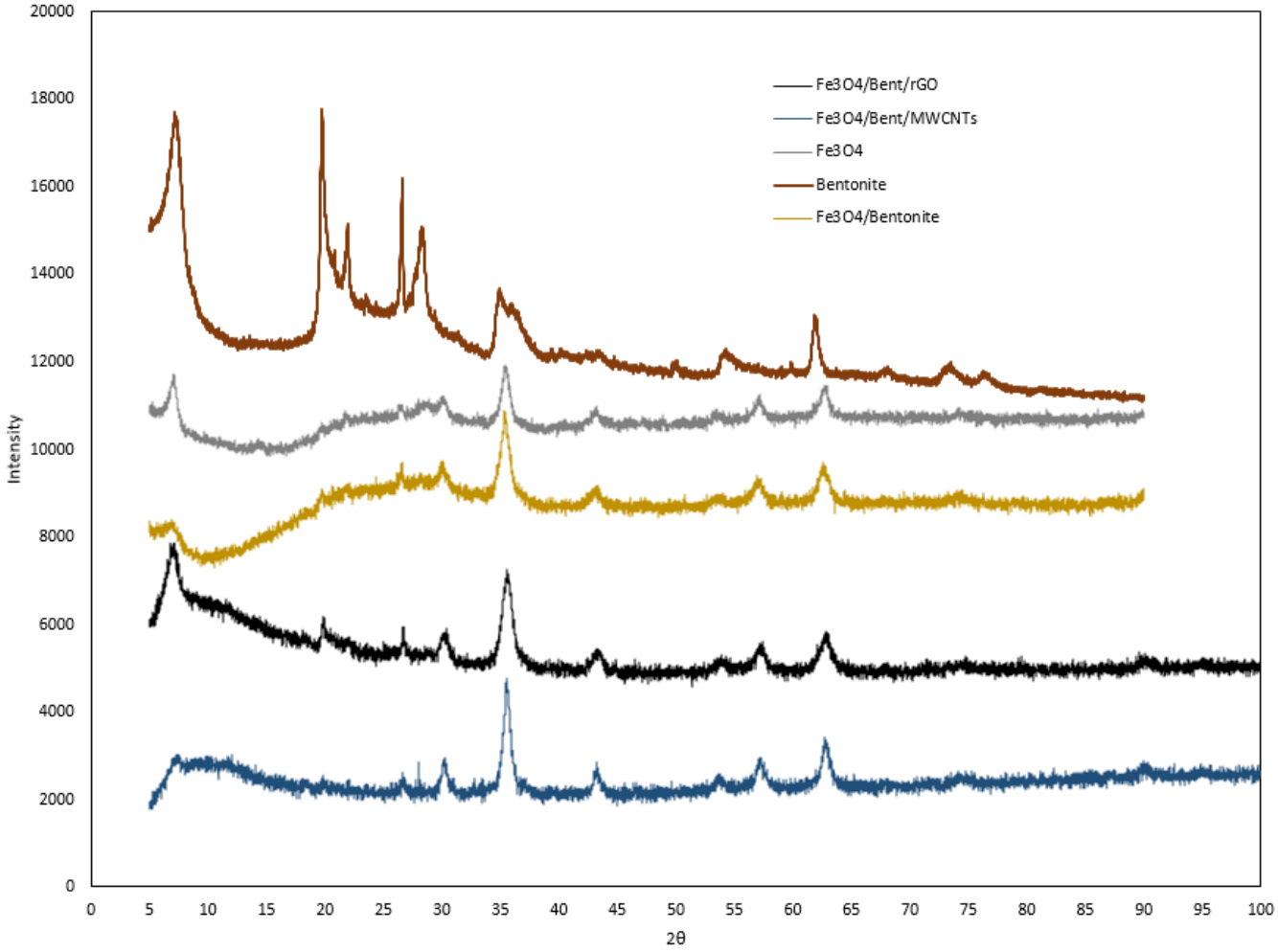

Figure 10: XRD pattern for Fe_3O_4, raw bentonite, Fe_3O_4/Bentonite, Fe_3O_4/Bent/rGO, and Fe_3O_4/Bent/MWCNTs.

4.1.2 Thermogravimetric analysis

The thermal stability of all composites was performed using TGA. As shown in Figure 11, the thermogram of Fe_3O_4/Bent/rGO showed a continuous decrease in the weight loss (19%) over temperature range 30℃-770℃ followed by slightly constant thermal stability. This could be attributed to the dehydration and the removal of oxygen present on rGO surface at temperature below 200 ℃. Above 200 ℃, the weight loss is attributed to the gasification of carbonadoes materials as a result of rGO oxidation and the transformation of Fe_3O_4 to Fe_2O_3 and $Fe(OH)_3$. The sudden decrease in weight loss at 435 ℃ might be due to the degradation of carbon material intercalated with bentonite [169]. The thermogram of Fe_3O_4/Bent/MWCNTs displayed a dehydration weight loss (7%) in temperature range 30℃-100 ℃ followed by a slightly constant thermal stability up to 600 ℃. Finally, a gradual weight loss (2%) continued up to 850 ℃, which could be due to the transformation of Fe_3O_4 to Fe_2O_3 and $Fe(OH)_3$. For Fe_3O_4/Bentonite, the composite attained showed continuous decrease in weight loss (~12%) up to temperature of 700 ℃, which could be due to the transformation of Fe_3O_4 to Fe_2O_3 and $Fe(OH)_3$. After that, the composite attained constant thermal stability up to temperature of 850 ℃. Overall, Fe_3O_4/Bent/rGO showed a better thermal stability over temperature range 30℃-250 ℃ [170]. From these results, it can be concluded that the combination of Fe_3O_4 NPs and MWCNT lead to positive synergism causing the composite (Fe_3O_4/Bent/MWCNTs) to exhibit higher temperature stability compared to Fe_3O_4/Bent/rGO and Fe_3O_4/Bentonite [171]. This is confirmed by the Fe amount presents in EDX analysis and Fe_3O_4 NPs shown in TEM images indicating the presence of less amount of Fe_3O_4 NPs on Fe_3O_4/Bent/MWCNTs composite, causing it to exhibit better thermal stability at higher temperatures.

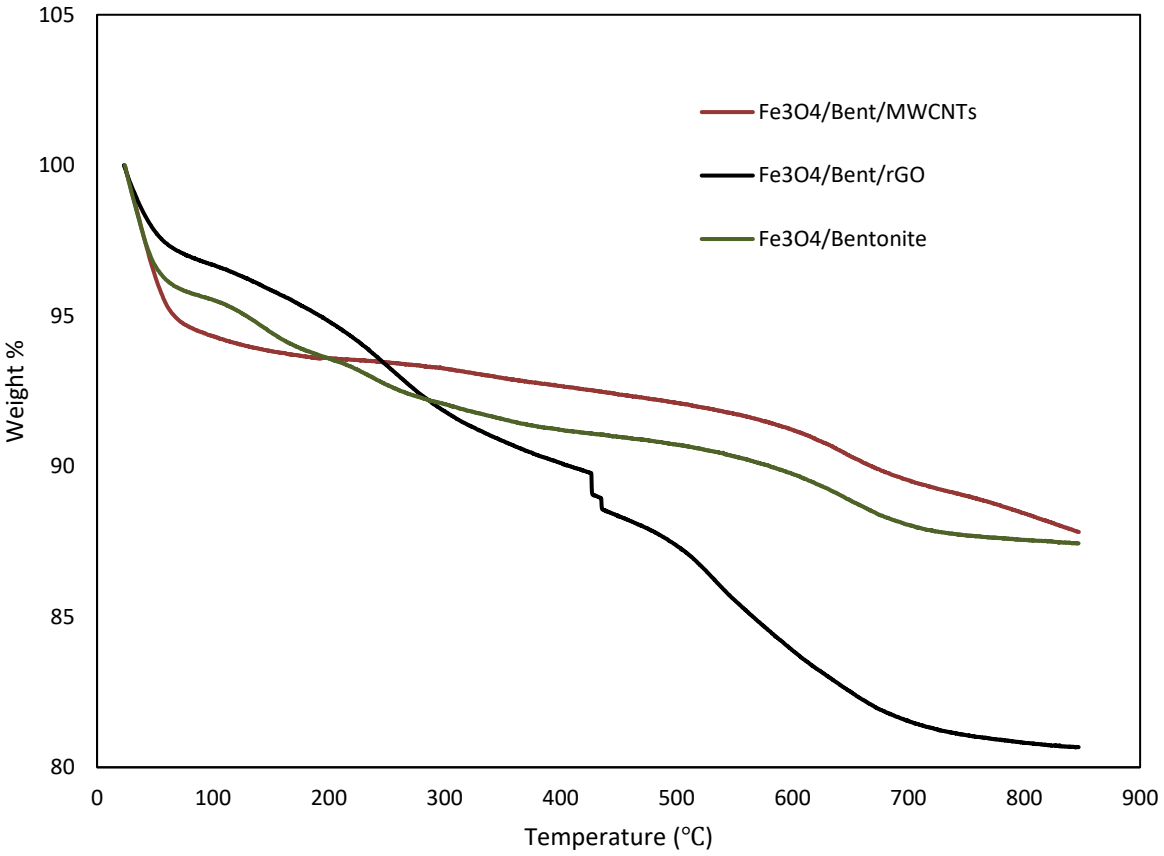

Figure 11: TGA specturm for Fe_3O_4/Bentonite, Fe_3O_4/Bent/rGO and Fe_3O_4/Bent/MWCNTs.

4.1.3 Scanning electron microscope/ Energy-dispersive X-ray spectroscopy

The SEM images are used to observe the surface structure, morphology, uniformity, and distribution of the samples. Figure 12 shows the SEM images for rGO, bentonite, Fe_3O_4 NPs, Fe_3O_4/Bentonite , Fe_3O_4/Bent/rGO and Fe_3O_4/Bent/MWCNTs at a different magnitude along with the elemental analysis on the surface presented in Table 5. Carbon (C), oxygen (O), and iron (Fe) are the main elements existing in all composites. The existence of Fe_3O_4 NPs is indicated by the existence of elements O and Fe. Moreover, the existence of the carbonaceous materials on bentonite surface are indicated by elemental Carbon. The EDX analysis also indicates the existence of silica (Si), Aluminum (Al) and magnesium (Mg) in all composites, which are related to

bentonite. In addition, the EDX analysis of Fe_3O_4/Bentonite indicated the presence of titanium (Ti) and Sodium (Na) elements, which do not present in other composites. These elements are constituents of bentonite clay that present in small quantities. Their absence in other composites reveal the presence of rGO, MWCNTs and Fe_3O_4 NPs on the composites surface in a considerable amount. Moreover, the existence of Na and absence of calcium (Ca) in all composites reveals that the bentonite is sodium-based, which was also confirmed by the XRD analysis.

Figure 12 shows the SEM for rGO, raw bentonite, Fe_3O_4 NPs, Fe_3O_4/Bentonite, Fe_3O_4/Bent/rGO, and Fe_3O_4/Bent/MWCNTs. The SEM image shown in Figure 12a indicate that rGO sheets are thin and possess wrinkled surface structure with distinct edges. On the other hand, bentonite is rock-like structure with a rough surface (Figure 12b). Moreover, Figure 11c shows the agglomeration of Fe_3O_4 NPs, which could be attributed to their high surface energy they attain, as a result of large surface-to-volume ratio [172]. Another reason could be the strength of the magnetic force between the particles [173]. Figure 12d shows the SEM images of Fe_3O_4/Bentonite confirming the successful decoration of bentonite with Fe_3O_4 NPs.

The SEM image of Fe_3O_4/Bent/rGO composite is shown in Figure 12e and 12f. rGO is believed to be formed on the surface of bentonite as indicated by the wrinkled edge structure and/or intercalated into bentonite layers [107]. It is worth noting that rGO sheet formed due to the application of high temperature during Fe_3O_4/Bent/rGO synthesis, which caused the transformation of Graphene oxide (GO) into rGO sheet [160, 174]. Similarly, the SEM images of Fe_3O_4/Bent/MWCNTs indicate that bentonite acts as a support for Fe_3O_4 NPs and MWCNTs (Figure 12g and h). In addition, it can be observed that MWCNTs are distributed over bentonite surface without any agglomeration. The SEM images of Fe_3O_4/Bentonite, Fe_3O_4/Bent/rGO and

Fe_3O_4/Bent/MWCNTs show that Fe_3O_4 NPs were formed randomly on rGO, bentonite, and MWCNTs surface with obvious agglomerations, which is also confirmed by the TEM images shown in Figure 13.

Table 5: EDX analysis for Fe_3O_4/Bentonite/ Fe_3O_4/Bent/rGO and Fe_3O_4/Bent/MWCNTs.

Element	**Fe_3O_4/Bentonite**	**Fe_3O_4/Bent/rGO**	**Fe_3O_4/Bent/MWCNTs**
C	14.44	35.63	64
O	31.35	41.23	23.21
Mg	0.17	0.43	0.16
Al	0.99	1.39	0.68
Si	2.11	3.15	1.93
Cl	-	0.69	0.2
Fe	49	18.49	9.82
Na	0.32	-	-
Ti	0.05	-	-

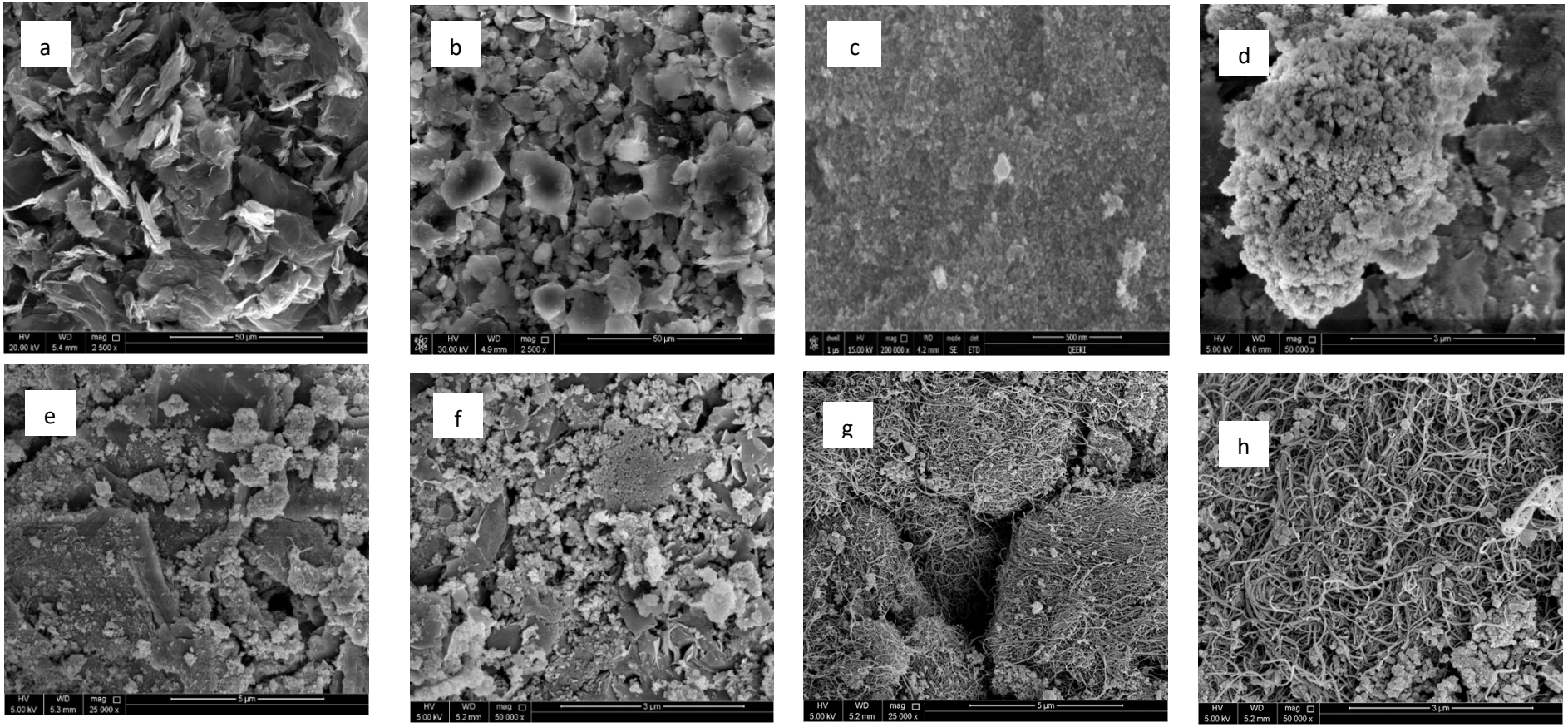

Figure 12: SEM images (a) rGO at 50 μm (b) Bentonite at 50 μm (c) Fe_3O_4 NPs at 0.5 μm(d) Fe_3O_4/Bentonite at 3 μm (e) Fe_3O_4/Bent/rGO at 5μm (f) Fe_3O_4/Bent/rGO at 3μm (g) Fe_3O_4/Bent/MWCNTs at 5μm (h) Fe_3O_4/Bent/MWCNTs at 3μm

4.1.4 Transmission electron microscopy

Figure 13 shows the TEM images for Fe_3O_4 NPs, Fe_3O_4/Bentonite, Fe_3O_4/Bent/rGO, and Fe_3O_4/Bent/MWCNTs. It can be observed that Fe_3O_4 NPs are agglomerated as was indicated by the SEM images due to their high surface energy (Figure 13a). After loading Fe_3O_4 NPs onto bentonite clay, it can be observed that Fe_3O_4 NPs are uniformly distributed on bentonite clay, which is due to the application of ultrasound waves during synthesis. The use of ultrasonic waves causes the particles to disperse due to cavitation and explosion process of bubbles that results from the high shear stress applied on the particles. Consequently, the process of cavitation can accelerate the sild particles to move with high speed and the resultant collisions can potentially produce significant changes in the morphology [173]. Additionally, the particle size of iron oxide nanoparticles on bentonite's surface are in the range of an average value of 13.55 nm. While Fe_3O_4 NPs at 100 nm average diameter attained a value of 13.65 nm. This indicates that ultrasound waves have a slight effect on the particle size, yet they significantly affected the distribution of iron oxide on bentonite surface.

Unlike Fe_3O_4/Bentonite, Fe_3O_4 NPs were agglomerated in Fe_3O_4/Bent/rGO, and Fe_3O_4/Bent/MWCNTs composites because the use of conventional co-precipitation method as the preparation method. The size of Fe_3O_4 NPs over Fe_3O_4/Bent/rGO and Fe_3O_4/Bent/MWCNTs were 11.6 nm and 8.83 nm, respectively. These values are smaller than Fe_3O_4 NPs size formed over Fe_3O_4/Bentonite composite. Although the same amount of precursors were used for the preparation of all composites, the amount of Fe_3O_4 NPs existing on Fe_3O_4/Bent/MWCNTs surface is less than the amount present in Fe_3O_4/Bent/rGO and Fe_3O_4/Bentonite composites. This fact is indicated by the amount of Fe and O in EDX analysis (Table 4) and further observed in the TEM images as well (Figure 13).

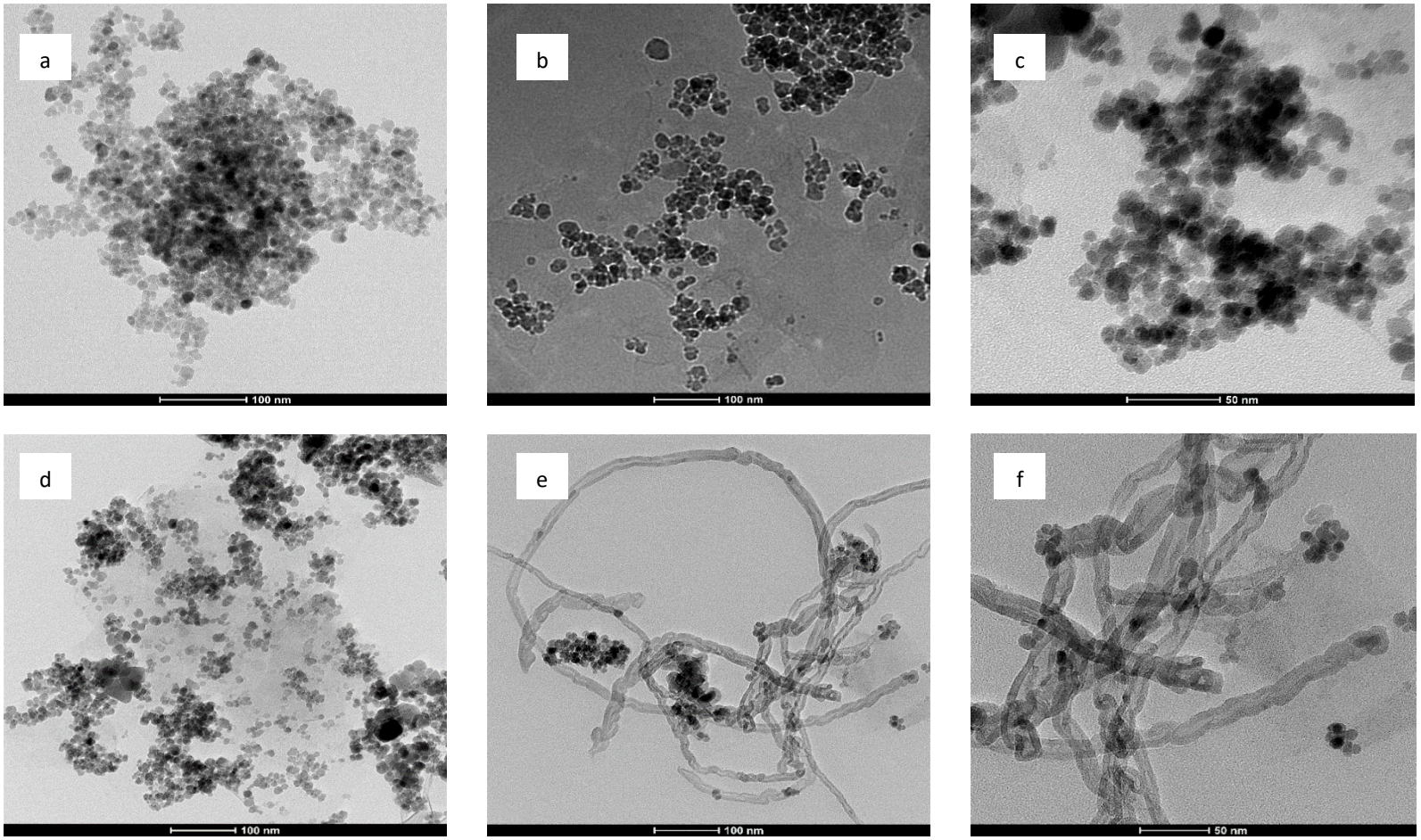

Figure 13: TEM image (a) Fe_3O_4 NPs at 100 nm (b) Fe_3O_4/Bentonite at 100 nm (c) Fe_3O_4/Bent/rGO at 50nm (d) Fe_3O_4/Bent/rGO at 100nm (e) Fe_3O_4/Bent/MWCNTs at 100 nm (f) Fe_3O_4/Bent/MWCNTs at 50 nm.

4.1.5 Brunauer Emmett Teller

The BET analysis for Fe_3O_4/Bentonite, Fe_3O_4/Bent/rGO and Fe_3O_4/Bent/MWCNTs is shown in Table 6. It is observed that Fe_3O_4/Bent/MWCNT attained higher BET surface area and pore volume compared to Fe_3O_4/Bent/rGO, which is expected to yield an enhancement in oil uptake. Generally, surface area and pore volume are important factors that influence the adsorbent uptake capacity. This is because surface area determines the number of effective collisions between the adsorbent and the contaminant [175], whereas higher pore volume allows to trap more contaminants within its pores. In addition, both adsorbents attained higher surface area compared to Fe_3O_4/Bentonite composite reported by Khatamiana et al. [102], which indicates that both composites are expected to attain better adsorption performance.

Table 6: BET analysis of the synthized composites.

Adsorbent	**BET surface Area (m^2/g)**	**total pore volume (cm^3/g)**	**Average pore radius (based on BHJ) (nm)**
Fe_3O_4/Bentonite [102]	44.82	-	-
Fe_3O_4/Bent/rGO	145.336	0.52816	7.27
Fe_3O_4/Bent/MWCNTs	156.26	0.85848	10.99

4.2 Adsorption results

4.2.1 Performance of iron oxide/Bentonite

Fe_3O_4/Bentonite is reported in the literature, but it has not been reported emulsified oil adsorption. Therefore, the adsorption experiments were carried out in order to compare the adsorptive performance of Fe_3O_4/Bentonite composite with the novel composites developed in this work.

4.2.1.1 Effect of adsorbent dosage

The impact of varying Fe_3O_4/Bentonite dosage from 0.05 grams to 0.2 grams on oil removal is represented in Figure 14 and the raw data are represented in Table 14 in the Appendix. All other experimental parameters were maintained constant. This includes initial oil concentration of 100 ppm, contact time of 90 minutes and 6.5 pH. The figure demonstrates a remarkable increase in oil removal percentage as the Fe_3O_4/Bentonite dosage was increased from 0.05 g to 0.1 g, which is attributed to the increase in the unoccupied adsorption sites and functional groups on the Fe_3O_4/ Bentonite surface. However, for the dosage increase from 0.1 g to 0.2 g, the change in the removal percentage was not significant. This could be due to the agglomeration of the composite, which potentially reduced the surface area available for adsorption [176]. This suggests that 0.1 g contains the required number of active sites to attain the maximum removal. Thus, a determined optimum mass of 0.1 g was then used to carry out the rest of the experiments.

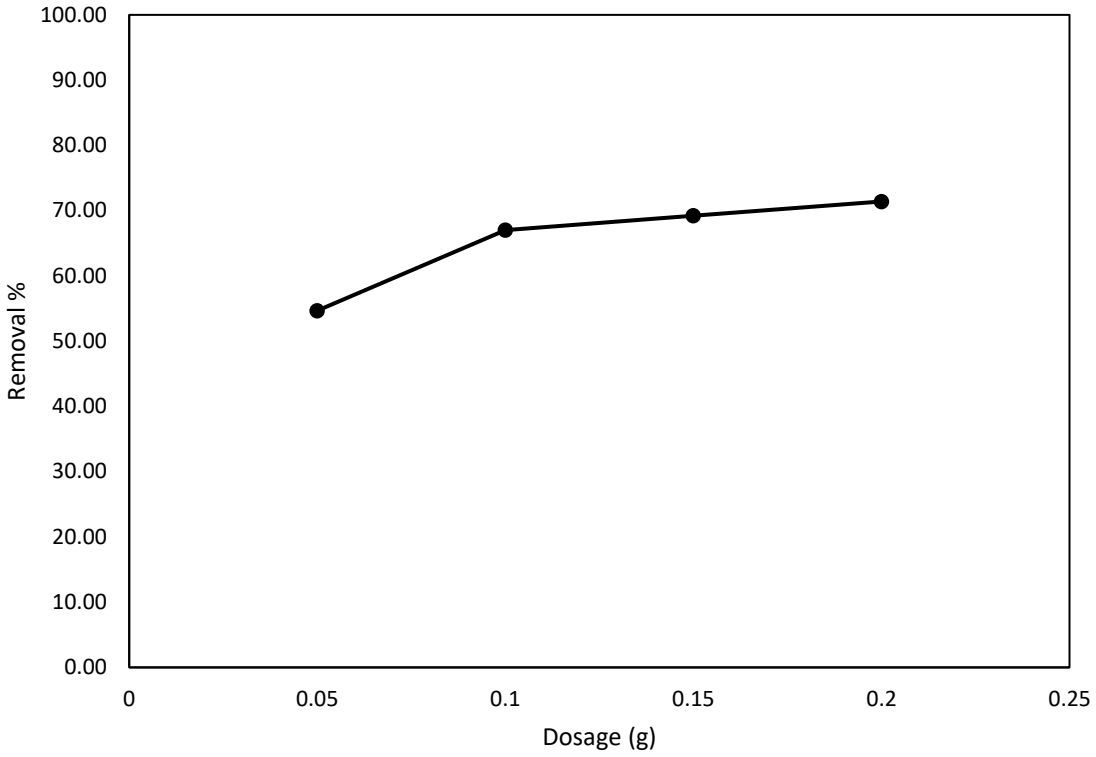

Figure 14: Effect of Fe_3O_4/Bentonite dosage on the removal of oil at 6.5 pH, 298K, oil concentration of 100 ppm, and contact time 90 min.

4.2.1.2 Effect of solution pH

The surface charge , adsorbent stability and pollutant structure are greatly affected by the changes in pH [177]. Therefore, the emulsified oil pH effect on Fe_3O_4/Bentonite adsorption capability was studied by varying the emulsified oil pH from 3.0 to 9.0 using 0.1 g of adsorbent and 100 ppm oil concentration for 90 min contact time. The raw data are represented in Table 16 in the appendix. As shown in figure 15, the oil removal increased by increasing pH up to a maximum pH of 6.5, which is the neutral pH of the emulsified oil solution. Then, the removal decreased to reach a minimum removal percentage at pH 9. Generally, the removal percentage in acidic or alkaline conditions are lower than the neutral condition. This behavior could be due to the partial dissociation of the surface functional groups in acidic or alkaline emulsified oil solution, which results in electrostatic repulsion between the oil droplets and

Fe_3O_4/Bentonite [177]. The poor performance in alkaline conditions compared to neutral and acidic conditions could attributed to the higher electrostatic repulsion between Fe_3O_4/Bentonite and the oil deports[178].

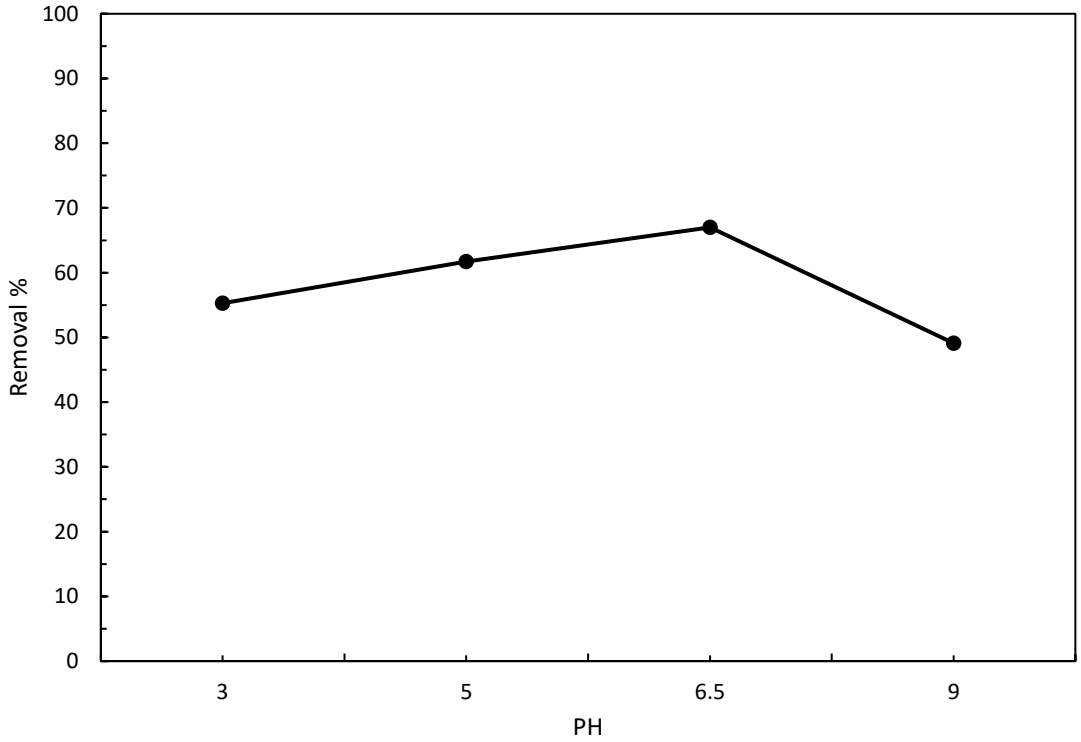

Figure 15: Effect of pH on oil removal by Fe_3O_4/Bentonite 298K ,dosage concentration of 0.1g, 90 min contact time and oil concentration 100 ppm.

4.2.1.3 Effect of contact time

Figure 16 shows the effect of varying the contact time between the Fe_3O_4/Bentonite and the emulsified oil solution on the removal capability of Fe_3O_4/Bentonite composite and the raw data are represented in Table 18 in the appendix. Initially, the oil removal percentage increased due to the availability of active sites on the composite. The equilibrium was reached after 90 minutes with a maximum removal of 67%. After that, no remarkable change in the emulsified oil concentration was observed, which indicates the saturation of adsorption sites [17].

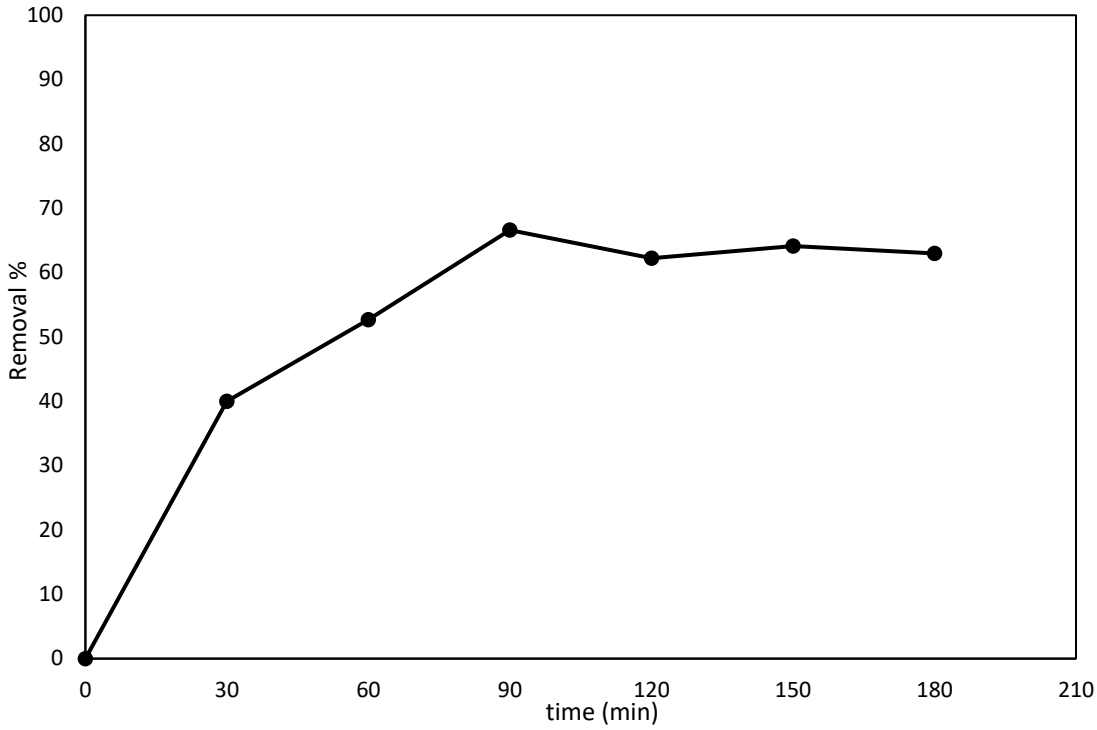

Figure 16: Effect of contact time on oil removal by Fe_3O_4/Bentonite at 298 K, initial concentration 100 ppm, 0.1 g dosage concentration and 6.5 pH

4.2.1.4 Effect of initial oil concentration

The effect of initial oil concentration on the removal percentage of emulsified oil by Fe_3O_4/Bentonite was carried out by changing the initial oil concentration from 66 to 170 mg/L at pH 6.5 using composite dosage of 0.1 g for 180 min. The raw data are represented in Table 17 in the appendix. The effect of initial emulsified oil concentration on the Fe_3O_4/Bentonite removal capability is shown in Figure 17. The figure indicates a negative correlation between removal percentage and initial oil concentration. This could be due to the reduction in the saturation concentration value with a higher initial concentration, which cause the removal percentage to decrease [179].

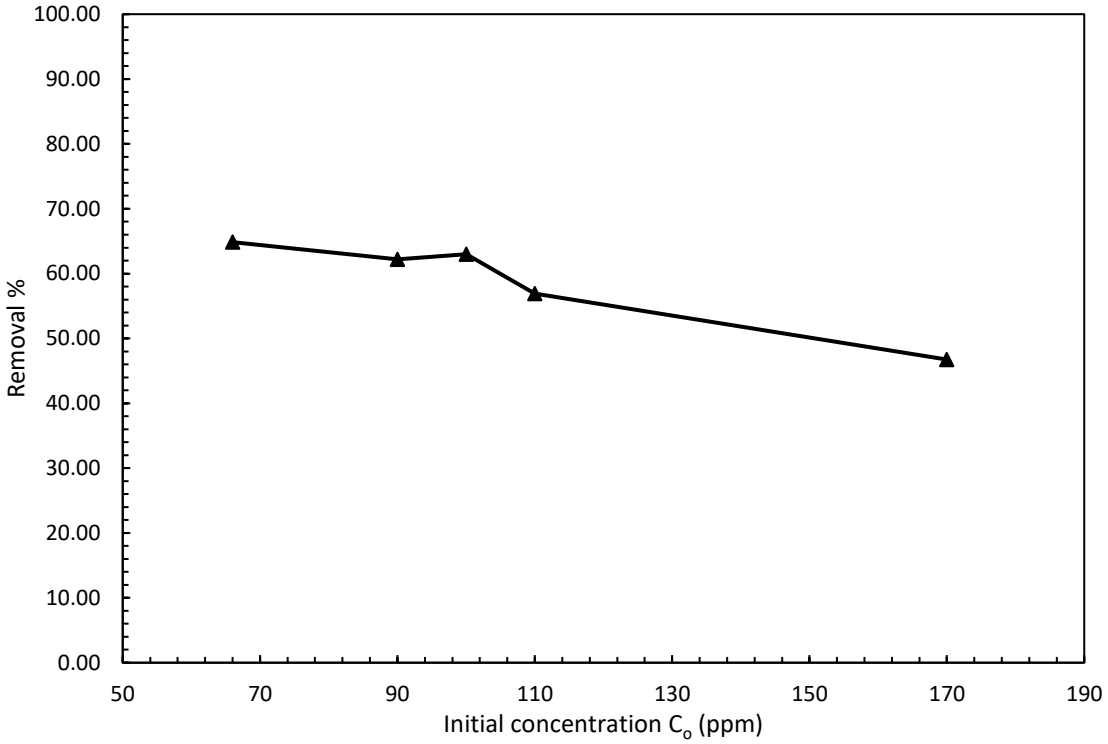

Figure 17: Effect of initial oil concentration on Removal percent using Fe_3O_4/Bentonite after 180 minutes at 298 K, dosage concentration 0.1 g and 6.5 pH.

4.2.1.5 Adsorption isotherms

The experimental adsorption data were fitted to Langmuir, Freundlich and sips models using non-linear regression by employing Marquardt-Levenberg algorithm to find the minimum function that is a sum of squares of nonlinear functions [180]. The fitting of adsorption oil data to the isotherm models using Fe_3O_4/Bentonite is represented in Figure 18. The isotherm parameters are displayed in Table 7. It can be observed that at low equilibrium concentration, the isotherms' curves exhibit higher slope due to the availability of active sites on Fe_3O_4/bentonite (Figure 18).

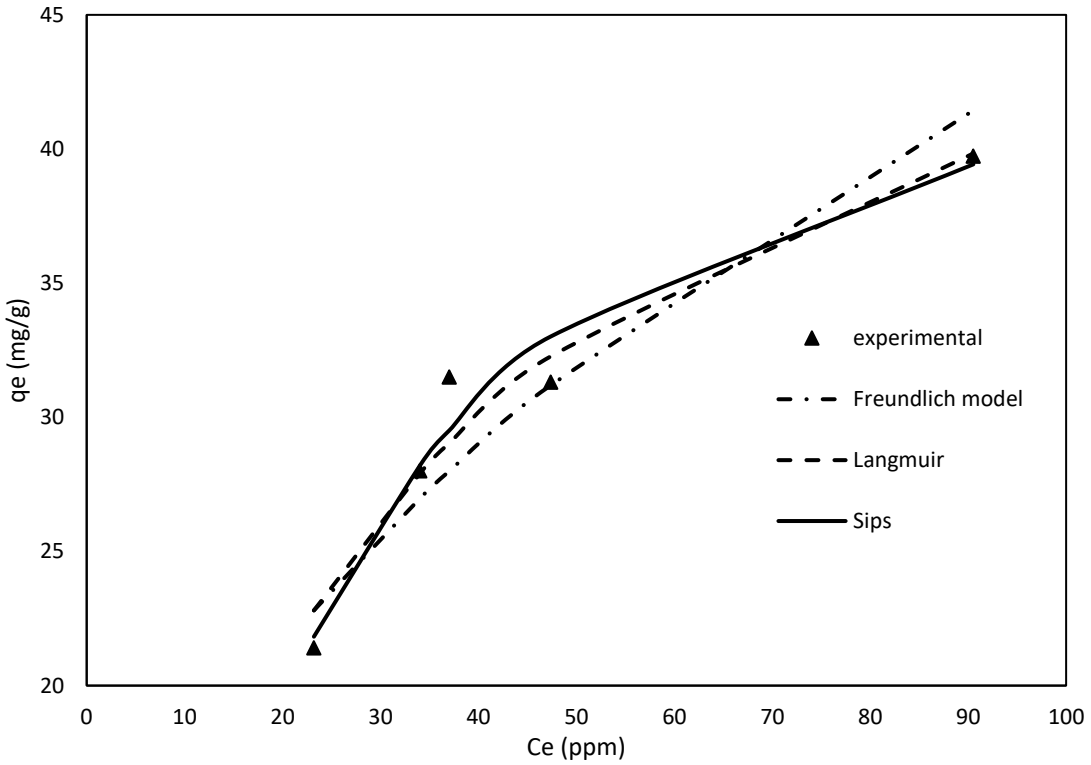

Figure 18: Non-linear isotherm model fitting for oil adsorption onto Fe_3O_4/Bentonite adsorbent.

Table 7: Isotherm parameters for Langmuir, Freundlich and Sips models for oil adsorption onto Fe_3O_4/Bentonite.

Isotherm Model	Parameter	Value
Langmuir	q_m(mg/g)	53.64
	k_L(L/mg)	0.0318
Freundlich	k_f $(mg.g^{-1})(L.mg^{-1})^{1/n}$	5.74
	n	2.28
Sips	q_m(mg/g)	44.54
	b (L/mg)	0.0078
	n	0.654

A comparison of the isotherm models was performed based on the sum of square errors (SSE), correlation coefficient (R^2) and Akaike Information Criterion (AIC) method [181]. AIC method compares between different models and identify the best model that fits the experimental data. Table 8 shows the SSE, R^2, AIC, AIC_c and w_i values of the three isotherm models for Fe_3O_4/Bentonite. The model that best fits the experimental data showed attain the lowest SSE, and AIC; while it should attain the highest R^2, and w_i considering that the sum of w_i is equal to 1. The results indicate that Langmuir model best fits the experimental data for the adsorption of emulsified oil onto Fe_3O_4/Bentonite with R^2=0.983 and w_i= 0.869. These results confirm the adsorption followed Langmuir model, which indicates a monolayer distribution of oil on identical and homogenous active sites. The maximum oil adsorption capacity was 53.64 mg/g.

Figure 19 shows the values of R_L for adsorption of emulsified oil onto Fe_3O_4/Bentonite, which indicates that the adsorption is favorable as R_L lies within the favorable limit ($0 < R_L < 1$) [182].

Table 8: A comparison of the adsorption isotherm models for oil adsorption onto Fe_3O_4/bentonite.

Model	SSE	R^2	AIC	AIC_c	w_i
Langmuir	8.986	0.983	5.74	8.74	0.869
Freundlich	18.25	0.966	10.708	13.708	0.0728
Sips	7.163	0.987	6.16	14.16	0.0580

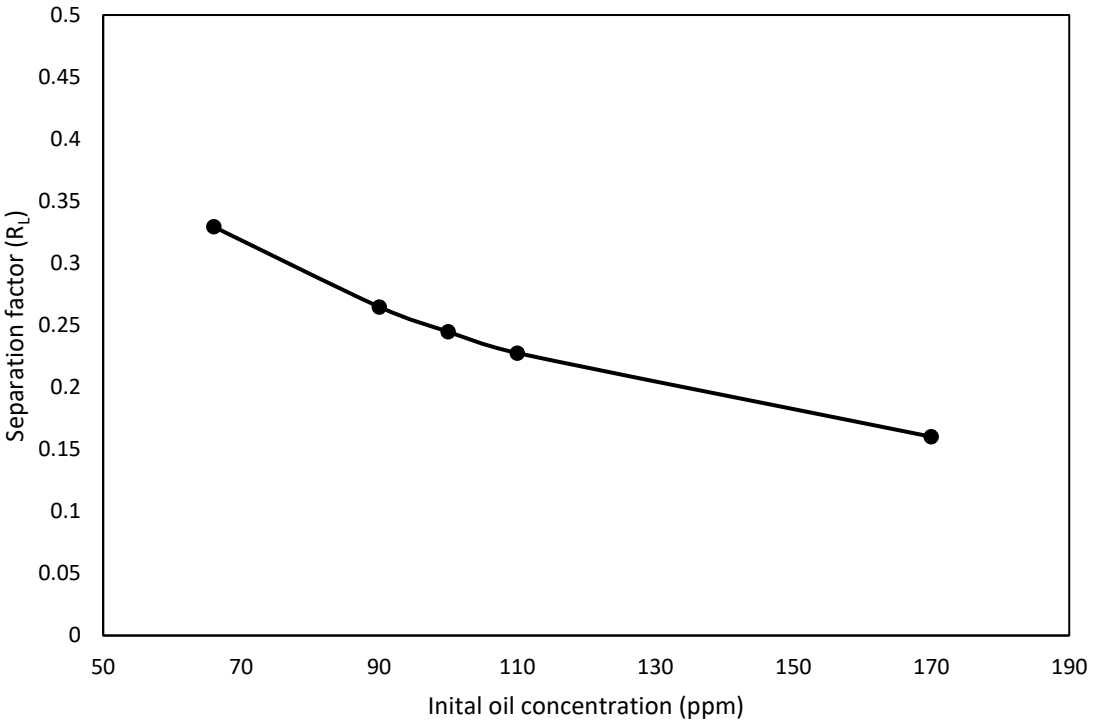

Figure 19: Separation factor (R_L) of emulsified oil adsorption onto Fe_3O_4/Bentonite.

4.2.1.6 Adsorption kinetics

The adsorption of oil kinetics using Fe_3O_4/Bentonite was investigated using the three different kinetics models, which are: PFO, PSO and intraparticle diffusion models. Figure 20 shows the linearized results for the three kinetics models. Additionally, the

kinetics parameters of the fitted models are presented in Table 9. It is clear from Figure 20a that the kinetics experimental data do not fit well PFO kinetic model since the correlation constant R^2 attained a value of 0.6709. However, pseudo second order kinetic model (Figure 20b) shows a better fitting to the experimental data as R^2 attained a value of 0.9868. This indicates that adsorption kinetics of oil onto Fe_3O_4/Bentonite is best described by PSO kinetic model. Figure 20c for the intra-particle diffusion model shows the involvement of three complex stages in the adsorption process, two linear and one curved transition portion. The first linear part is associated with the surface adsorption, in which the oil particles diffuse to the external surface of Fe_3O_4/Bentonite adsorbent with a diffusion rate constant of $k_{i1.}$ The second intermediate stage (curved portion) represents the external boundary layer diffusion. The Last linear stage corresponds to the diffusion through interior surface of Fe_3O_4/Bentonite with a diffusion rate constant k_{d3}. As shown in Table 8, the value of k_{d1} is greater than k_{d3}, which indicates that the interior pore-diffusion is the rate-limiting step [179]. The influence of the boundary layer is represented by the intercept C. the numerical values of C_1 and C_3 shown in Table 8, reveal that the intraparticle diffusion is not the only rate-limiting step since C does not pass through the zero point [179]. In addition, the larger the value of C, the greater the influence of the boundary layer on the diffusion process[182].

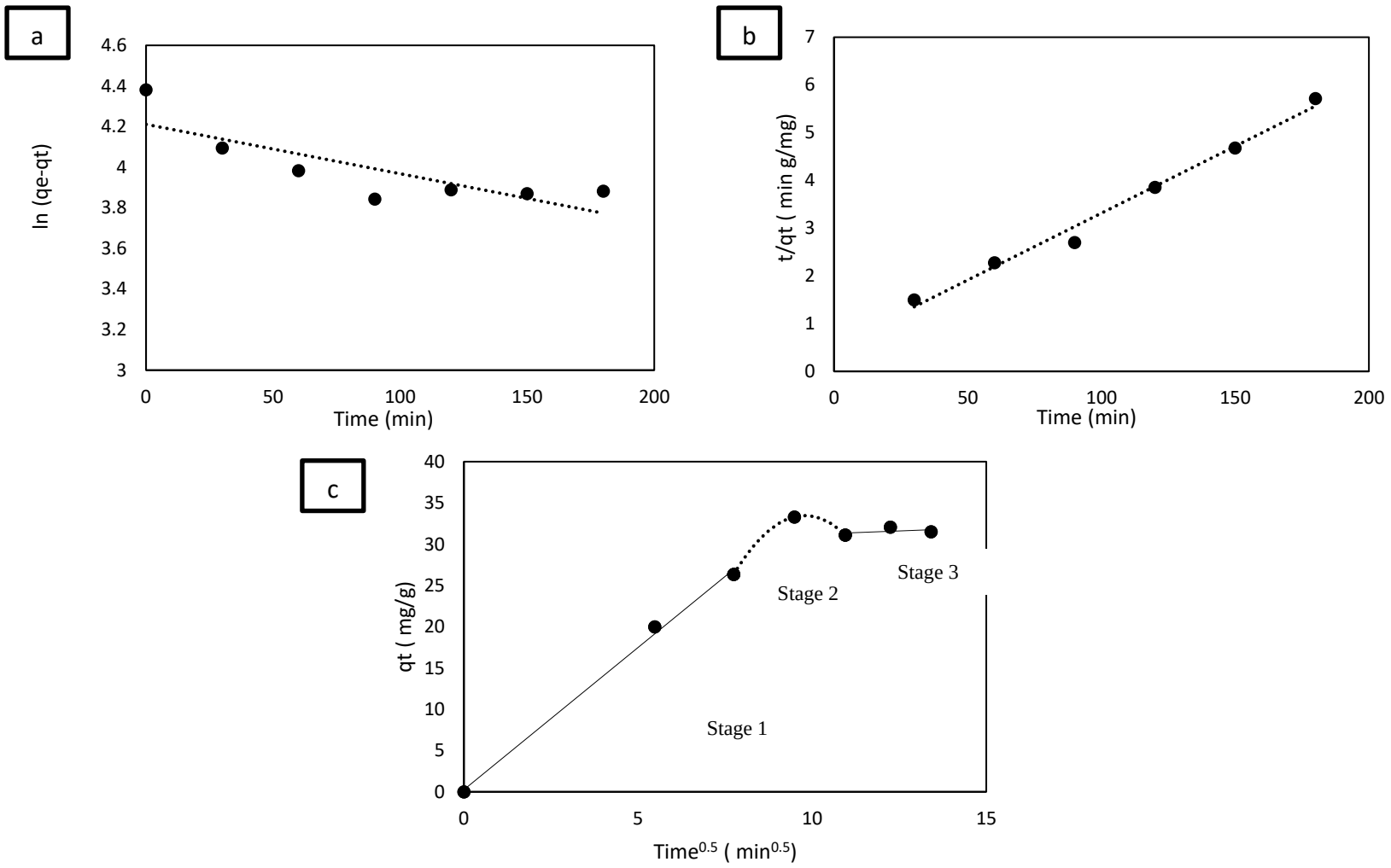

Figure 20: Kinetics models fitting for oil adsorption onto Fe_3O_4/Bentonite using (a) PFO (b) PSO (c) intraparticle diffusion model.

Table 9: Kintic models parameters for oil adsorption onto Fe_3O_4/Bentonite.

Kinetics Model	Parameter	Value
PFO	qe (mg/g)	67.41
	k_1(1/min)	0.0024
	R^2	0.6709
PSO	qe(mg/g)	35.67
	k_2 (g/mg.min)	0.00153
	R^2	0.9868
Intraparticle diffusion	k_{d1} (mg/g.$min^{0.5}$)	3.4458
	k_{d3} (mg/g.$min^{0.5}$)	0.1624
	C_1 (mg/g)	0.2552
	C_3 (mg/g)	29.575

4.2.1.7 Adsorption mechanism

The FTIR spectrum presented in Figure 21a shows the functional groups on the surface of Fe_3O_4/Bentonite. The absorption peak at approximately 598 cm^{-1} can be ascribed to Fe-O vibrational mode of Fe_3O_4 NPs. The absorption peaks at 3604 cm^{-1} and 1692 cm^{-1} correspond to stretching vibration of –OH (water) and -FeOO- [183]. Additionally, the other broad absorption peak at 1038 cm^{-1} can be attributed to Si-O-Si while 609 cm^{-1} can be ascribed to the bending vibration of Si-O-Al group [184]. These results show the successful decoration of Bentonite surface by Fe_3O_4 as confirmed by XRD and TEM analyses results. The FTIR spectra of Fe_3O_4/Bentonite after diesel oil adsorption is represented in Figure 21b. The figure clearly shows the appearance of new peaks at 1057 cm^{-1} and 2922 cm^{-1} which is attributed to the stretching vibration of C–O and C–H, respectively [185]. In addition, the peak sharpness intensity was increased at 1038 cm^{-1}, 1429 cm^{-1} and 3604 cm^{-1} and this confirms the interaction between Fe_3O_4/Bentonite with the hydrocarbon chain presented in the emulsified diesel oil. Moreover, the composite could have a hydrophobic interaction with oil and tends to adsorb oil molecules, due to the hydrophobic nature of bentonite and iron oxide [186, 187]. In addition, the FTIR spectra shows no shift in Fe_3O_4/Bentonite peaks after oil

adsorption, which indicates that the hydrophobicity interaction has an important role in the adsorption process [188]. It can be observed that the absorption peak of O-H after adsorption has increased, which indicates that hydrogen bonding is involved in the adsorption mechanism. In addition, the presence of positive ions as indicated by EDX analysis (Table 4) could results in an electrostatic interaction. Therefore, chemical, physical (e.g hydrogen), hydrophobic, and electrostatic interaction are involved in oil uptake mechanism. Figure 22 illustrates the feasible mechanism of oil removal using Fe_3O_4/ Bentonite.

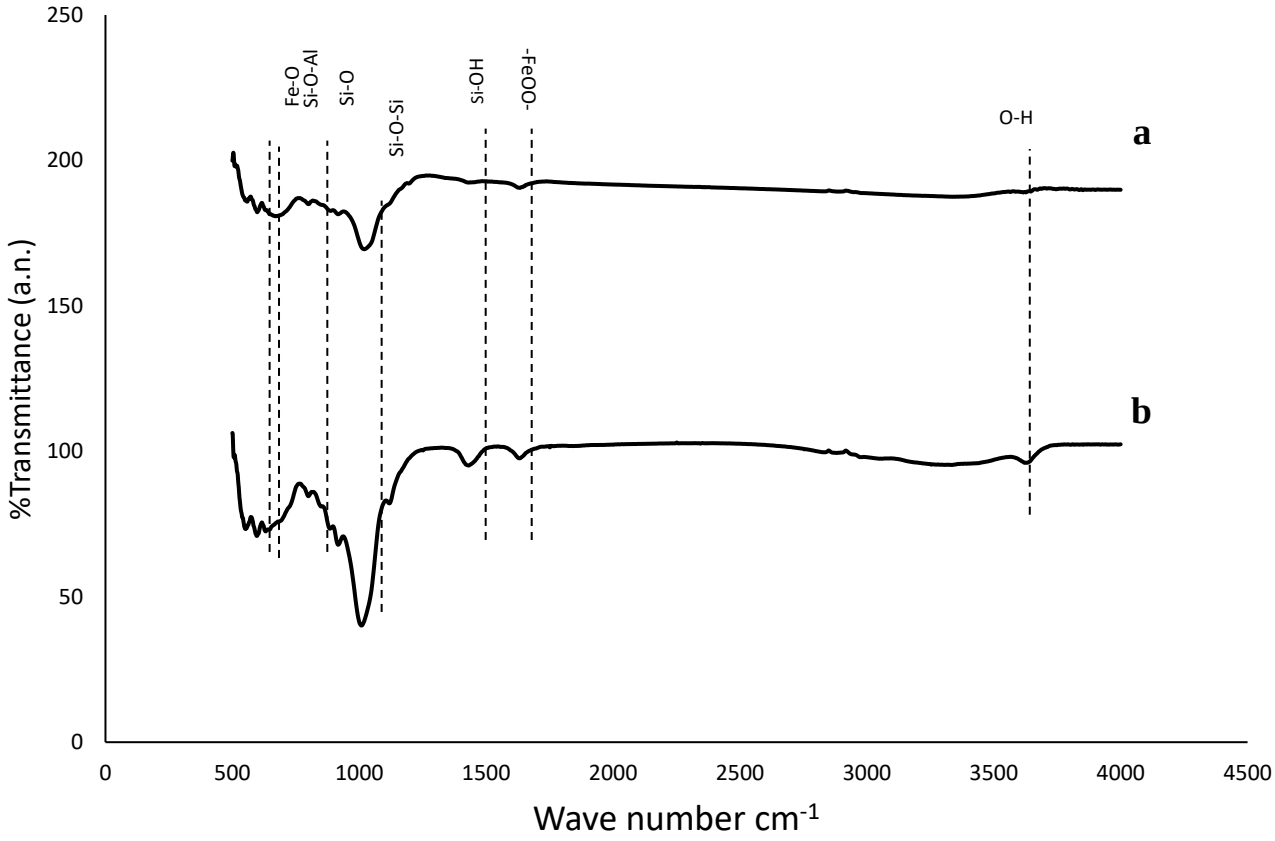

Figure 21 FTIR spectra of Fe_3O_4/Bentonite (a) before oil adsorption (b) after oil adsorption.

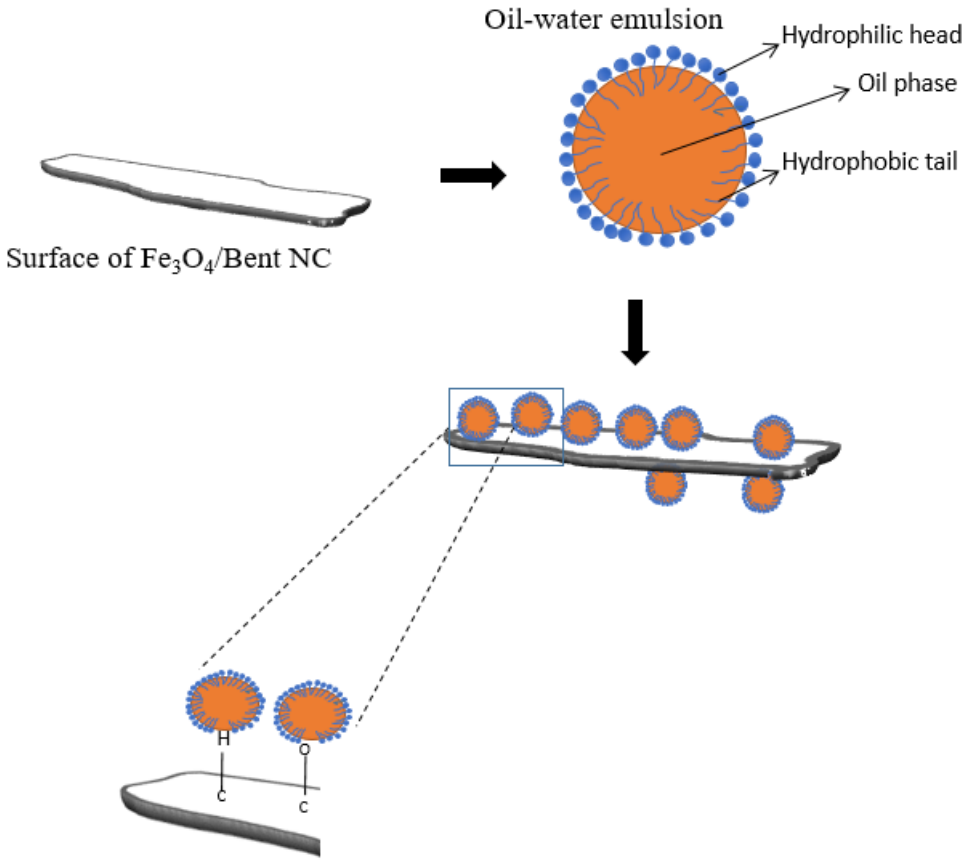

Figure 22 The possible adsorption mechanism of diesel oil by Fe_3O_4/bentonite.

4.2.2 Performance of Fe_3O_4/Bent/rGO and Fe_3O_4/Bent/MWCNTs

In order to compare the performance of the developed composites compared to Fe_3O_4/bentonite in oil removal, the adsorption experiments were conducted using the same adsorbent dosage (0.1 g), solution pH (6.5), temperature (303 K), and rotation speed (200 rpm). The effect of contact time and initial oil concentration were varied and fitted to isotherm and kinetics models to have insights into the removal capability of the developed composites as well as the adsorption mechanism.

4.2.2.1 Effect of contact time

The influence of contact time between the composites and the oil solution is shown in Figure 23 and the raw data are represented in table 20 and 22 in the appendix. The figure shows a rapid adsorption within the first 30 minutes followed by a gradual decrease until equilibrium was reached. This could be attributed to the availability of binding sites for adsorption in the first 30 minutes, after that, the sites become fully occupied and the adsorption starts to decrease. Moreover, it can be observed that Fe_3O_4/Bent/MWCNTs reached equilibrium faster than Fe_3O_4/Bent/rGO, which could be attributed to the higher pore volume that the composite possesses. The maximum oil removal using Fe_3O_4/Bent/MWCNTs and Fe_3O_4/Bent/rGO were 97.7% and 92.4 %, respectively.

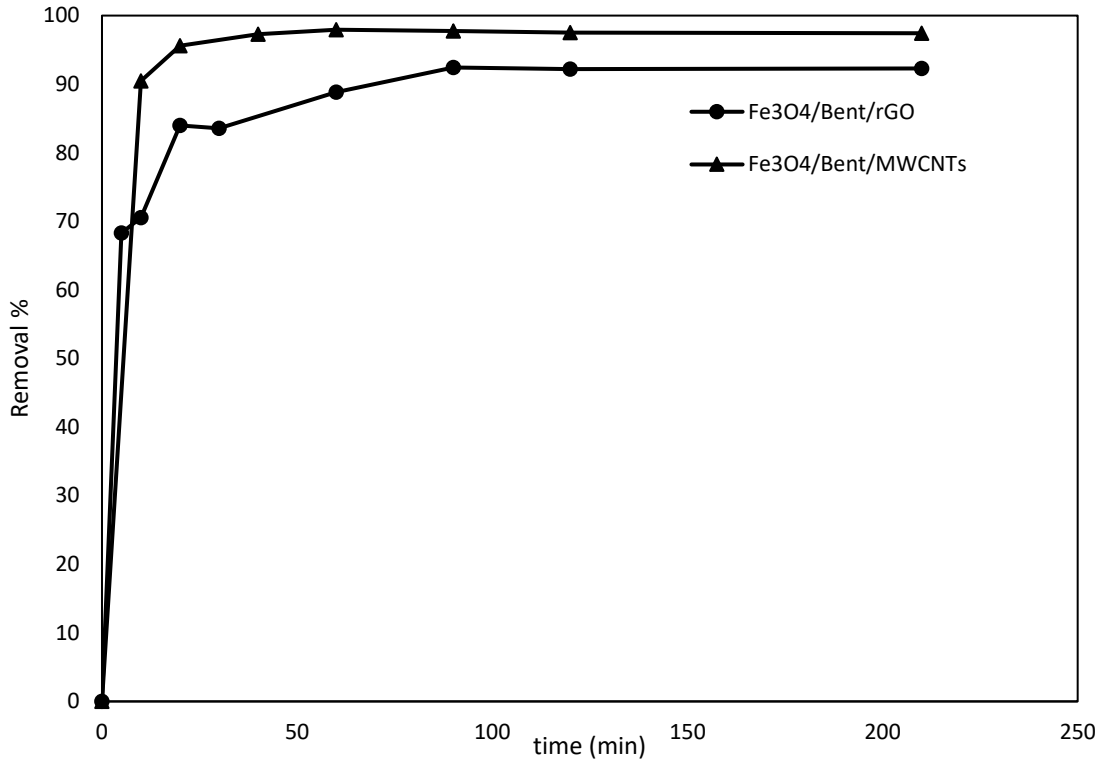

Figure 23: Effect of time on the adsorption capacity (Dosage 0.1 g, Oil Concentration 120 ppm, 6.5 pH and Temperature 303 K.

4.2.2.2 Effect of initial oil concentration

The influence of initial oil concentration on the adsorption capacities of Fe_3O_4/Bent/rGO and Fe_3O_4/Bent/MWCNTs is shown in Figure 24 and the raw data are represented in Table 19 and 21 in the appendix. The figure indicates that the removal capability of both composites increased as the initial concentration increased from 15 ppm to 90 ppm. This increase is attributed to the presence of greater amount of oil molecules at high concentrations that interact with the adsorbent's active sites due to the increase in the concentration gradient between the solution and the adsorbent. After that, the removal percentage remained roughly constant when initial oil concentration increased up to 150 ppm, which indicated that the saturation of oil molecules on the adsorbents and the active sites are fully occupied. Moreover, Fe_3O_4/Bent/MWCNTs showed similar removal capability to Fe_3O_4/Bent/rGO at concentration lower than 40

ppm. However, at higher initial oil concentration, Fe_3O_4/Bent/MWCNTs attained higher removal capability. This behavior could be due to the presence of more binding sites on Fe_3O_4/Bent/MWCNTs surface compared to that of Fe_3O_4/Bent/rGO. The higher BET surface area and average pore volume that Fe_3O_4/Bent/MWCNTs composite (Table 5) attains are expected to be responsible for the increase in oil removal compared to Fe_3O_4/Bent/rGO. This allows Fe_3O_4/Bent/MWCNTs to trap oil molecules within its structure and increase the oil molecules contact with the adsorbent functional groups, which increases the overall removal efficiency. Moreover, high specific surface area and lower pore radius are expected to be the main parameters that determine the enhancement in the adsorption capacity. Despite that Fe_3O_4/Bent/MWCNTs attained higher average pore radius and specific surface area, it showed a higher removal capability [189]. Consequently, pore volume has a vital role in determining the composite removal capability.

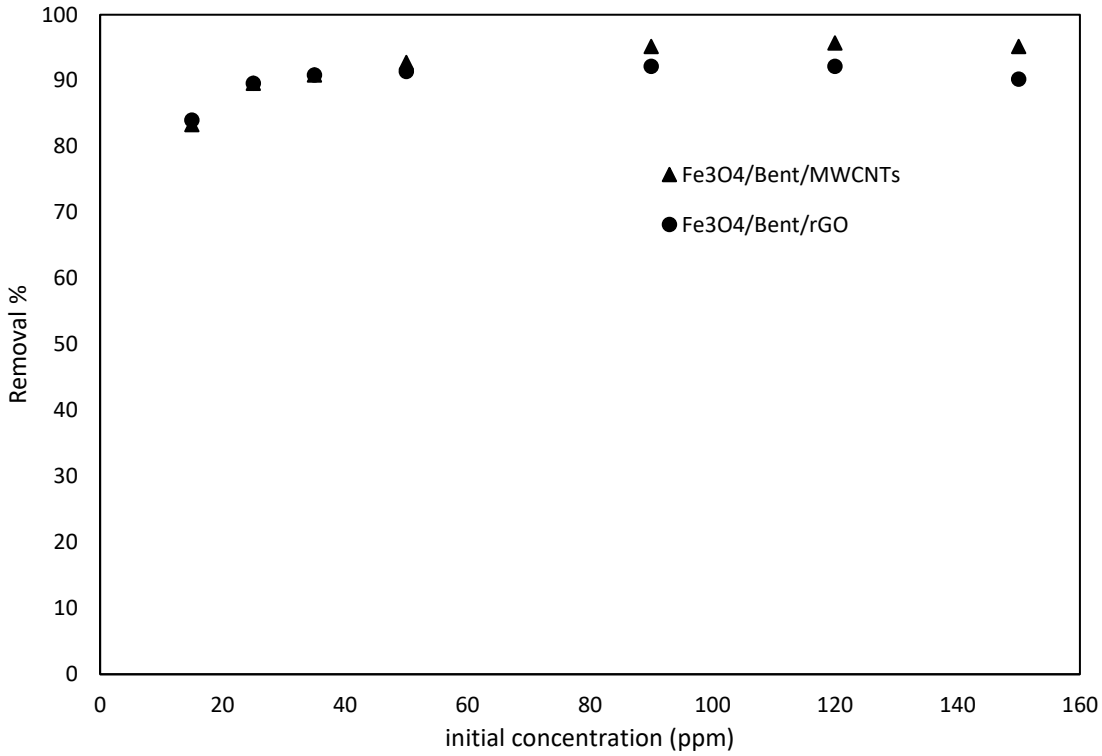

Figure 24: Effect of initial concentration on the adsorption capacity (Dosage 0.1 g, Time 210 minutes, 6.5 pH and Temperature 303 K).

4.2.2.3 Adsorption isotherms

The fitting of adsorption oil data to the isotherm models using Fe_3O_4/Bent/rGO and Fe_3O_4/Bent/MWCNTs are represented in Figure 25 and 26, respectively. The isotherm parameters are displayed in Table 10. Similar to Fe_3O_4/Bentonite, it can be observed that at low equilibrium concentration, the isotherms' curves of both composites exhibit higher slope due to the availability of active sites.

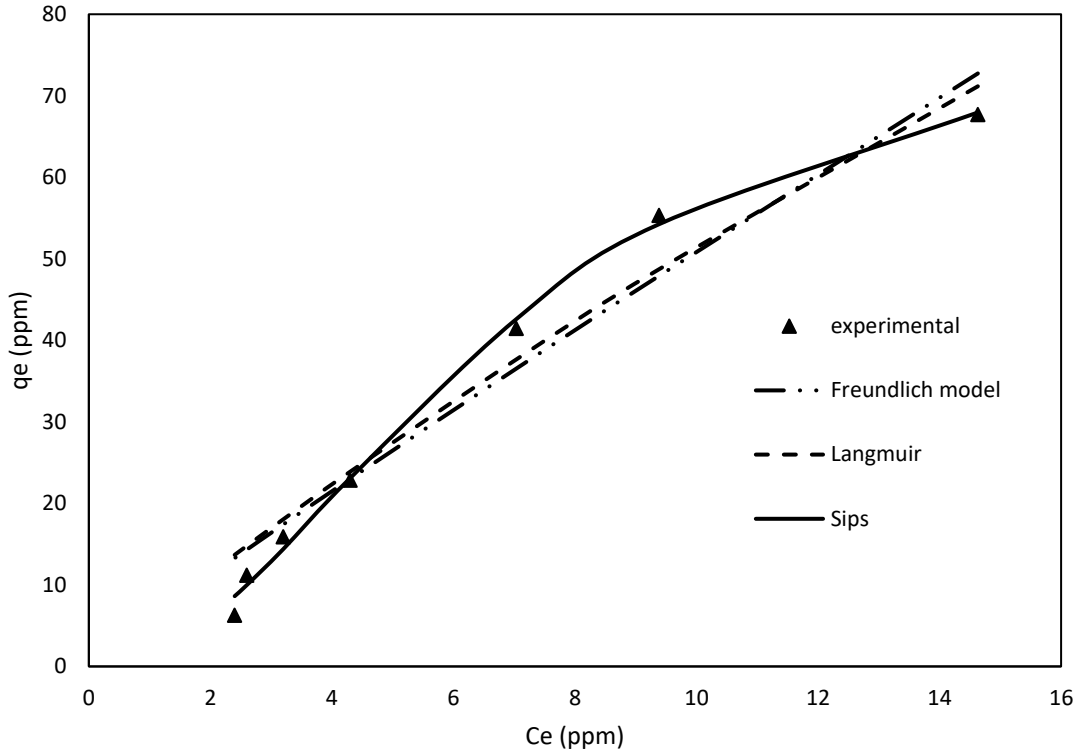

Figure 25: Non-linear isotherm model fitting for oil adsorption onto Fe_3O_4/Bent/rGO.

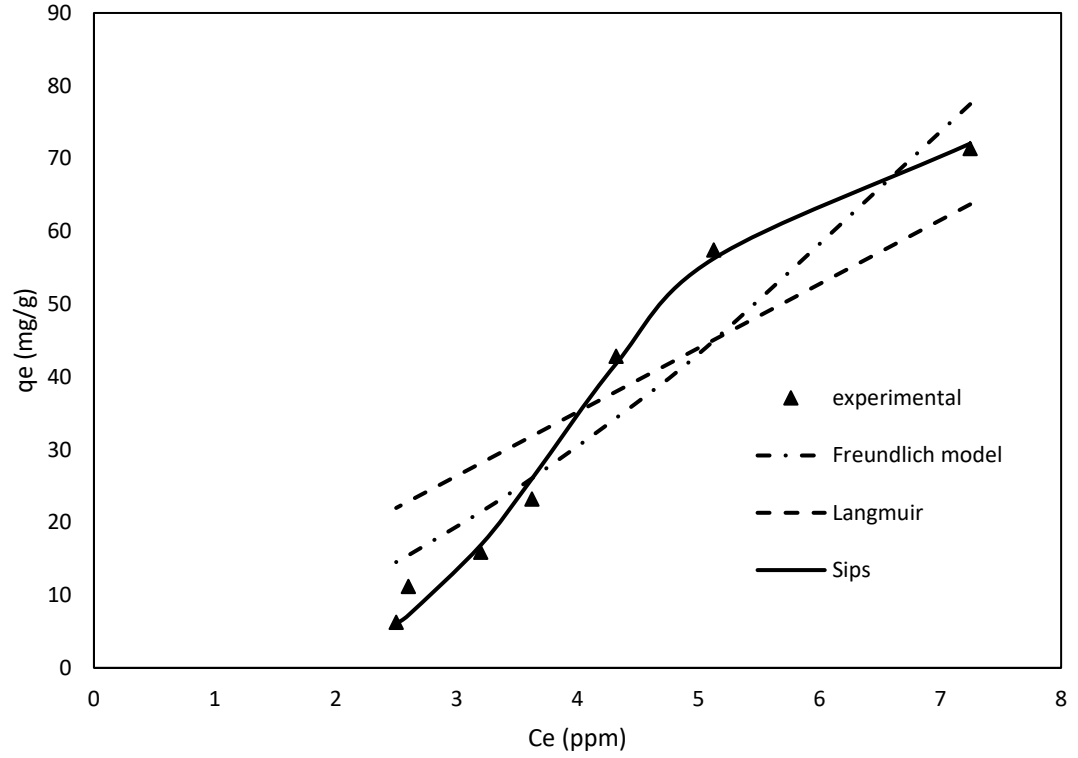

Figure 26: Non-linear isotherm model fitting for oil adsorption onto Fe_3O_4/Bent/MWCNTs.

Table 10: Isotherm parameters for Langmuir, Freundlich and Sips models for oil adsorption onto the novel composites.

Model	Parameter	Fe_3O_4/Bent/rGO	Fe_3O_4/Bent/MWCNTs
Langmuir	k_L (L/mg)	0.0146	0.000108
	q_m(mg/g)	404.21	81351.14
Freundlich	k_F $(mg.g^{-1})(L.mg^{-1})^{1/n}$	5.8344	3.446
	n_F	1.0634	0.636
Sips	q_m (mg/g)	81.65	77.12
	b (L/mg)	0.019	0.0010
	n	0.485	0.208

Table 11 and 12 shows the SSE, R^2, AIC, AIC_c and w_i values of the three isotherm models for Fe_3O_4/Bent/rGO and Fe_3O_4/Bent/MWCNTs, respectively. The model that best fits the experimental data showed attain the lowest SSE, and AIC; while it should attain the highest R^2, and w_i considering that the sum of w_i is equal to 1. The results indicate that Sips model best fits the experimental data for the adsorption of oil onto Fe_3O_4/Bentonite/rGO with R^2=0.997 and w_i= 0.9919. Similarly, the adsorption of oil onto Fe_3O_4/Bentonite/MWCNTs is best described by sips model with R^2=0.9926 and w_i= 0.9967. These results confirm the adsorption followed Freundlich model at lower concentrations and Langmuir model when the oil concentrations were increased, which indicates the involvement of both physical and chemical adsorption process. The maximum oil adsorption capacity were 81.65 mg/g and 77.12 mg/g for Fe_3O_4/Bentonite/rGO and Fe_3O_4/Bent/MWCNTs, respectively.

Table 11: A comparison of the adsorption isotherm models for oil adsorption onto Fe_3O_4/Bent/rGO.

Model	SSE	R^2	AIC	AIC_c	w_i
Langmuir	143.3	0.957	25.133	28.133	0.005
Freundlich	165.82	0.950	26.155	29.154	0.003
Sips (L-F)	11.654	0.997	9.568	17.568	0.9919

Table 12: A comparison of the adsorption isotherm models for oil adosrption onto Fe_3O_4/Bent/MWCNTs.

Model	SSE	R^2	AIC	AIC_c	w_i
Langmuir	843.59	0.7747	37.542	40.542	0.0002
Freundlich	390.26	0.8957	32.146	35.146	0.003
Sips	27.586	0.9926	15.599	23.599	0.9967

4.2.2.4 Adsorption kinetics

The fitted adsorption experimental data onto both composites to three kinetics models are shown in Figures 27 and 28. The kinetics parameter calculated from the related plots are shown in Table 13. The high R^2 values indicate that PSO model best describe the oil adsorption onto both composites. This implies that oil adsorption onto both composites involves chemisorption process [190]. In addition, the kinetics data were fitted to intraparticle diffusion model to have an insight into the adsorption rate controlling steps and the mechanism (Figure 27C and 28C). For both composites, the intraparticle diffusion model shows a multistage behavior. The first stage is the instantaneous adsorption of oil molecules represented by the sharp rise in qt with $t^{0.5}$.

In this stage, the adsorption is controlled by external mass transfer. The second stage is a curved portion, which shows a slow adsorption rate controlled by intraparticle diffusion. The third stage represents the equilibrium stage where internal diffusion occurs within the composite's pores. Moreover, the value of k_{d1} is greater than k_{d2} for both adsorbents (Table 12), which indicates that the rate limiting step is the interior pore-diffusion [191]. The intercept (C) describes the boundary layer thickness. The Larger the value of C, the greater the contribution of the surface adsorption in the rate controlling step. Finally, it can be observed that the plot of intraparticle diffusion model for both composites did not pass through the origin, which indicate that intraparticle diffusion is not the only rate-controlling step.

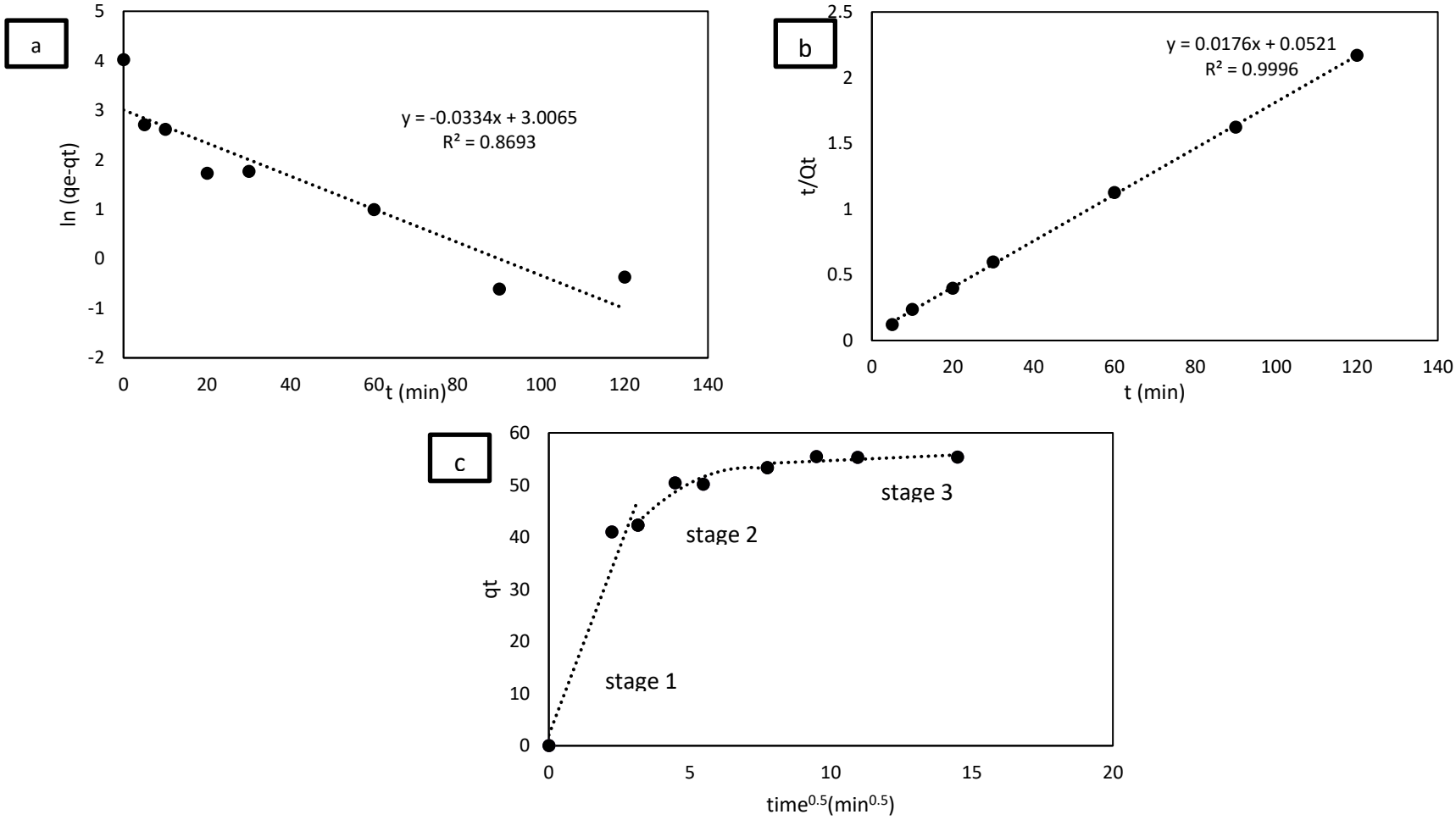

Figure 27: Kinetics models fitting for oil adsorption onto Fe_3O_4/Bent/rGO using (a) PFO (b) PSO (c) intraparticle diffusion model.

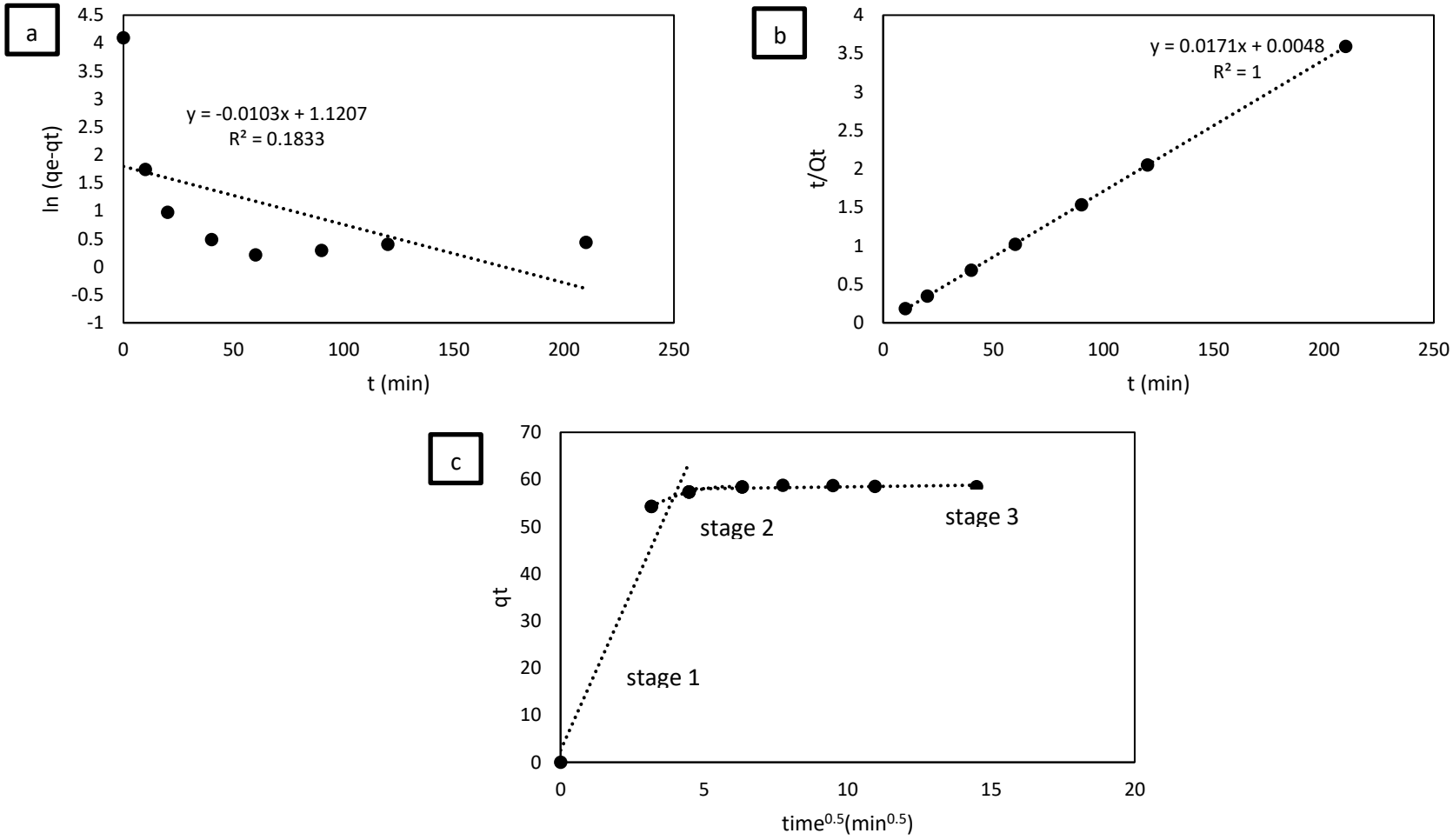

Figure 28: Kinetics models fitting for oil adsorption onto Fe_3O_4/Bent/MWCNTs using (a) PFO (b) PSO (c) intraparticle diffusion model.

Table 13: The kinetics parameters for oil adsorption onto novel composites.

Model	**Parameter**	**Fe_3O_4/Bent/rGO**	**Fe_3O_4/Bent/MWCNTs**
	k_1	0.0334	0.0103
PFO	q_e	20.217	3.067
	R^2	0.8693	0.1833
	k_2	0.00594	0.0609
PSO	q_e	56.818	58.479
	R^2	0.9996	1.000
	k_{d1}	14.292	13.65
Intraparticle	k_{d3}	0.24	0.0782
diffusion	C_1	2.040	2.5357
	C_3	52.297	57.651

4.3 Performance in fluidized bed

The performance of Fe_3O_4 NPs, Fe_3O_4/Bentonite, Fe_3O_4/Bent/rGO, and Fe_3O_4/Bent/MWCNTs in flidized bed reactor is shown in Figure 29 and The raw data are represented in Table 23 in the appendix. The figure Cleary indicates that the novel adsorbents developed in this work outperform Fe_3O_4 NPs and Fe_3O_4/Bentonite adsorbents, which is due to the addition of carbonaceous materials. Among the developed adsorbents in this work, it can be observed that Fe_3O_4/Bent/rGO was able to remove higher percentage of oil compared to Fe_3O_4/Bent/MWCNTs by more than 20% despite having lower specific surface area, and pore volume. Besides, in batch experiments, both adsorbents attained mostly similar adsorption behavior and adsorption capacity. This significant difference could be due to the different adsorbent size, density, and surface properties. The difference in the performance of the developed

composites could be due the difference in their particle size. From visual observation, the particles of Fe_3O_4/Bent/rGO were larger than those of Fe_3O_4/Bent/MWCNTs. Consequently, Fe_3O_4/Bent/rGO particles are capable to disintegrate larger bubbles that are evolved in fluidized bed resulting in a better contact between emulsified oil solution and the composite, which increases the removal percentage. kim and kang reported that particle size could be the most important factor that control the mass transfer in FBR [192]. Furthermore, surface properties including surface hydrophobicity, surface irregularity, and surface angles sharpness are important factors that influence the adsorbent removal capability significantly [193].

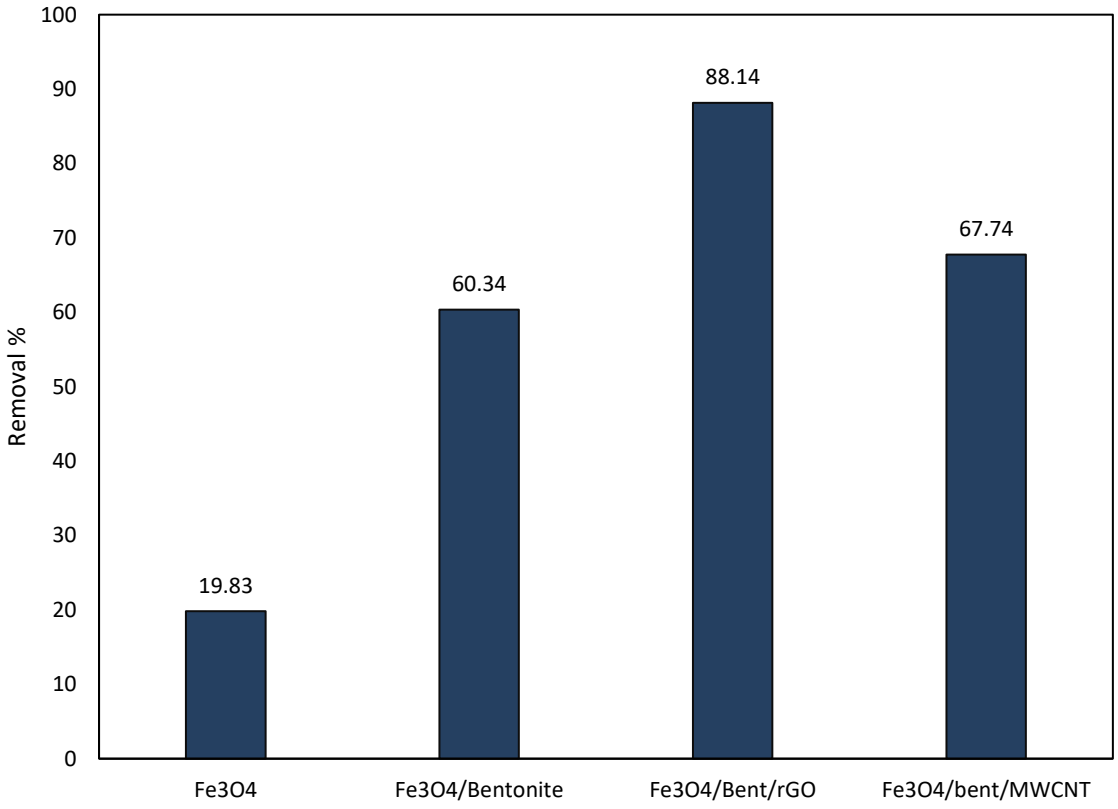

Figure 29: performance of Fe_3O_4 NPs, Fe_3O_4/Bentonite, Fe_3O_4/Bent/rGO and Fe_3O_4/Bent/MWCNTs in fluidized bed reactor.

4.4 Adsorption mechanism

The FTIR spectra shown in Figure 30 indicate the surface functional groups for both composites before and after diesel oil adsorption. The figure clearly indicates that both adsorbents attain similar absorption peaks except the absorption peak at 687 cm^{-1} that is observed for Fe_3O_4/Bent/MWCNTs, which is related to the strong bending of C=C bond. Moreover, the peaks observed at 3640 cm^{-1}, and 1040 cm^{-1}, are related to O–H, and C–O bond, respectively [194]. The bond stretching vibration of CO observed at 1107 cm^{-1} is related to the carbon attached to the epoxy groups, while the absorption peak at 1639 cm^{-1} is attributed to the C=O bond [195]. The peak observed at 1430 cm^{-1} is ascribed to the stretching vibration of CO_3^{-2} anion associated in dolomite that presents in bentonite as impurity [107]. The broad peak at 1038 cm^{-1} indicates the presence of Si–O–Si groups of the tetrahedral sheet. The peaks observed at 521 cm^{-1} and 467 cm^{-1} correspond to Al–O–Si and Si–O–Si, respectively [196, 197]. The stretching vibration in the region between 800 cm^{-1} and 930 cm^{-1} are related to C–H bond. The peak observed between 500 cm^{-1} and 600 cm^{-1} are related to the presence of Fe–O bond [102]. In addition, the stretching vibration in the region between 3300 cm^{-1} and 3600 cm^{-1} corresponds to the hydroxyl and carboxyl groups presented in GO [198]. The non-existence of absorption peaks at 1724 cm^{-1} confirms the successful reduction of GO into rGO [198]. After adsorption, the peaks' intensity in this region were reduced and new peaks at 2928 cm^{-1} and 2857 cm^{-1} were observed. These peaks indicate the presence of C–H bond, which indicate the chemical interaction between the adsorbents and the diesel oil molecules. The vibration region between 2309 cm^{-1}, and 2371 cm^{-1}observed in Figure 30d for Fe_3O_4/Bent/MWCNTs after adsorption is indication of C=O=C bond.

Based on these results, it is expected that the removal of oil molecules by the fabricated composites is based on a chemical interaction as observed by the FTIR spectra represented in Figure 30. Moreover, the hydrophobic interaction between oil molecules and the composites hydrophobic surface facilitated oil removal from the aqueous solution. The hydrophobic nature of the composites is determined by the presence of active functional groups with a lone pair of electrons such as O–H, and C–O groups that interact with the hydrophobic oil molecules. It can be observed from Figure 30c and d that the intensity of these groups was reduced after adsorption, which confirms the hydrophobic interaction. In addition, π-π interaction caused by the presence of graphene sheets and MWCNTs have primary role in oil molecules adsorption and accounts for the increase in oil adsorption compared to Fe_3O_4/Bentonite composite [199, 200]. Moreover, the existence of positively charged element such as Mg and Al (as indicated by the EDX analysis, Table 4) results in electrostatic interaction between the positively charged elements and the additives presents the Water-in-oil emulsion solution resulting in physical interaction. The possible adsorption pathway between the as-synthesized composites and oil molecules are illustrated in Figure 31.

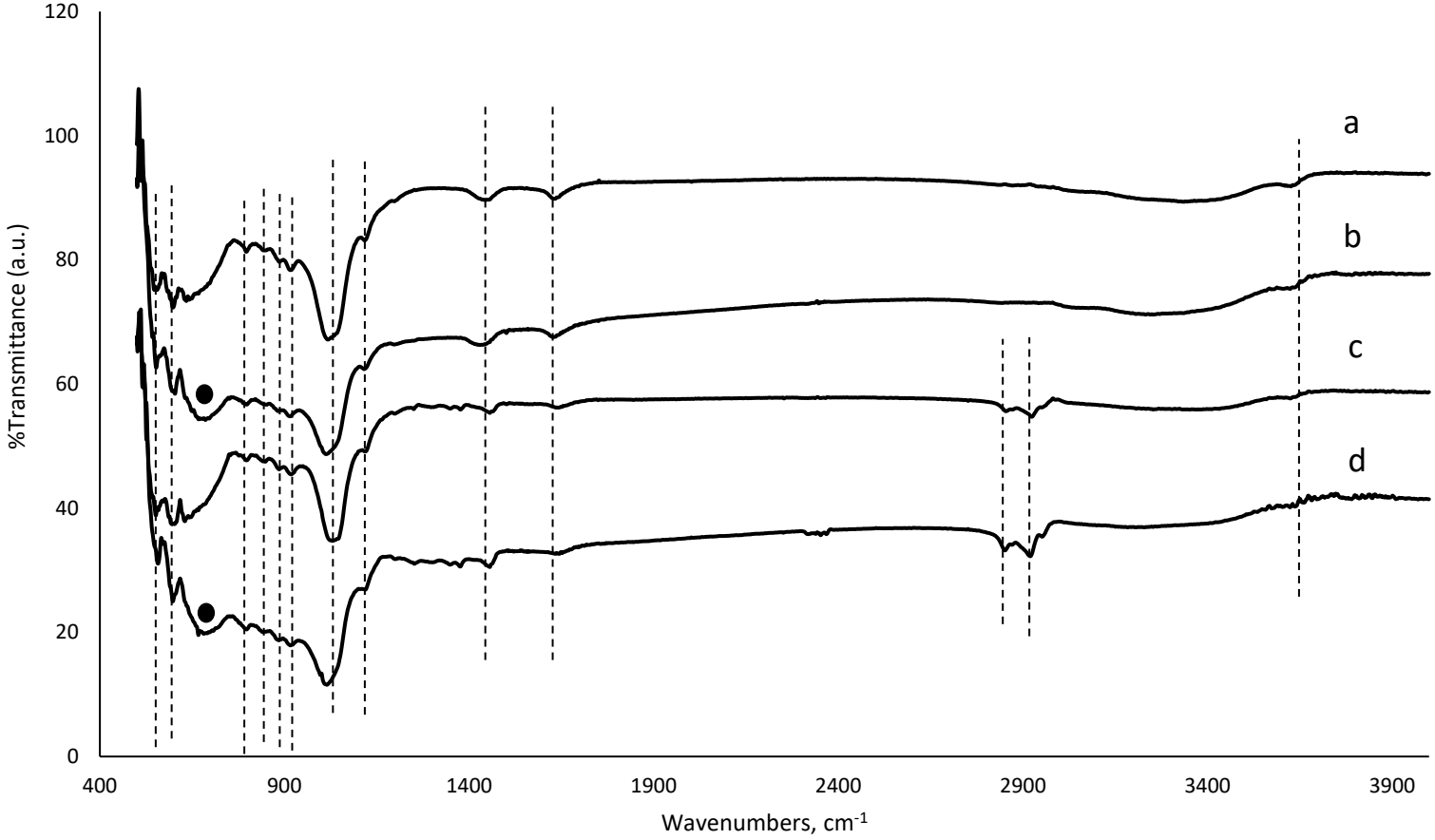

Figure 30: FTIR spectra of (a) Fe_3O_4/Bent/rGO before adsorption (b) Fe_3O_4/Bent/MWCNTs before adsorption (c) Fe_3O_4/Bent/rGO after adsorption (d) Fe_3O_4/Bent/MWCNTs after adsorption.

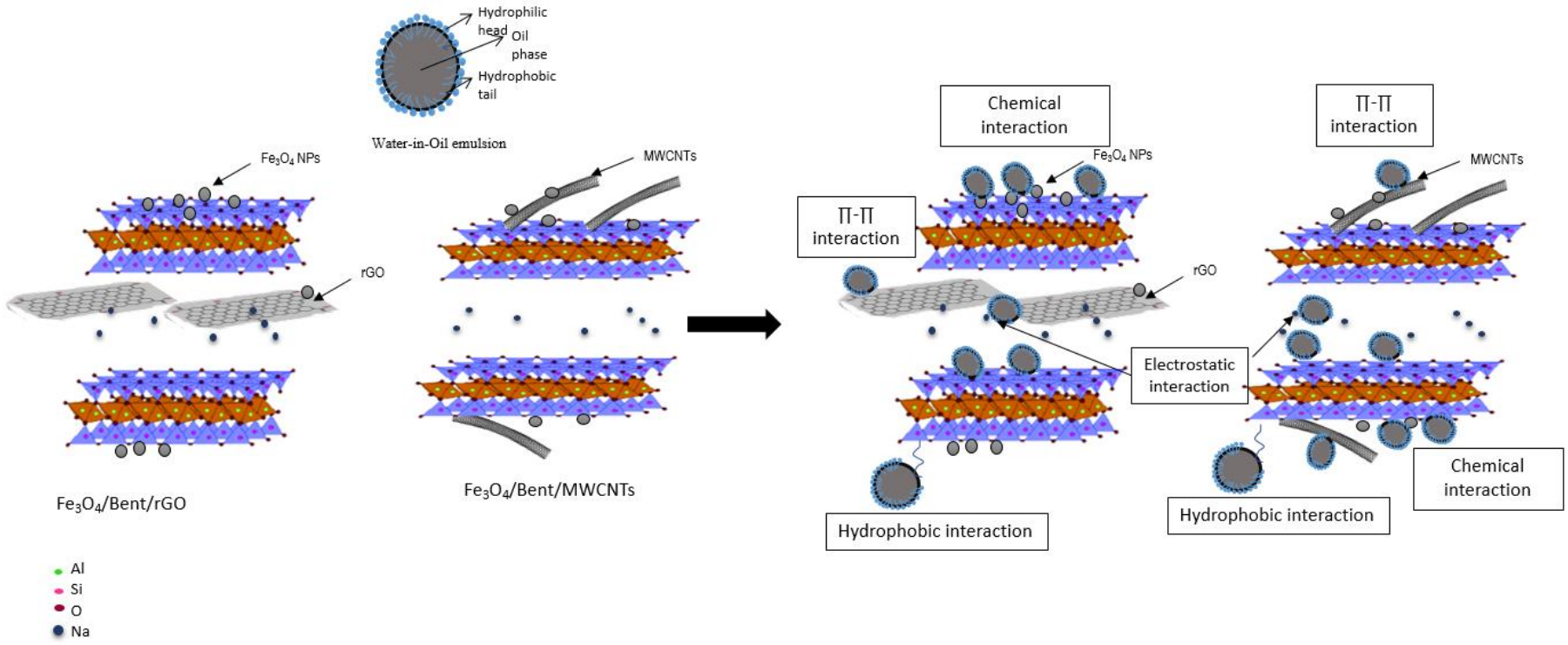

Figure 31: The possible adsorption mechanism of oil onto the novel composites.

4.5 Comparison of adsorbents

The novel composites reported in this work (Fe_3O_4/Bent/rGO and Fe_3O_4/Bent/MWCNTs) were developed to enhance oil uptake from emulsified oil solution. For this purpose, the removal capability of Fe_3O_4/bentonite composite, which is reported in the literature, was examined for oil removal and compared to the performance of the developed composites. The maximum adsorption capacity of Fe_3O_4/bentonite is 53.64 mg/g (obtained from Langmuir isotherm model) at pH 6.5, dosage 0.1 g, time 180 minutes under initial emulsified oil concentration between 66 mg/l and 170 mg/l. In addition, Fe_3O_4/bentonite reached equilibrium in 90 minutes in which no further adsorption occurs after the indicated time. On the other hand, the novel composites (Fe_3O_4/Bent/rGO and Fe_3O_4/Bent/MWCNTs) attained an adsorption capacity towards emulsified oil of 81.65 mg/g and 77.12 mg/g, respectively, under similar Fe_3O_4/bentonite adsorption experimental conditions. Furthermore, sips isotherm model best fitted the experimental data for Fe_3O_4/Bent/rGO and Fe_3O_4/Bent/MWCNTs. Whereas Langmuir isotherm model best fitted the adsorption data of emulsified oil onto Fe_3O_4/bentonite. This indicates that the adsorption mechanism and the type of interaction was affected. Furthermore, all composites followed PSO kinetic model, which suggests a chemisorption process. The intraparticle diffusion model for all adsorbents confirm the existence of three stages. first stage is the instantaneous adsorption of oil molecules represented by the sharp rise in qt with $t^{0.5}$. In this stage, the adsorption is controlled by external mass transfer. The second stage is a curved portion, which shows a slow adsorption rate controlled by intraparticle diffusion. The third stage represents the equilibrium stage where internal diffusion occurs within the adsorbents' pores. It can be observed that the curved portion in intraparticle diffusion model for Fe_3O_4/Bent/MWCNTs is closer to linearity compared

to other composites. This indicate that MWCNTs have a significant role in oil adsorption.

The adsorption mechanism of emulsified oil adsorption onto Fe_3O_4/Bentonite was mainly chemical interaction, electrostatic interaction, hydrophobic interaction, and hydrogen bonding. Whereas the adsorption mechanism of novel composites was mainly chemical, electrostatic, hydrophobic and π-π interaction. The absence of hydrogen bonding might be involved in the Fe_3O_4/Bent/rGO and Fe_3O_4/Bent/MWCNTs adsorption mechanism but might be insignificant.

Among all adsorbents, Fe_3O_4/Bent/rGO attained the highest adsorption capacity. However, the batch adsorption experiments showed that Fe_3O_4/Bent/MWCNTs attained slightly higher removal capability compared to Fe_3O_4/Bent/rGO at higher oil concentration and contact time. This could be explained by the observed higher Fe_3O_4/Bent/MWCNTs pore volume compared to Fe_3O_4/Bent/rGO. Moreover, the amount of Fe_3O_4 NPs in Fe_3O_4/Bent/MWCNTs were less than their amount in Fe_3O_4/Bent/rGO and Fe_3O_4/Bentonite as indicated by the EDX analysis, and TEM and SEM images despite using the same amount of iron-based precursors. This also contributed to more surface availability on Fe_3O_4/Bent/MWCNTs as observed in BET analysis (Table 6). Consequently, slightly higher adsorption of oil was observed onto Fe_3O_4/Bent/MWCNTs compared to the other composites. The observed maximum adsorption capacities of emulsified oil onto the novel composites were further compared to the ones reported in the literature as shown in Table 14. The results clearly show that the novel composites developed in this study exhibit superior adsorption capability and outperforms all the reported adsorbents towards emulsified oil. These observations further affirm the potential of the Fe_3O_4/Bent/MWCNTs and Fe_3O_4/Bent/rGO composites to be utilized for oil removal.

In fluidized bed reactor application, Fe_3O_4/Bent/rGO outperform Fe_3O_4 NPs, Fe_3O_4/Bentonite, and Fe_3O_4/Bent/MWCNTs, which might be due to the large particle size that Fe_3O_4/Bent/rGO possess.

The adsorption mechanism of oil onto Fe_3O_4/Bentonite was mainly electrostatic, hydrogen, hydrophobic and chemical interaction. Whereas, the adsorption of oil onto Fe_3O_4/Bent/rGO and Fe_3O_4/Bent/MWCNTs was mainly through electrostatic, hydrophobic, chemical and π-π interaction. It is observed that the addition of carbnonceous material to Fe_3O_4/Bentonite eliminated the interaction of the novel composites with oil through hydrogen bonding.

Table 14: Comparsion between the performance of different adsorbent twoards emlusifed oil.

Adsorbent	**Oil type**	**Adsorption capacity mg/g**	**Ref.**
Amberlite XAD 7	Gasoline	11.86	[16]
Optipore L 493		9.51	
Lewatit AF 5		13.35	
Bentonite	Diesel	38.5	[201]
Org-bentonite		48	
Fe_3O_4/Bentonite		53.64	This work
Fe_3O_4/Bent/rGO		81.65	This work
Fe_3O_4/Bent/MWCNTs		77.12	This work

CHAPTER 5: CONCLUSION AND FUTURE PERSPECTIVE

Oil and gas industry generates significate amounts of PW that contains various organic and inorganic contaminants, such as PAH, heavy metals, phenols, etc. The direct discharge of PW threats the aquatic ecosystem and exacerbate water scarcity issue. Therefore, proper management and treatment of PW is required.

The literature review indicated that PW management and proper treatment is required due to its content of toxic, persistent and hazardous compounds, especially with the increase in its amount in old and depleted fields. Treatment technologies discussed in this work such as membrane, and EC are promising, but still significant efforts are required to make them economically feasible. Adsorption stands among the most effective technologies that can reduce the contaminants concentration significantly with the use of the suitable adsorbent. Besides, adsorption process is cost effective and known for its simplicity and ease of operation. A suitable adsorbent should be able to remove high quantities of contaminants, non-toxic, inexpensive, environmentally friendly, and can be regenerated and used for several cycles. CMs meet these criteria, however, its dispersity in aqueous solution and relatively low adsorption capacity towards organic compounds limit their application. More recently, composites gained a great deal of attention due to their superior adsorption capacity towards several classification of organic contaminants and enhanced physiochemical properties compared to the composite individual components. Moreover, the studies related to the composite's utilization for oil removal, which is a major constituent of PW are rare in the literature.

In this work, Fe_3O_4/Bentonite was used to remove emulsified oil, which is a good representation of PW organic concentration. Moreover, new composites were developed in this study, which are Fe_3O_4/Bent/rGO and Fe_3O_4/Bent/MWCNTs. The

new composites adsorptive behavior was compared to the performance of Fe_3O_4/Bentonite by examining different experimental parameters.

The characterization analysis showed that Fe_3O_4 NPs were less in quantity over Fe_3O_4/Bent/MWCNTs despite using the same amount of iron-based precursor. This contributed to the increase in its thermal stability compared to other composites at higher temperatures as revealed by TGA. However, Fe_3O_4/Bent/rGO attained the highest thermal stability at temperature less than 100 ℃. Furthermore, the SEM images revealed that bentonite acts as a support for Fe_3O_4 NPs, rGO and MWCNTs. In addition, it is expected that rGO is formed on the surface of bentonite as indicated by the wrinkled edge structure and/or intercalated into bentonite layers. TEM images showed a good distribution of Fe_3O_4 NPs over the three composites. Moreover, the particle size of Fe_3O_4 NPs was estimated to be 13.55 nm, 11.6 nm, and 8.83 nm for Fe_3O_4/Bentonite, Fe_3O_4/Bent/rGO and Fe_3O_4/Bent/MWCNTs, respectively.

The adsorption results showed that Fe_3O_4/Bentonite was able to remove almost 67% of oil after 90 min. The adsorption data were best described by Langmuir isotherm model with a maximum adsorption capacity of 53.64 mg/g. Whereas, Fe_3O_4/Bent/rGO and Fe_3O_4/Bent/MWCNTs followed Sips isotherm model with a maximum adsorption capacity of 81.65 mg/g and 77.12 mg/g, respectively. Moreover, the composites were able to reach equilibrium time in 50 minutes, which is less than the equilibrium time reached by Fe_3O_4/Bentonite composite. The kinetics studies showed that all composites followed PSO kinetic model confirming a chemisorption process. In fluidized bed reactor, Fe_3O_4/Bent/rGO outperform all composites reported in this study, which is mainly due to its particle size rather than its specific surface area and pore volume.

The adsorption mechanism of oil onto Fe_3O_4/Bentonite was mainly electrostatic, hydrogen, hydrophobic and chemical interaction. Whereas the adsorption of oil onto

Fe_3O_4/Bent/rGO and Fe_3O_4/Bent/MWCNTs was mainly through electrostatic, hydrophobic, chemical and π-π interaction. It is believed that the high adsorption capacity that the developed composites possess is due to the π-π interaction that the carbonaceous material provided. The above findings well manifest that the prepared composite is promising in effectively purifying oily water.

Future work should assess the regeneration through different techniques including chemical, ultrasound and MW regeneration. In addition, the composites morphology, physiochemical after regeneration should be investigated to reveal the composite stability. The performance of the developed composites in multipollutant system and real industrial wastewater with high COD value should be investigated. Other parameters such as salinity, TDS, temperature should be assessed. Moreover, the composite adsorption capability in fluidized bed reactor connected to a regeneration column under various parameters need to be assessed. Finally, plans should be implemented to deal with the spent adsorbents in which they cannot be regenerated further.

References

[1] F. Yu, X. Bai, M. Liang, J. Ma, Recent progress on metal-organic framework-derived porous carbon and its composite for pollutant adsorption from liquid phase, Chemical Engineering Journal, 405 (2021) 126960.

[2] T. Al-Farra, Water Security in the Gulf Region, in, Al Jazeera Center for Studies, 2015.

[3] D. Ewis, A. Benamor, M.M. Ba-Abbad, M. Nasser, M. El-Naas, H. Qiblawey, Removal of Oil Content from Oil-Water Emulsions Using Iron Oxide/Bentonite Nano Adsorbents, Journal of Water Process Engineering, 38 (2020) 101583.

[4] M. Mofokeng, L.N. Nthunya, L. Gutierrez, P. Matabola, S. Mishra, E.N. Nxumalo, Perfluorooctyltriethoxy silane and carbon nanotubes-modified PVDF superoleophilic nanofibre membrane for oil-in-water adsorption and recovery, Journal of Environmental Chemical Engineering, 8 (2020) 104497.

[5] W. Chao, S. Wang, Y. Li, G. Cao, Y. Zhao, X. Sun, C. Wang, S.-H. Ho, Natural sponge-like wood-derived aerogel for solar-assisted adsorption and recovery of high-viscous crude oil, Chemical Engineering Journal, 400 (2020) 125865.

[6] A. Echchelh, T. Hess, R. Sakrabani, Reusing oil and gas produced water for irrigation of food crops in drylands, Agricultural Water Management, 206 (2018) 124-134.

[7] M.A. Al-Ghouti, M.A. Al-Kaabi, M.Y. Ashfaq, D.A. Da'na, Produced water characteristics, treatment and reuse: A review, Journal of Water Process Engineering, 28 (2019) 222-239.

[8] M.H. Ibrahim, D.T. Moussa, M.H. El-Naas, M.S. Nasser, A perforated electrode design for passivation reduction during the electrochemical treatment of produced water, Journal of Water Process Engineering, 33 (2020).

[9] Abass A. Olajire, Recent advances on the treatment technology of oil and gas produced water for sustainable energy industry-mechanistic aspects and process chemistry perspectives, Chemical Engineering Journal Advances, 4 (2020) 100049.

[10] T. Zhang, C. Zhang, G. Zhao, C. Li, L. Liu, J. Yu, F. Jiao, Electrospun composite membrane with superhydrophobic-superoleophilic for efficient water-in-oil emulsion separation and oil adsorption, Colloids and Surfaces A: Physicochemical and Engineering Aspects, 602 (2020) 125158.

[11] U.S.E.P. Agency, NPDES Compliance Inspection Manual in, 2017, pp. 1-43.

[12] Y. Deng, C. Peng, M. Dai, D. Lin, I. Ali, S.S. Alhewairini, X. Zheng, G. Chen, J. Li, I. Naz, Recent development of super-wettable materials and their applications in oil-water separation, Journal of Cleaner Production, 266 (2020) 121624.

[13] D. Ewis, N.A. Ismail, M. Hafiz, A. Benamor, A.H. Hawari, Nanoparticles functionalized ceramic membranes: fabrication, surface modification, and performance, Environmental Science and Pollution Research, (2021).

[14] M. Zhang, P. Gu, S. Yan, Y. Liu, G. Zhang, Effective removal of radioactive cobalt from aqueous solution by a layered metal sulfide adsorbent: Mechanism, adsorption performance, and practical application, Separation and Purification Technology, 256 (2021) 117775.

[15] S.-Y. Liu, J. Gao, B. Qu, Y.-J. Yang, X.J.W.m. Xin, research, Kinetic models for the adsorption of lead ions by steel slag, 28 (2010) 748-753.

[16] H. Albatrni, H. Qiblawey, F. Almomani, S. Adham, M. Khraisheh, Polymeric adsorbents for oil removal from water, Chemosphere, 233 (2019) 809-817.

[17] T. Shahnaz, C. Patra, V. Sharma, N. Selvaraju, A comparative study of raw, acid-modified and EDTA-complexed Acacia auriculiformis biomass for the removal of hexavalent chromium, Chemistry and Ecology, 36 (2020) 360-381.

[18] G. Crini, Non-conventional low-cost adsorbents for dye removal: a review, Bioresour Technol, 97 (2006) 1061-1085.

[19] E.I. Unuabonah, A. Taubert, Clay–polymer nanocomposites (CPNs): Adsorbents of the future for water treatment, Applied Clay Science, 99 (2014) 83-92.

[20] M.A. Sakr, M.G.A. Mohamed, R. Wu, S.R. Shin, D. Kim, K. Kim, S. Siddiqua, Development of bentonite-gelatin nanocomposite hybrid hydrogels for tissue engineering, Applied Clay Science, 199 (2020) 105860.

[21] D.O.B. Apriandanu, Y. Yulizar, CuO-bentonite-gold nanocomposites: Facile green preparation and their characterization, Materials Letters, 284 (2021) 128911.

[22] R. Gusain, K. Gupta, P. Joshi, O.P. Khatri, Adsorptive removal and photocatalytic degradation of organic pollutants using metal oxides and their composites: A comprehensive review, Adv Colloid Interface Sci, 272 (2019) 102009.

[23] B.S. Damasceno, A.F.V. da Silva, A.C.V. de Araújo, Dye adsorption onto magnetic and superparamagnetic Fe3O4 nanoparticles: A detailed comparative study, Journal of Environmental Chemical Engineering, 8 (2020) 103994.

[24] M. Yu, L. Wang, L. Hu, Y. Li, D. Luo, S. Mei, Recent applications of magnetic composites as extraction adsorbents for determination of environmental pollutants, TrAC Trends in Analytical Chemistry, 119 (2019) 115611.

[25] F. Marrakchi, B.H. Hameed, E.H. Hummadi, Mesoporous biohybrid epichlorohydrin crosslinked chitosan/carbon–clay adsorbent for effective cationic and anionic dyes adsorption, International Journal of Biological Macromolecules, 163 (2020) 1079-1086.

[26] L. Qin, W.-f. Liu, X.-g. Liu, Y.-z. Yang, L.-a. Zhang, A review of nano-carbon based molecularly imprinted polymer adsorbents and their adsorption mechanism, New Carbon Materials, 35 (2020) 459-485.

[27] X. Liang, Y. Lu, Z. Li, C. Yang, C. Niu, X. Su, Bentonite/carbon composite as highly recyclable adsorbents for alkaline wastewater treatment and organic dye removal, Microporous and Mesoporous Materials, 241 (2017) 107-114.

[28] A. Fakhru'l-Razi, A. Pendashteh, L.C. Abdullah, D.R.A. Biak, S.S. Madaeni, Z.Z. Abidin, Review of technologies for oil and gas produced water treatment, Journal of Hazardous Materials, 170 (2009) 530-551.

[29] J. Zheng, B. Chen, W. Thanyamanta, K. Hawboldt, B. Zhang, B. Liu, Offshore produced water management: A review of current practice and challenges in harsh/Arctic environments, Marine Pollution Bulletin, 104 (2016) 7-19.

[30] P.J.C. Tibbetts, I.T. Buchanan, L.J. Gawel, R. Large, A Comprehensive Determination of Produced Water Composition, in: J.P. Ray, F.R. Engelhardt (Eds.) Produced Water: Technological/Environmental Issues and Solutions, Springer US, Boston, MA, 1992, pp. 97-112.

[31] J.P. Fillo, S.M. Koraido, J.M. Evans, Sources, Characteristics, and Management of Produced Waters from Natural Gas Production and Storage Operations, in: J.P. Ray, F.R. Engelhardt (Eds.) Produced Water: Technological/Environmental Issues and Solutions, Springer US, Boston, MA, 1992, pp. 151-161.

[32] K.L. Benko, J.E. Drewes, Produced Water in the Western United States: Geographical Distribution, Occurrence, and Composition, Environmental Engineering Science, 25 (2008) 239-246.

[33] D.B. MacGowan, R.C. Surdam, Difunctional carboxylic acid anions in oilfield waters, Organic Geochemistry, 12 (1988) 245-259.

[34] H.S. Dórea, J.R.L. Bispo, K.A.S. Aragão, B.B. Cunha, S. Navickiene, J.P.H. Alves, L.P.C. Romão, C.A.B. Garcia, Analysis of BTEX, PAHs and metals in the oilfield produced water in the State of Sergipe, Brazil, Microchemical Journal, 85

(2007) 234-238.

[35] D. Callaghan, W.E. Baumgartner, Characterization of Residual Hydrocarbons in Produced Water Discharged From Gas Production Platforms, in, 1990.

[36] S. Johnsen, T.I. Røe Utvik, E. Garland, B. de Vals, J. Campbell, Environmental fate and effect of contaminants in produced water, in: SPE International Conference on Health, Safety, and Environment in Oil and Gas Exploration and Production, Society of Petroleum Engineers, 2004.

[37] W.U. Rahman, M.D. Khan, M.Z. Khan, G. Halder, Anaerobic biodegradation of benzene-laden wastewater under mesophilic environment and simultaneous recovery of methane-rich biogas, Journal of Environmental Chemical Engineering, 6 (2018) 2957-2964.

[38] L. Sellaoui, M. Kehili, E.C. Lima, P.S. Thue, A. Bonilla-Petriciolet, A.B. Lamine, G.L. Dotto, A. Erto, Adsorption of phenol on microwave-assisted activated carbons: Modelling and interpretation, Journal of Molecular Liquids, 274 (2019) 309-314.

[39] S.B. Kane Driscoll, M.E. McArdle, C.A. Menzie, M. Reiss, J.A. Steevens, A framework for using dose as a metric to assess toxicity of fish to PAHs, Ecotoxicology and Environmental Safety, 73 (2010) 486-490.

[40] P. Bauerová, T. Krajzingrová, M. Těšický, H. Velová, J. Hraníček, S. Musil, J. Svobodová, T. Albrecht, M. Vinkler, Longitudinally monitored lifetime changes in blood heavy metal concentrations and their health effects in urban birds, Science of The Total Environment, 723 (2020) 138002.

[41] P.J. McCabe, Oil and Natural Gas: Global Resources, in: R. Malhotra (Ed.) Fossil Energy: Selected Entries from the Encyclopedia of Sustainability Science and Technology, Springer New York, New York, NY, 2013, pp. 7-23.

[42] J.M. Dickhout, J. Moreno, P. Biesheuvel, L. Boels, R.G. Lammertink, W.M.J.J.o.c.

de Vos, i. science, Produced water treatment by membranes: a review from a colloidal perspective, 487 (2017) 523-534.

[43] P.J.J.F.E. McCabe, Oil and natural gas: global resources, (2020) 5-16.

[44] G.W.J.G.W.I.P. Intelligence, Produced Water Market: Opportunities in the oil, shale and gas sectors in North America, (2011).

[45] J.M. Dickhout, J. Moreno, P.M. Biesheuvel, L. Boels, R.G.H. Lammertink, W.M. de Vos, Produced water treatment by membranes: A review from a colloidal perspective, Journal of Colloid and Interface Science, 487 (2017) 523-534.

[46] M. al-kaabi, Enhancing produced water quality using modified activated carbon in: College of Arts and Sciences Qatar University 2016.

[47] Z. Khatib, P.J.J.o.P.T. Verbeek, Water to value-produced water management for sustainable field development of mature and green fields, 55 (2003) 26-28.

[48] E.T. Igunnu, G.Z. Chen, Produced water treatment technologies, International Journal of Low-Carbon Technologies, 9 (2014) 157-177.

[49] F.C. Dolan, T.Y. Cath, T.S. Hogue, Assessing the feasibility of using produced water for irrigation in Colorado, Science of The Total Environment, 640-641 (2018) 619-628.

[50] Z.-h. Liu, Y. Kanjo, S. Mizutani, Removal mechanisms for endocrine disrupting compounds (EDCs) in wastewater treatment — physical means, biodegradation, and chemical advanced oxidation: A review, Science of The Total Environment, 407 (2009) 731-748.

[51] C. Igwe, A. Saadi, Optimal Options for Treatment of Produced Water in Offshore Petroleum Platforms, Journal of Pollution Effects & Control, 01 (2013).

[52] D.T. Moussa, M.H. El-Naas, M. Nasser, M.J. Al-Marri, A comprehensive review of electrocoagulation for water treatment: Potentials and challenges, Journal of

Environmental Management, 186 (2017) 24-41.

[53] N. Esmaeilirad, K. Carlson, P.O.J.J.o.h.m. Ozbek, Influence of softening sequencing on electrocoagulation treatment of produced water, 283 (2015) 721-729.

[54] S. Zhao, G. Huang, G. Cheng, Y. Wang, H.J.D. Fu, Hardness, COD and turbidity removals from produced water by electrocoagulation pretreatment prior to reverse osmosis membranes, 344 (2014) 454-462.

[55] P.K. Holt, G.W. Barton, C.A.J.C. Mitchell, The future for electrocoagulation as a localised water treatment technology, 59 (2005) 355-367.

[56] E. Bazrafshan, L. Mohammadi, A. Ansari-Moghaddam, A.H.J.J.o.e.h.s. Mahvi, engineering, Heavy metals removal from aqueous environments by electrocoagulation process–a systematic review, 13 (2015) 1-16.

[57] M.Y. Mollah, P. Morkovsky, J.A. Gomes, M. Kesmez, J. Parga, D.L.J.J.o.h.m. Cocke, Fundamentals, present and future perspectives of electrocoagulation, 114 (2004) 199-210.

[58] S. Al-Amshawee, M.Y.B.M. Yunus, A.A.M. Azoddein, D.G. Hassell, I.H. Dakhil, H.A. Hasan, Electrodialysis desalination for water and wastewater: A review, Chemical Engineering Journal, 380 (2020) 122231.

[59] V.A. Shaposhnik, K. Kesore, An early history of electrodialysis with permselective membranes, Journal of Membrane Science, 136 (1997) 35-39.

[60] P.A. Sosa-Fernandez, J.W. Post, H. Bruning, F.A.M. Leermakers, H.H.M. Rijnaarts, Electrodialysis-based desalination and reuse of sea and brackish polymer-flooding produced water, Desalination, 447 (2018) 120-132.

[61] A. Campione, L. Gurreri, M. Ciofalo, G. Micale, A. Tamburini, A. Cipollina, Electrodialysis for water desalination: A critical assessment of recent developments on process fundamentals, models and applications, Desalination, 434 (2018) 121-160.

[62] An Integrated Framework for Treatment and Management of Produced Water: Technical Assessment Of Produced Water Treatment Technologies in: s. EDITION (Ed.) RPSEA Project 07122-12 2009

[63] M. Ebrahimi, K.S. Ashaghi, L. Engel, D. Willershausen, P. Mund, P. Bolduan, P. Czermak, Characterization and application of different ceramic membranes for the oil-field produced water treatment, Desalination, 245 (2009) 533-540.

[64] M. Ebrahimi, D. Willershausen, K.S. Ashaghi, L. Engel, L. Placido, P. Mund, P. Bolduan, P. Czermak, Investigations on the use of different ceramic membranes for efficient oil-field produced water treatment, Desalination, 250 (2010) 991-996.

[65] T. Bilstad, E. Espedal, Membrane separation of produced water, Water Science and Technology, 34 (1996) 239-246.

[66] Q. Alsalhy, Produced Water Treatment Using Ultrafiltration and Nanofiltration Membranes, Al-Khwarizmi Engineering Journal, 12 (2016) 10-18.

[67] S. Mondal, S.R. Wickramasinghe, Produced water treatment by nanofiltration and reverse osmosis membranes, Journal of Membrane Science, 322 (2008) 162-170.

[68] R.A. Maltos, J. Regnery, N. Almaraz, S. Fox, M. Schutter, T.J. Cath, M. Veres, B.D. Coday, T.Y. Cath, Produced water impact on membrane integrity during extended pilot testing of forward osmosis – reverse osmosis treatment, Desalination, 440 (2018) 99-110.

[69] S. Tang, L. Zhang, Y. Peng, J. Liu, Z. Zhang, Fenton cleaning strategy for ceramic membrane fouling in wastewater treatment, Journal of Environmental Sciences, 85 (2019) 189-199.

[70] M.A. Islam, M.R. Awual, M.J. Angove, A review on nickel(II) adsorption in single and binary component systems and future path, Journal of Environmental Chemical Engineering, 7 (2019) 103305.

[71] M. Plebon, M. Saad, S. Fraser, FURTHER ADVANCES IN PRODUCED WATER DE OILING UTILIZING A TECHNOLOGY THAT REMOVES AND RECOVERS DISPERSED OIL IN PRODUCED WATER 2 MICRONS AND LARGER, (2005).

[72] J. Ren, Z. Zhu, Y. Qiu, F. Yu, J. Ma, J. Zhao, Magnetic field assisted adsorption of pollutants from an aqueous solution: A review, Journal of Hazardous Materials, 408 (2021) 124846.

[73] S.M.R. Shaikh, M.S. Nasser, I. Hussein, A. Benamor, S.A. Onaizi, H. Qiblawey, Influence of polyelectrolytes and other polymer complexes on the flocculation and rheological behaviors of clay minerals: A comprehensive review, Separation and Purification Technology, 187 (2017) 137-161.

[74] F. Bergaya, G. Lagaly, Chapter 1 - General Introduction: Clays, Clay Minerals, and Clay Science, in: F. Bergaya, G. Lagaly (Eds.) Developments in Clay Science, Elsevier, 2013, pp. 1-19.

[75] H. Cheng, Q. Zhu, Z. Xing, Adsorption of ammonia nitrogen in low temperature domestic wastewater by modification bentonite, Journal of Cleaner Production, 233 (2019) 720-730.

[76] G.L. Li, C.H. Zhou, S. Fiore, W.H. Yu, Interactions between microorganisms and clay minerals: New insights and broader applications, Applied Clay Science, 177 (2019) 91-113.

[77] A. Busch, S.J.T. Hangx, J.D. Marshall, H.M. Wentinck, Swelling clay minerals and containment risk assessment for the storage seal of the Peterhead CCS project, International Journal of Greenhouse Gas Control, 94 (2020) 102924.

[78] M.S. Nasser, S.A. Onaizi, I.A. Hussein, M.A. Saad, M.J. Al-Marri, A. Benamor, Intercalation of ionic liquids into bentonite: Swelling and rheological behaviors,

Colloids and Surfaces A: Physicochemical and Engineering Aspects, 507 (2016) 141-151.

[79] Y. Zhang, X. Song, Y. Xu, H. Shen, X. Kong, H. Xu, Utilization of wheat bran for producing activated carbon with high specific surface area via NaOH activation using industrial furnace, Journal of Cleaner Production, 210 (2019) 366-375.

[80] K.S. Ahmad, Adsorption Evaluation of Herbicide Iodosulfuron Followed by Cedrus deodora Sawdust-Derived Activated Carbon Removal, Soil and Sediment Contamination: An International Journal, 28 (2019) 65-80.

[81] E. Şeyma Seyrek, E. Yalçin, M. Yilmaz, B. Vural Kök, H. Arslanoğlu, Effect of activated carbon obtained from vinasse and marc on the rheological and mechanical characteristics of the bitumen binders and hot mix asphalts, Construction and Building Materials, 240 (2020) 117921.

[82] J.M.V. Nabais, C. Laginhas, M.M.L.R. Carrott, P.J.M. Carrott, J.E.C. Amorós, A.V.N. Gisbert, Surface and porous characterisation of activated carbons made from a novel biomass precursor, the esparto grass, Applied Surface Science, 265 (2013) 919-924.

[83] J.C. Lee, B.H. Lee, B.G. Kim, M.J. Park, D.Y. Lee, I.H. Kuk, H. Chung, H.S. Kang, H.S. Lee, D.H. Ahn, The effect of carbonization temperature of PAN fiber on the properties of activated carbon fiber composites, Carbon, 35 (1997) 1479-1484.

[84] M. Dizbay-Onat, U.K. Vaidya, C.T. Lungu, Preparation of industrial sisal fiber waste derived activated carbon by chemical activation and effects of carbonization parameters on surface characteristics, Industrial Crops and Products, 95 (2017) 583-590.

[85] Y.-R. Son, S.-J. Park, Preparation and characterization of mesoporous activated carbons from nonporous hard carbon via enhanced steam activation strategy, Materials

Chemistry and Physics, 242 (2020) 122454.

[86] X. Lu, J. Jiang, K. Sun, X. Xie, Y. Hu, Surface modification, characterization and adsorptive properties of a coconut activated carbon, Applied Surface Science, 258 (2012) 8247-8252.

[87] I. Ali, V.K. Gupta, Advances in water treatment by adsorption technology, Nature Protocols, 1 (2006) 2661-2667.

[88] M.F. Hassan, M.A. Sabri, H. Fazal, A. Hafeez, N. Shezad, M. Hussain, Recent trends in activated carbon fibers production from various precursors and applications—A comparative review, Journal of Analytical and Applied Pyrolysis, 145 (2020) 104715.

[89] H. Khayyam, R.N. Jazar, S. Nunna, G. Golkarnarenji, K. Badii, S.M. Fakhrhoseini, S. Kumar, M. Naebe, PAN precursor fabrication, applications and thermal stabilization process in carbon fiber production: Experimental and mathematical modelling, Progress in Materials Science, 107 (2020) 100575.

[90] F. Wei, H.-f. Zhang, X.-j. He, H. Ma, S.-a. Dong, X.-y. Xie, Synthesis of porous carbons from coal tar pitch for high-performance supercapacitors, New Carbon Materials, 34 (2019) 132-139.

[91] F.M. Marsin, W.A. Wan Ibrahim, H.R. Nodeh, M.M. Sanagi, New magnetic oil palm fiber activated carbon-reinforced polypyrrole solid phase extraction combined with gas chromatography-electron capture detection for determination of organochlorine pesticides in water samples, Journal of Chromatography A, 1612 (2020) 460638.

[92] X. Duan, C. Srinivasakannan, X. Wang, F. Wang, X. Liu, Synthesis of activated carbon fibers from cotton by microwave induced H3PO4 activation, Journal of the Taiwan Institute of Chemical Engineers, 70 (2017) 374-381.

[93] A. Bhatnagar, W. Hogland, M. Marques, M. Sillanpää, An overview of the modification methods of activated carbon for its water treatment applications, Chemical Engineering Journal, 219 (2013) 499-511.

[94] M.M. Hassan, C.M. Carr, Biomass-derived porous carbonaceous materials and their composites as adsorbents for cationic and anionic dyes: A review, Chemosphere, 265 (2021) 129087.

[95] N.H. Abdullah, K. Shameli, E.C. Abdullah, L.C. Abdullah, Solid matrices for fabrication of magnetic iron oxide nanocomposites: Synthesis, properties, and application for the adsorption of heavy metal ions and dyes, Composites Part B: Engineering, 162 (2019) 538-568.

[96] B.O. Otunola, O.O. Ololade, A review on the application of clay minerals as heavy metal adsorbents for remediation purposes, Environmental Technology & Innovation, 18 (2020) 100692.

[97] H. Najafi, S. Farajfaed, S. Zolgharnian, S.H. Mosavi Mirak, N. Asasian-Kolur, S. Sharifian, A comprehensive study on modified-pillared clays as an adsorbent in wastewater treatment processes, Process Safety and Environmental Protection, 147 (2021) 8-36.

[98] T. E, D. Ma, S. Yang, X. Hao, Graphene oxide-montmorillonite/sodium alginate aerogel beads for selective adsorption of methylene blue in wastewater, Journal of Alloys and Compounds, 832 (2020) 154833.

[99] B.A. Fil, Isotherm, kinetic, and thermodynamic studies on the adsorption behavior of malachite green dye onto montmorillonite clay, Particulate Science and Technology, 34 (2016) 118-126.

[100] A. Liu, W. Zhou, K. Shen, J. Liu, X. Zhang, One-pot hydrothermal synthesis of hematite-reduced graphene oxide composites for efficient removal of malachite green

from aqueous solution, RSC Advances, 5 (2015) 17336-17342.

[101] M.J. Ahmed, B.H. Hameed, E.H. Hummadi, Review on recent progress in chitosan/chitin-carbonaceous material composites for the adsorption of water pollutants, Carbohydrate Polymers, 247 (2020) 116690.

[102] M. Khatamian, B. Divband, R. Shahi, Ultrasound assisted co-precipitation synthesis of Fe3O4/ bentonite nanocomposite: Performance for nitrate, BOD and COD water treatment, Journal of Water Process Engineering, 31 (2019) 100870.

[103] F.I. El-Dib, F.M. Tawfik, G. Eshaq, H.H.H. Hefni, A.E. ElMetwally, Remediation of distilleries wastewater using chitosan immobilized Bentonite and Bentonite based organoclays, International Journal of Biological Macromolecules, 86 (2016) 750-755.

[104] G.L. Dotto, F.K. Rodrigues, E.H. Tanabe, R. Fröhlich, D.A. Bertuol, T.R. Martins, E.L. Foletto, Development of chitosan/bentonite hybrid composite to remove hazardous anionic and cationic dyes from colored effluents, Journal of Environmental Chemical Engineering, 4 (2016) 3230-3239.

[105] S.H. Vithalkar, R.M. Jugade, Adsorptive removal of crystal violet from aqueous solution by cross-linked chitosan coated bentonite, Materials Today: Proceedings, 29 (2020) 1025-1032.

[106] D.S. Tong, C.W. Wu, M.O. Adebajo, G.C. Jin, W.H. Yu, S.F. Ji, C.H. Zhou, Adsorption of methylene blue from aqueous solution onto porous cellulose-derived carbon/montmorillonite nanocomposites, Applied Clay Science, 161 (2018) 256-264.

[107] W. Xu, Y. Chen, W. Zhang, B. Li, Fabrication of graphene oxide/bentonite composites with excellent adsorption performances for toluidine blue removal from aqueous solution, Advanced Powder Technology, 30 (2019) 493-501.

[108] Y. Kong, L. Wang, Y. Ge, H. Su, Z. Li, Lignin xanthate resin–bentonite clay

composite as a highly effective and low-cost adsorbent for the removal of doxycycline hydrochloride antibiotic and mercury ions in water, Journal of Hazardous Materials, 368 (2019) 33-41.

[109] A. Rotaru, C. Cojocaru, I. Cretescu, M. Pinteala, D. Timpu, L. Sacarescu, V. Harabagiu, Performances of clay aerogel polymer composites for oil spill sorption: Experimental design and modeling, Separation and Purification Technology, 133 (2014) 260-275.

[110] D. Garmia, H. Zaghouane-Boudiaf, C.V. Ibbora, Preparation and characterization of new low cost adsorbent beads based on activated bentonite encapsulated with calcium alginate for removal of 2,4-dichlorophenol from aqueous medium, International Journal of Biological Macromolecules, 115 (2018) 257-265.

[111] Y. Cao, G. Zhou, R. Zhou, C. Wang, B. Chi, Y. Wang, C. Hua, J. Qiu, Y. Jin, S. Wu, Green synthesis of reusable multifunctional γ-Fe2O3/bentonite modified by doped TiO2 hollow spherical nanocomposite for removal of BPA, Science of The Total Environment, 708 (2020) 134669.

[112] W. Guo, W. Hu, J. Pan, H. Zhou, W. Guan, X. Wang, J. Dai, L. Xu, Selective adsorption and separation of BPA from aqueous solution using novel molecularly imprinted polymers based on kaolinite/Fe3O4 composites, Chemical Engineering Journal, 171 (2011) 603-611.

[113] S. Barreca, S. Orecchio, A. Pace, The effect of montmorillonite clay in alginate gel beads for polychlorinated biphenyl adsorption: Isothermal and kinetic studies, Applied Clay Science, 99 (2014) 220-228.

[114] A.V. Samrot, C.S. Sahithya, J. Selvarani A, S.K. Purayil, P. Ponnaiah, A review on synthesis, characterization and potential biological applications of superparamagnetic iron oxide nanoparticles, Current Research in Green and

Sustainable Chemistry, 4 (2021) 100042.

[115] C. Burda, X. Chen, R. Narayanan, M.A.J.C.r. El-Sayed, Chemistry and properties of nanocrystals of different shapes, 105 (2005) 1025-1102.

[116] A. Tavakoli, M. Sohrabi, A.J.c.p. Kargari, A review of methods for synthesis of nanostructured metals with emphasis on iron compounds, 61 (2007) 151-170.

[117] P.G. Jamkhande, N.W. Ghule, A.H. Bamer, M.G. Kalaskar, Metal nanoparticles synthesis: An overview on methods of preparation, advantages and disadvantages, and applications, Journal of Drug Delivery Science and Technology, 53 (2019) 101174.

[118] K.E. Haque, Microwave energy for mineral treatment processes—a brief review, International Journal of Mineral Processing, 57 (1999) 1-24.

[119] M. Bhattacharya, T. Basak, On the analysis of microwave power and heating characteristics for food processing: Asymptotes and resonances, Food Research International, 39 (2006) 1046-1057.

[120] L. Guo, H. Luo, J. Gao, L. Guo, J. Yang, Microwave hydrothermal synthesis of barium titanate powders, Materials Letters, 60 (2006) 3011-3014.

[121] A. Sosnik, G. Gotelli, G. Abraham, Microwave-assisted polymer synthesis (MAPS) as a tool in biomaterials science: How new and how powerful, Progress in Polymer Science, 36 (2011) 1050-1078.

[122] K. Dharmalingam, D. Pamu, R. Anandalakshmi, Comparison of solid state synthesis of zinc calcium phosphorous oxide (ZCAP) ceramics under conventional and microwave heating methods, Materials Letters, 212 (2018) 207-210.

[123] H.M. Williams, G.M.B. Parkes, Activation of a phenolic resin-derived carbon in air using microwave thermogravimetry, Carbon, 46 (2008) 1169-1172.

[124] F.K. Yuen, B.H. Hameed, Recent developments in the preparation and regeneration of activated carbons by microwaves, Advances in Colloid and Interface

Science, 149 (2009) 19-27.

[125] D.E. Clark, D.C. Folz, J.K. West, Processing materials with microwave energy, Materials Science and Engineering: A, 287 (2000) 153-158.

[126] R.R. Menezes, P.M. Souto, R.H.G.A. Kiminami, Microwave hybrid fast sintering of porcelain bodies, Journal of Materials Processing Technology, 190 (2007) 223-229.

[127] P. Yadoji, R. Peelamedu, D. Agrawal, R. Roy, Microwave sintering of Ni–Zn ferrites: comparison with conventional sintering, Materials Science and Engineering: B, 98 (2003) 269-278.

[128] W. Wei, Z. Shao, Y. Zhang, R. Qiao, J. Gao, Fundamentals and applications of microwave energy in rock and concrete processing – A review, Applied Thermal Engineering, 157 (2019) 113751.

[129] S.P. Masinga, E.N. Nxumalo, B.B. Mamba, S.D. Mhlanga, Microwave-induced synthesis of β-cyclodextrin/N-doped carbon nanotube polyurethane nanocomposites for water purification, Physics and Chemistry of the Earth, Parts A/B/C, 67-69 (2014) 105-110.

[130] E. Yagmur, S. Turkoglu, A. Banford, Z. Aktas, The relative performance of microwave regenerated activated carbons on the removal of phenolic pollutants, Journal of Cleaner Production, 149 (2017) 1109-1117.

[131] C. Saucier, M.A. Adebayo, E.C. Lima, R. Cataluna, P.S. Thue, L.D.T. Prola, M.J. Puchana-Rosero, F.M. Machado, F.A. Pavan, G.L. Dotto, Microwave-assisted activated carbon from cocoa shell as adsorbent for removal of sodium diclofenac and nimesulide from aqueous effluents, J Hazard Mater, 289 (2015) 18-27.

[132] K.Y. Foo, B.H. Hameed, Microwave-assisted preparation of oil palm fiber activated carbon for methylene blue adsorption, Chemical Engineering Journal, 166 (2011) 792-795.

[133] X. Ge, F. Tian, Z. Wu, Y. Yan, G. Cravotto, Z. Wu, Adsorption of naphthalene from aqueous solution on coal-based activated carbon modified by microwave induction: Microwave power effects, Chemical Engineering and Processing: Process Intensification, 91 (2015) 67-77.

[134] H. Chen, K. Lv, Y. Du, H. Ye, D. Du, Microwave-assisted rapid synthesis of Fe2O3/ACF hybrid for high efficient As(V) removal, Journal of Alloys and Compounds, 674 (2016) 399-405.

[135] H. Chen, Y. Du, Q. Lu, H. Ye, D. Du, K. Lv, J. Li, J. Li, Microwave-assisted rapid synthesis of Mn 3 O 4 /ACF hybrid for high efficient As(V) removal, Chemical Engineering Research and Design, 121 (2017) 431-437.

[136] H. Wang, H. Gao, M. Chen, X. Xu, X. Wang, C. Pan, J. Gao, Microwave-assisted synthesis of reduced graphene oxide/titania nanocomposites as an adsorbent for methylene blue adsorption, Applied Surface Science, 360 (2016) 840-848.

[137] S. Kumar N, D. Grekov, P. Pré, B.J. Alappat, Microwave mode of heating in the preparation of porous carbon materials for adsorption and energy storage applications – An overview, Renewable and Sustainable Energy Reviews, 124 (2020) 109743.

[138] N.M. Mubarak, J.N. Sahu, E.C. Abdullah, N.S. Jayakumar, P. Ganesan, Single stage production of carbon nanotubes using microwave technology, Diamond and Related Materials, 48 (2014) 52-59.

[139] R. Yañez-Macias, E. Hernandez-Hernandez, C.A. Gallardo-Vega, R. Ledezma-Rodríguez, R.F. Ziolo, Y. Mendoza-Tolentino, S. Fernández-Tavizon, C.A. Avila-Orta, Z. Garcia-Hernandez, P. Gonzalez-Morones, Covalent grafting of unfunctionalized pristine MWCNT with Nylon-6 by microwave assist in-situ polymerization, Polymer, 185 (2019) 121946.

[140] S. Deng, C. Yu, J. Niu, J. Liao, X. Liu, Microwave assisted synthesis of

phosphorylated PAN fiber for highly efficient and enhanced extraction of U(VI) ions from water, Chemical Engineering Journal, (2019).

[141] L.N.F. Queiroga, M.B.B. Pereira, L.S. Silva, E.C. Silva Filho, I.M.G. Santos, M.G. Fonseca, T. Georgelin, M. Jaber, Microwave bentonite silylation for dye removal: Influence of the solvent, Applied Clay Science, 168 (2019) 478-487.

[142] J. Wang, X. Guo, Adsorption isotherm models: Classification, physical meaning, application and solving method, Chemosphere, 258 (2020) 127279.

[143] K.Y. Foo, B.H. Hameed, Insights into the modeling of adsorption isotherm systems, Chemical Engineering Journal, 156 (2010) 2-10.

[144] S. Kundu, A.J.C.E.J. Gupta, Arsenic adsorption onto iron oxide-coated cement (IOCC): regression analysis of equilibrium data with several isotherm models and their optimization, 122 (2006) 93-106.

[145] K.R. Hall, L.C. Eagleton, A. Acrivos, T. Vermeulen, Pore- and Solid-Diffusion Kinetics in Fixed-Bed Adsorption under Constant-Pattern Conditions, Industrial & Engineering Chemistry Fundamentals, 5 (1966) 212-223.

[146] B. Turner, B. Henley, S. Sleap, S.J.I.j.o.e.s. Sloan, technology, Kinetic model selection and the Hill model in geochemistry, 12 (2015) 2545-2558.

[147] M.H. El-Naas, M.A. Alhaija, S.J.E.S. Al-Zuhair, P. Research, Evaluation of an activated carbon packed bed for the adsorption of phenols from petroleum refinery wastewater, 24 (2017) 7511-7520.

[148] M. Ahmadi, B. Ramavandi, S.J.C.E.C. Sahebi, Efficient degradation of a biorecalcitrant pollutant from wastewater using a fluidized catalyst-bed reactor, 202 (2015) 1118-1129.

[149] M. Andalib, E. Elbeshbishy, N. Mustafa, H. Hafez, G. Nakhla, J.J.R.E. Zhu, Performance of an anaerobic fluidized bed bioreactor (AnFBR) for digestion of primary

municipal wastewater treatment biosolids and bioethanol thin stillage, 71 (2014) 276-285.

[150] N. Abidi, E. Errais, J. Duplay, A. Berez, A. Jrad, G. Schäfer, M. Ghazi, K. Semhi, M.J.J.o.c.p. Trabelsi-Ayadi, Treatment of dye-containing effluent by natural clay, 86 (2015) 432-440.

[151] M. Bello, M. Nourouzi, L.C. Abdullah, T.S. Choong, Y. Koay, S.J.J.o.h.m. Keshani, POME is treated for removal of color from biologically treated POME in fixed bed column: applying wavelet neural network (WNN), 262 (2013) 106-113.

[152] D. Zhou, Z. Xu, Y. Wang, J. Wang, D. Hou, S.J.E.S. Dong, P. Research, Simultaneous removal of multi-pollutants in an intimate integrated flocculation-adsorption fluidized bed, 22 (2015) 3794-3802.

[153] K. Mohanty, D. Das, M.N. Biswas, Treatment of phenolic wastewater in a novel multi-stage external loop airlift reactor using activated carbon, Separation and Purification Technology, 58 (2008) 311-319.

[154] R.-C. Wang, S.-C. Chang, Adsorption/desorption of phenols onto granular activated carbon in a liquid–solid fluidized bed, Journal of Chemical Technology & Biotechnology, 74 (1999) 647-654.

[155] K. Mohanty, D. Das, M.N.J.S. Biswas, P. Technology, Treatment of phenolic wastewater in a novel multi-stage external loop airlift reactor using activated carbon, 58 (2008) 311-319.

[156] R.C. Wang, S.C.J.J.o.C.T. Chang, E. Biotechnology: International Research in Process, C. Technology, Adsorption/desorption of phenols onto granular activated carbon in a liquid–solid fluidized bed, 74 (1999) 647-654.

[157] V. Vimonses, B. Jin, C.W. Chow, C.J.C.E.J. Saint, Development of a pilot fluidised bed reactor system with a formulated clay–lime mixture for continuous

removal of chemical pollutants from wastewater, 158 (2010) 535-541.

[158] N. Balaji, K. Meera, M. Begum, N. Anantharaman, M. Uddin, Adsorption and desorption of L-phenylalanine on nano-sized magnetic particles, Journal of Engineering and Applied Sciences, 4 (2009).

[159] R. Balog, B. Jørgensen, L. Nilsson, M. Andersen, E. Rienks, M. Bianchi, M. Fanetti, E. Lægsgaard, A. Baraldi, S. Lizzit, Z. Sljivancanin, F. Besenbacher, B. Hammer, T.G. Pedersen, P. Hofmann, L. Hornekær, Bandgap opening in graphene induced by patterned hydrogen adsorption, Nature Materials, 9 (2010) 315-319.

[160] M. Moshari, A. Mehrehjedy, M. Heidari-Golafzania, M. Rabbani, S. Farhadi, Adsorption study of lead ions onto sulfur/reduced graphene oxide composite, Chemical Data Collections, 31 (2021) 100627.

[161] M. Khatamian, B. Divband, R. Shahi, Ultrasound assisted co-precipitation synthesis of Fe3O4/ bentonite nanocomposite: Performance for nitrate, BOD and COD water treatment, Journal of Water Process Engineering, 31 (2019).

[162] W.S. Peternele, V. Monge Fuentes, M.L. Fascineli, J. Rodrigues da Silva, R.C. Silva, C.M. Lucci, R. Bentes de Azevedo, Experimental Investigation of the Coprecipitation Method: An Approach to Obtain Magnetite and Maghemite Nanoparticles with Improved Properties, Journal of Nanomaterials, 2014 (2014) 682985.

[163] H.S. Abd El-Gawad, Oil and Grease Removal from Industrial Wastewater Using New Utility Approach, Advances in Environmental Chemistry, 2014 (2014) 1-6.

[164] L. Andrini, R. Moreira Toja, M.R. Gauna, M.S. Conconi, F.G. Requejo, N.M. Rendtorff, Extended and local structural characterization of a natural and 800°C fired Na-montmorillonite–Patagonian bentonite by XRD and Al/Si XANES, Applied Clay Science, 137 (2017) 233-240.

[165] M.S. Raghu, K. Yogesh Kumar, M.K. Prashanth, B.P. Prasanna, R. Vinuth, C.B. Pradeep Kumar, Adsorption and antimicrobial studies of chemically bonded magnetic graphene oxide-Fe3O4 nanocomposite for water purification, Journal of Water Process Engineering, 17 (2017) 22-31.

[166] H. Saleem, M. Haneef, H. Abbasi, Synthesis Route of Reduced Graphene Oxide Via Thermal Reduction of Chemically Exfoliated Graphene Oxide, Materials Chemistry and Physics, 204 (2017).

[167] R. Andrews, D. Jacques, D. Qian, E.C. Dickey, Purification and structural annealing of multiwalled carbon nanotubes at graphitization temperatures, Carbon, 39 (2001) 1681-1687.

[168] M.M. Ba-Abbad, M.S. Takriff, A. Benamor, A.W. Mohammad, Size and shape controlled of α-Fe2O3 nanoparticles prepared via sol–gel technique and their photocatalytic activity, Journal of Sol-Gel Science and Technology, 81 (2017) 880-893.

[169] M. Saraf, K. Natarajan, Shaikh M. Mobin, Microwave assisted fabrication of a nanostructured reduced graphene oxide (rGO)/Fe2O3 composite as a promising next generation energy storage material, RSC Advances, 7 (2017) 309-317.

[170] A.A. Umar, M.F. Abdul Patah, F. Abnisa, W.M.A.W. Daud, Preparation of magnetized iron oxide grafted on graphene oxide for hyperthermia application, Reviews in Chemical Engineering, (2020) 000010151520200001.

[171] H. Sadegh, R. Shahryari-ghoshekandi, M. Kazemi, Study in synthesis and characterization of carbon nanotubes decorated by magnetic iron oxide nanoparticles, International Nano Letters, 4 (2014) 129-135.

[172] Y. Na, S. Yang, S. Lee, Evaluation of citrate-coated magnetic nanoparticles as draw solute for forward osmosis, Desalination, 347 (2014) 34-42.

[173] R. Rahmawati, A. Taufiq, S. Sunaryono, A. Fuad, B. Yuliarto, S. Suyatman, D.

Kurniadi, Synthesis of Magnetite (Fe3O4) Nanoparticles from Iron sands by Coprecipitation-Ultrasonic Irradiation Methods, Journal of Materials and Environmental Science, 9 (2018) 155-160.

[174] G. Ersan, O.G. Apul, F. Perreault, T. Karanfil, Adsorption of organic contaminants by graphene nanosheets: A review, Water Research, 126 (2017) 385-398.

[175] Y. Muhammad, H.U. Rashid, S. Subhan, A.U. Rahman, M. Sahibzada, Z. Tong, Boosting the hydrodesulfurization of dibenzothiophene efficiency of Mn decorated (Co/Ni)-Mo/Al2O3 catalysts at mild temperature and pressure by coupling with phosphonium based ionic liquids, Chemical Engineering Journal, 375 (2019) 121957.

[176] C.-C. Lin, C.-Y. Lee, Adsorption of ciprofloxacin in water using Fe3O4 nanoparticles formed at low temperature and high reactant concentrations in a rotating packed bed with co-precipitation, Materials Chemistry and Physics, 240 (2020) 122049.

[177] T. Xia, N. Yan, S. Li, Y. Lin, T. Su, Adsorption of tylosin and sulfamethazine by carbon nanotubes and titanium dioxide nanoparticles: pH-dependent mechanisms, Colloids and Surfaces A: Physicochemical and Engineering Aspects, 581 (2019).

[178] H. Xu, W. Jia, S. Ren, J. Wang, Novel and recyclable demulsifier of expanded perlite grafted by magnetic nanoparticles for oil separation from emulsified oil wastewaters, Chemical Engineering Journal, 337 (2018) 10-18.

[179] J. Liu, N. Wang, H. Zhang, J. Baeyens, Adsorption of Congo red dye on FexCo3-xO4 nanoparticles, J Environ Manage, 238 (2019) 473-483.

[180] F. Yan, Y. Chu, K. Zhang, F. Zhang, N. Bhandari, G. Ruan, Z. Dai, Y. Liu, Z. Zhang, A.T. Kan, M.B. Tomson, Determination of adsorption isotherm parameters with correlated errors by measurement error models, Chemical Engineering Journal, 281 (2015) 921-930.

[181] H. Akaike, Information theory and an extension of the maximum likelihood principle, in: Selected papers of hirotugu akaike, Springer, 1998, pp. 199-213.

[182] B.H. Hameed, Equilibrium and kinetics studies of 2,4,6-trichlorophenol adsorption onto activated clay, Colloids and Surfaces A: Physicochemical and Engineering Aspects, 307 (2007) 45-52.

[183] R.M. Cornell, U. Schwertmann, The iron oxides : structure, properties, reactions, occurrences, and uses., 1996.

[184] F. Tomul, Influence of Synthesis Conditions on the Physicochemical Properties and Catalytic Activity of Fe/Cr-Pillared Bentonites, Journal of Nanomaterials, 2012 (2012) 1-14.

[185] E. Wembabazi, P.J. Mugisha, A. Ratibu, D. Wendiro, J. Kyambadde, P.C. Vuzi, Spectroscopic Analysis of Heterogeneous Biocatalysts for Biodiesel Production from Expired Sunflower Cooking Oil, Journal of Spectroscopy, 2015 (2015) 714396.

[186] Z. Yaghoubi, J. Basiri-Parsa, Modification of ultrafiltration membrane by thermo-responsive Bentonite-poly(N-isopropylacrylamide) nanocomposite to improve its antifouling properties, Journal of Water Process Engineering, 34 (2020) 101067.

[187] F. Soetaert, P. Korangath, D. Serantes, S. Fiering, R. Ivkov, Cancer therapy with iron oxide nanoparticles: Agents of thermal and immune therapies, Advanced Drug Delivery Reviews, (2020).

[188] S. Ren, J. Deng, Z. Meng, T. Wang, T. Xie, S. Xu, Enhanced removal of phenol by novel magnetic bentonite composites modified with amphoteric-cationic surfactants, Powder Technology, 356 (2019) 284-294.

[189] N.D. Mu'azu, N. Jarrah, T.S. Kazeem, M. Zubair, M. Al-Harthi, Bentonite-layered double hydroxide composite for enhanced aqueous adsorption of Eriochrome Black T, Applied Clay Science, 161 (2018) 23-34.

[190] R.-r. Shan, L.-g. Yan, K. Yang, Y.-f. Hao, B. Du, Adsorption of Cd(II) by Mg–Al–CO3- and magnetic Fe3O4/Mg–Al–CO3-layered double hydroxides: Kinetic, isothermal, thermodynamic and mechanistic studies, Journal of Hazardous Materials, 299 (2015) 42-49.

[191] J. Liu, N. Wang, H. Zhang, J. Baeyens, Adsorption of Congo red dye on FexCo3-xO4 nanoparticles, Journal of Environmental Management, 238 (2019) 473-483.

[192] S.D. Kim, Y. Kang, Heat and mass transfer in three-phase fluidized-bed reactors—an overview, Chemical Engineering Science, 52 (1997) 3639-3660.

[193] M.M. Bello, A.A. Abdul Raman, M. Purushothaman, Applications of fluidized bed reactors in wastewater treatment – A review of the major design and operational parameters, Journal of Cleaner Production, 141 (2017) 1492-1514.

[194] C. Yu, J. Shao, W. Sun, X. Yu, Treatment of lead contaminated water using synthesized nano-iron supported with bentonite/graphene oxide, Arabian Journal of Chemistry, 13 (2020) 3474-3483.

[195] M. Parastar, S. Sheshmani, S. Shokrollahzadeh, Cross-linked chitosan into graphene oxide-iron(III) oxide hydroxide as nano-biosorbent for Pd(II) and Cd(II) removal, International Journal of Biological Macromolecules, 166 (2021) 229-237.

[196] W. Wang, B. Zheng, Z. Deng, Z. Feng, L. Fu, Kinetics and equilibriums for adsorption of poly(vinyl alcohol) from aqueous solution onto natural bentonite, Chemical Engineering Journal, 214 (2013) 343-354.

[197] J. Liu, C. Zhao, H. Tu, J. Yang, F. Li, D. Li, J. Liao, Y. Yang, J. Tang, N. Liu, U(VI) adsorption onto cetyltrimethylammonium bromide modified bentonite in the presence of U(VI)-CO3 complexes, Applied Clay Science, 135 (2017) 64-74.

[198] J.U. Halpegama, P.M.C.J. Bandara, L. Jayarathna, A. Bandara, C.-Y. Yeh, J.-Y. Chen, C. Kuss, U. Dahanayake, A.C. Herath, S.K. Weragoda, X. Chen, R.

Weerasooriya, Facile fabrication of nano zerovalent iron – Reduced graphene oxide composites for nitrate reduction in water, Environmental Advances, 3 (2021) 100024.

[199] J. Xiao, W. Lv, Z. Xie, Y. Tan, Y. Song, Q. Zheng, Environmentally friendly reduced graphene oxide as a broad-spectrum adsorbent for anionic and cationic dyes via π–π interactions, Journal of Materials Chemistry A, 4 (2016) 12126-12135.

[200] R. Benda, G. Zucchi, E. Cancès, B. Lebental, Insights into the π – π interaction driven non-covalent functionalization of carbon nanotubes of various diameters by conjugated fluorene and carbazole copolymers, The Journal of Chemical Physics, 152 (2020) 064708.

[201] E. Emam, Modified Activated Carbon and Bentonite Used to Adsorb Petroleum Hydrocarbons Emulsified in Aqueous Solution, American Journal of Environmental Protection, 2 (2013) 161.

APPENDIX

Table 15: Raw data for the effect of varying Fe_3O_4/Bentonite dosage on its removal capability .

Dosage	**Equilibrium concentration (ppm)**	**Average equilibrium concentration (ppm)**
0.05	47.4	45.33±2.07
	45.1	
	43.49	
0.1	34.5	33±3.51
	35.01	
	29.49	
0.15	30.1	30.8±1.96
	32.76	
	29.54	
0.2	29.1	28.6±0.5
	28.5	
	28.2	

Table 16: Raw data for the effect of varying solution pH on Fe_3O_4/Bentonite removal capability.

pH	**equilibrium concentration (ppm)**	**Average equilibrium concentration (ppm)**
3	47.4	44.71±3.08
	45.1	
	41.63	
5	37.56	38.3±4.03
	35.01	
	42.33	
6.5	34.78	33±1.54
	32.76	
	31.46	
9	52.9	50.89±2.01
	50.1	
	49.67	

Table 17: Raw data for effect of initial oil concentration on Fe_3O_4/Bentonite removal capability.

Initial concentration (ppm)	**equilibrium concentration (ppm)**	**Average equilibrium concentration (ppm)**
66	21	23.2±3.4
	22	
	26.6	
90	33.1	34±2.9
	32	
	36.9	
100	38.1	37.01±3.48
	39.4	
	33.53	
110	48.1	47.38±0.78
	46.6	
	47.44	
170	93.2	90.53±2.67
	90.1	
	88.29	

Table 18: Raw data for effect of varying contact time on Fe_3O_4/Bentonite removal capability.

Time (min)	**Equilibrium concentration (ppm)**	**Average equilibrium concentration (ppm)**
0	101	100±1.5
	100.5	
	98.5	
30	62.5	60±3.8
	61.3	
	56.2	
60	47	47.34±1.28
	46.4	
	48.62	
90	33.1	33.4±0.5
	33.9	
	33.2	
120	37.1	37.76±0.66
	38.4	
	37.78	
150	34.9	35.89±1.01
	35.87	
	36.9	
180	37	37.01±0.62
	36.4	
	37.63	

Table 19: Raw data for effect of varying initial oil concentration on Fe_3O_4/Bent/rGO removal capability.

Initial concentration (ppm)	**Equilibrium concentration (ppm)**	**Average equilibrium concentration (ppm)**
150	14.63	14.63±1.3
	13.5	
	15.76	
120	9.3	9.383±1.117
	10.5	
	8.349	
90	9.6	7.035±2.565
	6.5	
	5.005	
50	5	4.3±0.7
	4.1	
	3.8	
35	4.1	3.2±1.2
	3.5	
	2	
25	2.1	2.6±0.6
	2.5	
	3.2	
15	2	2.4±0.7
	2.1	
	3.1	

Table 20: Raw data for the effect of varying contact time on Fe_3O_4/Bent/rGO removal capability.

Time (min)	**Equilibrium concentration (ppm)**	**Average equilibrium concentration (ppm)**
0	120.1	120 ±1.1
	121	
	118.9	
5	38	38.07±0.43
	38.5	
	37.7	
10	34	35.38±3.56
	33.2	
	38.94	
20	20.1	19.24±1.02
	19.4	
	18.22	
30	20.2	19.72±1.86
	21.1	
	17.86	
60	13.1	13.4±0.8
	12.9	
	14.2	
90	9.1	9.084±1.134
	10.2	
	7.95	
120	9.1	9.383±0.867
	8.8	
	10.25	
210	8.8	9.27±1.03
	10.3	
	8.71	

Table 21: Raw data for the effect of varying initial oil concentration on Fe_3O_4/Bent/MWCNTs removal capability.

Initial concentration (ppm)	**Equilibrium concentration (ppm)**	**Average equilibrium concentration (ppm)**
150	9.1	7.248±1.852
	7.1	
	5.54	
120	5.1	5.128±1.072
	6.2	
	4.08	
90	3.9	4.32±0.42
	4.5	
	4.56	
50	4.1	3.623±0.654
	3.8	
	2.969	
35	3.1	3.2±0.1
	3.2	
	3.3	
25	2.1	2.6±0.6
	2.5	
	3.2	
15	2	2.5±0.9
	2.1	
	3.4	

Table 22: Raw data for the effect of contact time on Fe_3O_4/Bent/MWCNTs removal capability.

Time (min)	**Equilibrium concentration (ppm)**	**Average equilibrium concentration (ppm)**
0	120.1	120±1.1
	121	
	118.9	
10	12.3	11.44±0.92
	11.5	
	10.52	
20	6.2	5.304±1.092
	5.5	
	4.212	
40	3.5	3.262±0.276
	3.3	
	2.986	
60	2.57	2.474±0.222
	2.6	
	2.252	
90	2.1	2.679±0.579
	2.8	
	3.13	
120	3.3	3±1.1
	3.8	
	1.9	
210	2.1	3.1±1.9
	2.2	
	5	

Table 23: Raw data for performance of Fe_3O_4 NPs, Fe_3O_4/Bentonite, Fe_3O_4/Bent/rGO, and Fe_3O_4/Bent/MWCNTs in fluidzied bed reactor.

Composite	**Equilibrium concentration (ppm)**	**Average equilibrium concentration (ppm)**
Fe_3O_4	95.1	95±2.3
	97.2	
	92.7	
Fe_3O_4/Bentonite	47.4	47±0.4
	46.98	
	46.98	
Fe_3O_4/Bent/rGO	15.1	14.06±1.44
	14.56	
	12.62	
Fe_3O_4/bent/MWCNTs	37.87	38.23±1.05
	37.54	
	39.28	